Title
Next Generation Magnetic Resonance Imaging Contrast Agents

Author
Klemm, Piper Julia

Publication Date
2012

Peer reviewed|Thesis/dissertation

Next Generation Magnetic Resonance Imaging Contrast Agents

By

Piper Julia Klemm

A dissertation submitted in partial satisfaction of the

requirements for the degree of

Doctor of Philosophy

in

Chemistry

in the

Graduate Division

of the

University of California, Berkeley

Committee in charge:

Professor Kenneth N. Raymond, Chair
Professor Christopher J. Chang
Professor Michael Lustig

Fall 2012

Next Generation Magnetic Resonance Imaging Contrast Agents

by Piper Julia Klemm

Abstract

Next Generation Macromolecular Magnetic Resonance Imaging Contrast Agents

by

Piper Julia Klemm

Doctor of Philosophy in Chemistry

University of California, Berkeley

Professor Kenneth N. Raymond, Chair

Magnetic resonance imaging (MRI) is one of the most powerful diagnostic techniques at the disposal of the medical community. Its success in the clinic, with 75 to 90 million scans performed worldwide annually, can be attributed in part to the use of injectable contrast agents to improve signal differentiation between healthy and pathological tissue. These contrast agents primarily use Gd(III) as the paramagnetic metal ion to induce contrast. With seven unpaired electrons, Gd(III) has the most paramagnetic character of any nonradioactive element. Aqueous Gd(III), however, is highly toxic; hence contrast agents use chelators to encapsulate the Gd(III) ion, which protects the patient from from the Gd(III) ion.

While these chelators are necessary, they greatly decrease the relaxivity of the current commercial contrast agents. Commercial contrast agents are similar in that they are heteroatom chelators (N, O) and octadentate coordination, leaving only one open site for water coordination. Additionally, given their steric bulk, the water exchange mechanism with bulk solvent is a laboriously hindered dissociative mechanism. These factors contribute to the low efficiency of these Gd(III) complexes, as measured in relaxivity. Diagnostic scans typically inject 8-10 g of these complexes to achieve sufficient signal.

Hydroxypyridinone (HOPO) chelators have emerged as a superior alternative to current commercial compounds. Using a tris(2-aminoethyl)amine (TREN) capping moiety, three bidentate HOPO chelators form a hexadentate ligand. These TREN-*tris*-HOPO ligands leave multiple open sites for water coordination and exhibit rapid water exchange with bulk solvent, due to their reduced steric bulk and associative exchange mechanism. These ligands use all-oxygen-donor chelators, capitalizing on the oxophilicity of Gd(III) to form highly stable complexes.

From this superior family of chelators, a variety of approaches can be used to develop the next generation of MRI contrast agents. Increasing molecular weight and

tumbling time has been a strategy for increasing relaxivity and efficiency of MRI contrast agents. Through macromolecular conjugation, relaxivity is readily increased; simultaneously, these macromolecules provide the potential for building multimodal and multifunctional diagnostic and therapeutic agents. The potential applications for this class of materials are further increased with the addition of targeting functionality. These agents must have the ability to be fully and rapidly excreted and have facile and uniform large-scale syntheses to be candidates for the clinic.

The esteramide (EA) dendrimer is one such macromolecular platform. With eight sites for contrast agent conjugation, the esteramide dendrimer readily loads many distinct HOPO ligands with multiple lanthanides for multimodal imaging. With close to 40 kDa of polyethylene glycol units, the Gd-HOPO-EA macromolecular architecture is highly soluble and biocompatible. Furthermore, the ester core of the dendrimer is degradable under *in vivo* conditions, easing renal clearance with four smaller moieties. The superior properties of this system inspired investigation into a variety of other macromolecular systems.

Porous silica mesoparticles provide a rigid architecture that is much larger than other macromolecules evaluated and can hold greater than 10^8 small molecule MRI contrast complexes. The surfaces of these particles are readily functionalized and suitable for conjugation with most small molecule MRI contrast agents. These structures use a nontoxic silica infrastructure and are excreted renally despite their large size, making them viable candidates for further *in vitro* and *in vivo* study.

Gold nanoparticles (AuNP) as a solid-support system have the most potential for use as multifunctional diagnostic and therapeutic compounds. AuNP have been long used for enhancing computed tomography (CT) imaging and have recently emerged as a cancer therapeutic when their structure is irradiated. These compounds are readily synthesized in large scales and have loading sites that are close together to hold multi-tethered Gadolinium-HOPO systems for multifunctional imaging.

Using a variety of macromolecules to capitalize on the structural relationship between relaxivity and size, per-Gd and per-macromolecule-Gd relaxivity have been increased dramatically at clinically and physiologically relevant conditions. These improvements show that the combination of carefully designed macromolecules with excellent HOPO chelators produces an ideal MRI contrast agent for the clinic of the future.

Acknowledgements

First and foremost, I would like to acknowledge my advisor and mentor, Professor Kenneth N. Raymond. Ken has been both an inspiration and a mentor to me from my first days in the group. He has constantly supported me in my advancement as a scientist, giving me freedom to pursue many projects in many fields. Ken always showed me that I could pursue my ambitions and follow them through to success. It is due to his tremendous support that I have been successful in this program.

Within the Raymond group, so many people have worked with me to expand the MRI project. Dr. Sylvie L. Pailloux has been ever patient with synthetic advice, Dr. Christopher M. Andolina has been a fountain of luminescent data and advice, Oanh P. Lam has encouraged me to have fun during time off from research, Dr. P. Aru Hill got me through those initial syntheses, Dr. David Koster, and of course, Dr. Jide Xu. I have had the privilege of working with fabulous undergraduate researchers- Anna E. R. Faris, Michelle N. Keyser and Danil E. Smiles. Their research accomplishments have been some of my most happy and proud times in graduate school. All of my other labmates have made my time fun and productive and for that I am grateful. Allyson Sia, Ben Allred, Dr. Tatsuya Fukushima, Dr. Jenny Diwu, Dr. Tommy Sun, Billy Hart-Cooper, Tiffany Pham, Vicky Jun, David Tatum, Chen Zhao, Dr. Kristen Clary, Dr. Casey Brown, Dr. Jeff Mugridge, and Jenna Bernard.

Much of the experimental data described herein is due to the support of wonderful collaborators. These people lent their time, labs, and expertise, teaching me skills about their research and working to expand the scope of this research. William C. ("Tripp") Floyd III in the Fréchet Laboratory got me off on the right foot with dendritic macromolecules. Always more of a friend, Tripp has always been there to cheers the victories and cheers the sorrows. Professor Jill Millstone (University of Pittsburgh) has been an amazing source of knowledge and support. She graciously hosted me at her laboratory so that I could make gold nanoparticle conjugates for MRI. She continuously inspires me that self-discipline will get me to my goals. Patrick Straney and Dr. Christopher Andolina in the Millstone lab have spent much time teaching me the ropes of nanoparticle synthesis and characterization. Alexandra Kasmer Duncan and Professor Christopher Landry (University of Vermont) have been wonderful collaborators of silica mesoparticle conjugation chemistry. Michael Winter in the Marletta Group was finally able to hit his four year goal of teaching me protein bioinorganic chemistry and protein crystallography with our HNOx project. As the person who convinced me to go to Berkeley on my visit weekend, our research collaboration was the result of a long friendship and preppy person support system.

Many of the experiments conducted here used instrumentation in Professor Christopher Chang and Professor Carolyn Bertozzi's labs. Lab members, including

Genieve van der Bittner, Carl Onak, Lauren Wagner and Chelsea Gordon, have been especially helpful to my research pursuits.

There are many others who have been an important part of my time here- my friends and cheerleaders, who went on endless coffee runs: Stephanie R. Jones, John Weinstein, Justin A. Bours, Rebecca Murphy, Dr. Peter R. Wich, Hoang Doan, Dr. Andre K. Isaacs, Chandra Richards, members of Iota Sigma Pi & the Graduate Life Committee.

I also wish to thank Adam D. Hill for the constant encouragement and all of the Table of Contents figures on demand. My papers would certainly have been less exciting without the addition of the Raymond Group Zoo (and TOC ROFL would certainly have much less to blog about).

I also wish to thank the people outside of chemistry who have been so supportive: my parents- Drs. R. Christopher and Roberta Klemm; my other parents- Lee Sullivan and Gary Hill; the San Francisco Zoo II Committee; Fairbanks; and my pony Brighton Boast A Bit, who kept my spirits up by winning every single day of grad school. In the span of several months, I got to watch her win West Coast Pony Finals, culminating over ten years of training and have my first paper published in the Journal of the American Chemical Society.

Thank you all, friends!

to my parents,

Christopher and Robin Klemm,

with love

Table of Contents

List of Figures

Chapter 1

Chapter 2

Chapter 6

Chapter 7

Chapter 8

List of Equations

List of Tables

Chapter 6

Chapter 7

Chapter 8

List of Abbreviations

Ab	**A**nti**b**ody
CA	**C**ontrast **A**gent
CPP	**C**ell **P**enetrating **P**eptide
CT	**C**omputed **T**omography
DO3A	1,4,7,10-tetraazacyclododecane-1,4,7 trisacetic acid
DOTA	1,4,7,10-tetraazacyclododecane-1,4,7,10-tetraacetic
DTPA	**D**iethylene**t**riamine**p**enta**a**cetic acid
EDTA	**E**thylene**d**iamine**t**etra**a**cetic acid
FDA	U.S. **F**ood and **D**rug **A**dministration
HA	**H**ydroxy**a**paptite (or hydroxylapatite)
HOPO	3-**H**ydroxy-1-methyl-2-**o**xo-1,2-dihydro-**p**yridine-4-carb**o**xylic acid
HSA	**H**uman **S**erum **A**lbumin
MRI	**M**agnetic **R**esonance **I**maging
NMR	**N**uclear **M**agnetic **R**esonance
NMRD	**N**uclear **M**agnetic **R**esonance **D**ispersion
PEG	**P**oly**e**thylene **G**lycol
PET	**P**ositron **E**mission **S**pectroscopy
SPECT	**S**ingle-**P**hoton **E**mission **C**omputerized **T**omography
$t_{1/2}$	half-life
TAM	2,3 dihydroxy**t**erephthal**am**ide
TACN	1,4,7 **T**ri**a**za**c**yclo**n**onane
TREN	Tris(2-amino-ethyl) amine

List of Symbols

B	(T)	static magnetic field
Δ^2		mean square zero field splitting
q		number of coordinated inner-sphere water molecules
r_1	($mM_{Gd}^{-1}s^{-1}$)	longitudinal relaxivity
$r_1^{I.S.}$	($mM_{Gd}^{-1}s^{-1}$)	inner-sphere contribution to longitudinal relaxivity
$r_1^{2nd.S.}$	($mM_{Gd}^{-1}s^{-1}$)	2nd sphere contribution to longitudinal relaxivity
$r_1^{O.S.}$	($mM_{Gd}^{-1}s^{-1}$)	outer-sphere contribution to the longitudinal relaxivity
r_{Gd-H}	angstrom	Gd^{3+} electron spin-proton distance
T_1	s^{-1}	spin-lattice or longitudinal relaxation time
T_2	s^{-1}	spin-spin or transverse relaxation time
T_{1e}	s^{-1}	longitudinal electron-spin relaxation time
τ_m	ns	water residence time
τ_R	ps	rotational correlation time of the metal-proton vector
τ_v	ps	correlation time for the modulation of the zero-field-splitting interaction
ω_L	s^{-1}	Larmor frequency

Chapter 1- Introduction to Magnetic Resonance Imaging Contrast Agents

Abstract

In order to improve the efficacy and efficiency of magnetic resonance imaging contrast agents, macromolecular conjugation to gadolinium contrast agents may be employed to circumvent many common problems encountered by common therapeutic or imaging moieties. These drawbacks may include low solubility, short blood residence time, minor accumulation in targeted tissues, inadequate signal or response, and fast excretion from the body. Through macromolecular conjugation, an imaging contrast agent lacking ideal properties is bound to a large carrier exhibiting a more favorable efficiency and biocompatibility profile. Depending on the desired imaging procedure, the attached agent may be designed for introduction into a target tissue and bound in a permanent way to ensure its eventual excretion commensurate with the macromolecular conjugate. In this introduction, the overall motivations and approaches for this macromolecular-based imaging, with particular regard to gadolinium-hydroxypyridinone complexes are discussed.

Introduction

Drawbacks to Commercial Contrast Agents

Since diagnostic imaging modalities were introduced in the second half of the twentieth century, mitigating their respective inherent weaknesses has been at forefront of imaging research. Positron emission tomography (PET) has sought to increase throughput, computed tomography (CT) has sought to increase resolution of soft tissue, optical imaging has sought to increase depth penetration, and magnetic resonance imaging (MRI) has sought to increase sensitivity.[1] Diagnostics for all of these imaging modalities have turned to contrast agents (CA) to improve the efficiency and diagnostic power.

All current commercial CA utilize small molecules, with MRI using paramagnetic gadolinium (III) to shorten water relaxation time. Once administered, these MRI-CA are rapidly distributed by the blood to tissues throughout the body, eventually accumulating in larger concentrations in tumors and pathogenic tissue. Being small molecules, many of these small molecule agents are unfortunately cleared rapidly from the body (~ 3 h for full clearance) before a lengthy scan can be carried out.[2] Commercial CA are also highly inefficient and require inject into patients of large quantities of Gd(III), which is toxic to all living tissues and cells in the aqueous form.[2] Due to their widespread and predominantly indiscriminate distribution in the body, efficiency can be greatly increased through the design of high relaxivity and selectivity MRI-CA.

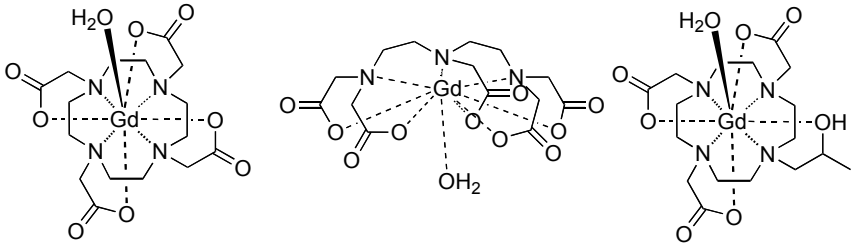

Gd-DOTA Gd-DTPA Gd-DO3A

Figure 1. Several commercially available but inefficient magnetic resonance imaging contrast agents.

The ideal MRI contrast agent would be extremely efficient and have high kinetic stability. It would be easily formulated, administered in a low dose, and then be renally excreted with all of the Gd(III) chelate intact.[2] However, the difficulty of finding a CA with high relaxivity and without regard to these further specifications is already challenging enough. As inorganic Gd(III) complexes, most CA prospects lack the necessary solubility in blood, presenting a daunting obstacle to their being delivered to a patient.

One common method for addressing these concerns is to continue the search for slight niche modifications to current commercial agents for slightly different functions.[2] This generally involves targeting a specific protein or site *in vivo* in search of more tailored CA that are similar enough to the approved commercial agents to be likely candidates for Food & Drug Administration (FDA) or European Medicines Agency (EMA) approval. This approach is effective in discovering new MRI-CA to take to the clinic, but progress is typically slow and the process is highly inefficient.[3] CA with similar synthetic architectures to current commercial agents cannot overcome inherent inefficiencies from using octadentate heteroatom chelators.[2]

Another common approach is the development of macromolecular nanoparticles or similar type metal oxide structures for use as larger CA.[4] While much signal enhancement can be delivered to a desired location, iron(III) oxide nanoparticles have been voluntarily withdrawn from the market by drug companies due to toxicity concerns.[5] In research phases, these compounds with Gd(III) or other lanthanides have metal leaching and stability concerns and their variability in size and shape during synthesis have potential unpredictable changes in CA diagnosis and pharmacokinetics.[6] Additionally, many CA present a synthetic challenge in their having too few viable synthetic handles with which to craft any improvement demanded by changes in diagnostic instruments or clinical administration.

While this goal of development of new CA is imperative, many complexes already known to exhibit potential in improving relaxivity are excluded from medical consideration due to their lack of solubility, kinetic stability, or high toxicity.[7] This delivery problem is not unique to CA, however, as many drugs, drug delivery organic structures, and nanoparticles suffer the same drawbacks. Because drugs and drug candidates are generally small organic molecules designed to be delivered in a specific then elicit a specific response (i.e., pain relief, cancer reduction), their commonly

encountered impediments do not significantly diverge from those of CA, at least with regards to the pharmacokinetic standpoint. For instance, many drug and drug candidates are similarly highly insoluble, toxic, or incapable of accumulating specifically in a region of interest. Because of these similarities, solutions to the challenges one class of molecule may be easily translated into progress for the other.[8] One attractive route for addressing these concerns of practicality and biocompatibility is to inject the agent as a conjugate to a macromolecule.[9]

Mechanism of Gadolinium-based Contrast Agents

MRI-CA function by accumulating a Gd(III) (or theoretically any paramagnetic metal center) in a tissue of interest and shortening the water relaxation time in that area.[10] Water is a significant fraction of the human body, ranging from 45-75% (with statistical averages based on age, gender, and lifestyle, reaching the generally accepted average at 60%.)[11] Bulk solvent (water) interactions with a paramagnetic metal center shorten the water relaxation time and enhance signal in a MRI instrument, which operates on the principles of nuclear magnetic resonance (NMR) spectroscopy. These agents accelerate the rate at which water protons relax when pulsed with the radio frequencies utilized in MRI, allowing for increased image contrast.[12]

The concept of a using a CA to enhance signal was first proposed in the early seventies with the introduction of MRI into the clinic, and was realized when Gd-DTPA was approved by the FDA in 1988.[13] Gadolinium(III) is the preferred metal of choice because it has seven unpaired electrons in its *f* orbitals. As such, it has the most paramagnetic character of any non-radioactive element. Additionally, Gd(III) has a large magnetic moment (7.9-8.0), which is inferior to only Tb(III), Dy(III), Ho(III), and Er(III), all of which have fewer unpaired electrons.[14] However, Gd(III) in its aqueous form is highly toxic *in vivo*. Its size and charge make it easily slide through Ca(II) ion channels, interrupting Ca(II) messages. It has been linked with incurable diseases termed Nephrogenic Systemic Fibrosis (NSF) and Nephrogenic Fibrosing Dermapathy (NFD), forms of Gd(III) poisoning.[15] For safety purposes, Gd(III) is chelated to an organic ligand. The complex used must have high solubility in blood, have high stability, be nontoxic, exhibit favorable accumulation in areas of interest, and also be injected in large enough quantities for Gd(III) to illuminate an MRI diagnosis.

Two families of commercial agents have made it successfully to the clinical market. Both Gd-DTPA and Gd-DOTA and their derivatives (Figure 1), which comprises all ten current commercial MRI-CA on the worldwide market in 2012, use a Gd(III) metal center with an octadentate heteroatom organic chelator. They are similar structures, are generally safe and effective with one noted structural difference. Gd-DTPA is an open-chain structure; while this has high thermodynamic stability, it does not lend to high kinetic stability, with decomplexation on the order of three weeks *in vivo*. Gd-DOTA is a macrocyclic structure, so while there is a high energy barrier for Gd(III) to enter the cage in the metallation synthetic step, once the Gd(III) is in the DOTA ligand, it has very high kinetic stability with a decomplexation time on the order of 6,000 years *in vivo.* [2] Both families of ligands are designed to bind strongly to Gd(III), accumulate to achieve signal

at tumor and pathogenic sites *in vivo*, and excrete (intact) renally with the Gd(III) metal ion shielded from the body.

These currently approved families of MRI CA's are water-soluble and are injected at hundreds of millimolar concentrations, which is necessary based on their low efficiency. With relaxivities of around 3 $mM^{-1}s^{-1}$ for all current CA, quantities of 8-10 g need to be administered to acquire signal.[2] Both complex families use heteroatom chelators of both nitrogen and oxygen donors, which does not fully capitalize on the stability that can be obtained from Gd(III)'s oxophilicity and the desire for a hard-hard metal-ligand interaction. Both families have octadentate architectures, which allow a q value (number of water molecules directly coordinated to the metal center) of one per Gd(III). Since Gd(III) has a coordination number of 8-9, a ligand with less denticity would allow for a higher q value, faster water exchange with bulk solvent, and a higher per Gd(III) relaxivity.[12]

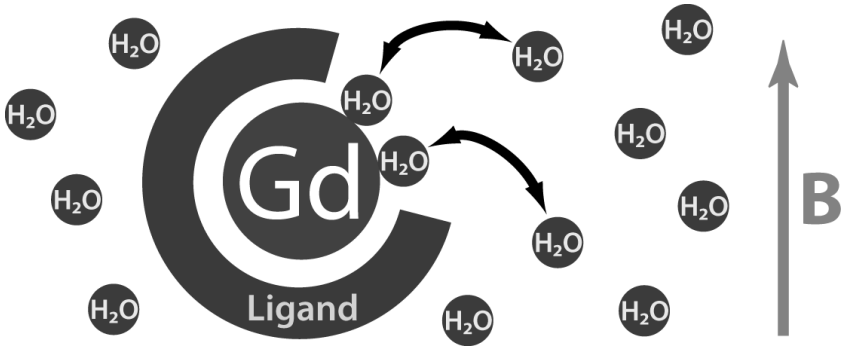

Figure 2. Bulk solvent exchange with the gadolinium(III) metal center, describing the mechanism of relaxivity enhancement in pathological tissue.

$$(1/T_1) = qP_m[1/(T_{1m} + \tau_m)]$$

$$\frac{1}{T_{1m}} = \frac{2}{15}\frac{\gamma^2 g^2 \mu_B^2 S(S+1)}{r^6}\left[\frac{3\tau_{c1}}{(1+\omega_1^2\tau_{c1}^2)} + \frac{7\tau_{c2}}{(1+\omega_S^2\tau_{c2}^2)}\right]$$

$$1/\tau_{ci} = 1/\tau_R + 1/T_{ie} + 1/\tau_m \text{ with } i = 1,2$$

r_i = relaxivity (inner-sphere) T_{im} = relaxation time of bound water

q = number of bound solvent nuclei τ_c = correlation time

P_m = mole fraction of bound water τ_R = rotational correlation time

τ_m = mean water residence time T_{ie} = electronic longitudinal relaxation time

Equation 1. The Solomon-Bloembergen-Morgan Equations[12] for determining relaxivity parameters. The parameters that can be synthetically modified to achieve larger relaxivities are q, τ_R, and τ_M (Equation from reference 12).

The Solomon-Bloembergen-Morgan Equations were developed in the 1960s to describe the interaction of paramagnetic metals with bulk solvent.[12] Of their many parameters (Equation 1), chemists have focused on the three that can be synthetically modified- q, τ_R, and τ_M. The q value can be increased using ligands with fewer chelators, however, this cannot be at the expense of kinetic or thermodynamic stability and the

potential leaching of Gd(III) into the body. The mean water residence time can be increased by having an associative versus dissociative water exchange on the metal center, having a strong hydrogen bonding network of second and outer sphere coordination with bulk solvent and the metal, and by reducing steric bulk around the metal center to allow exchange to occur more rapidly.[16] The rotational correlation time can be decreased (and relaxivity increased) through the conjugation to a macromolecule, which has been explored through use of dendrimers,[17] viral capsids,[18] proteins,[19] micelles,[20] nanobins,[21] nanoparticles,[22] microparticles,[23] nanodiamonds,[9] and many other macromolecular architectures. The addition of macromolecular architechtures offers a much larger degree of synthetic versatility in many of these systems allows for the introduction of other agents for multimodal imaging, drug delivery and other therapeutics,[24] cell penetrating peptides,[25] and targeting groups[26] to enhance and tailor the biodistribution properties of the conjugate.

Oxygen Donor Chelator Gd(III) Complexes

In this introduction and the following chapters, the emphasis is placed on relaxivity enhancement using Gd-Hydroxypyridonate (HOPO) complexes conjugated to various macromolecules. These advances in macromolecular conjuagation are possible due to the extensive research in the Raymond group over the last several decades in the form of the HOPO and TAM chelating moieties. This work has focused on designing, synthesizing, and optimizing small molecule Gd-HOPO complexes for the best properties,[27-30] which have been optimized by dozens of researchers in the Raymond Group since the breakout MRI paper in 1995. This body of research allows the focus of current research to investigate and optimize the macromolecular approach and optmize the largest relaxivities to date. Small molecule Gd-HOPO compounds (e.g. Figure 3) increase the relaxivity properties three fold or more as compared to commercial agents. Compared to other systems, the Gd-HOPO platform introduces the drawback of a larger synthetic investment; Gd-DOTA, Gd-DTPA, and relevant macromolecules are often formed in just a few synthetic steps. However, this synthetic investment is well worth the high q value of 2-3, high thermodynamic stability, rapid water exchange, and approximately three-fold increase in molecular weight to slow the tumbling time. These HOPO systems also feature the TAM chelating moiety, a synthetic handle that is easily modified to conjugate a solubilizing moiety or macromolecule. The hexadentate Gd-HOPO framework, capped by a tridentate moiety, provides an exceptional inorganic complex which not only improves greatly on commercial agents on its own, it also dramatically increases relaxivity through conjugation to various macromolecules.

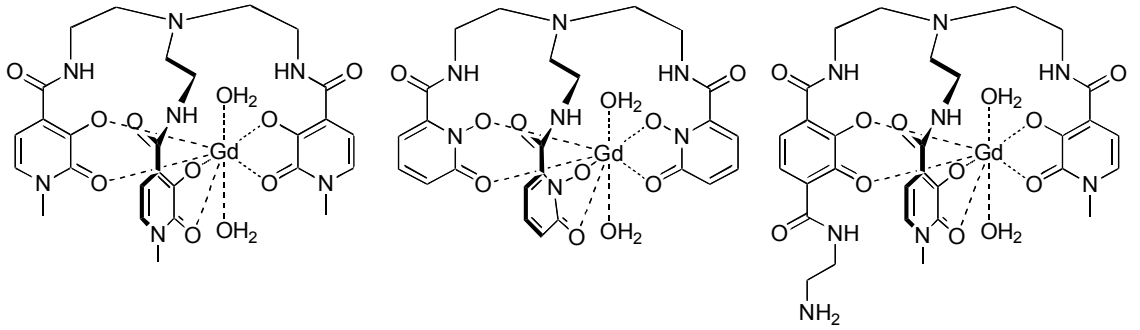

Figure 3. Representative structures of oxygen-donor hydroxypyridinone (HOPO) and terephthalamide (TAM) chelators developed by the Raymond Group.[27-30]

This ability to covalently link a Gd-HOPO CA to a specific region of the macromolecule is an important feature, as some systems allow exposed agents to interact with solvents[31] and some provide additional kinetic stability by protecting and shielding the agent from the surrounding environment.[32] While both methodologies have their advantages, as safety is the primary concern and efficiency second, it can be highly beneficial to conjugate a CA near the core of the macromolecule, whether it be a dendrimer, protein, or nanoparticle decorated with PEG chains. This manner of conjugation also allows the macromolecule to confer solubility and biocompatibility increases to the small molecule complex. These macromolecules must be large enough to hold several Gd-HOPO complexes, but they must not be so large that they will have difficulty filtering through the kidney for renal excretion.[33] This can be a particular issue for macromolecules that are not synthesized at a constant size and molecular weight; macromolecular polydispersity can lead to differing distribution and excretion profiles.

For conjugation to Gd-HOPO complexes, macromolecules were chosen that have had prior evaluation of their pharmacokinetic properties *in vivo* in mice to evaluate their potential. Precise control over synthesis and formation of macromolcules was also a criteria for clinical potential. For example, dendritic macromolecules with a facile ester core hydrolysis mechanism (Chapters 3 & 4) were used over linear PEG chains due to the precise control over their synthesis, rapid renal excretion when the core hydrolyzed after imaging scans, tightly packed bundle (~40 kDa in only ~10 nm diameter), low polydispersity, and high solubility and biocompatibility.[32-34] These dendritic macromolecules also have synthetic handles for other imaging agents to formulate multimodal CA (Chapter 4) and the ability to add targeting groups to the periphery of the dendrimer.[35] By combining chemistries optimized by the Raymond Laboratory for many years in the form of the Gd-HOPO complex and dendritic macromolecules optimized by the Fréchet Laboratory, in this example, truly novel and record changing performances can be achieved with a large degree of structural control, versatility, precision, and biocompatibility.

Commonly Employed Chemistries

When evaluating chemistries for use in conjugating small molecule Gd-HOPO complexes to macromolecules, covalent bonding is essential unless binding to a naturally occurring macromolecule, such as MS-325. It allows us to synthesize on a biologically relevant scale and ensure that the conjugate is stable in a biological system throughout the imaging and (for the theranostic agents) therapeutic processes. Using selective attachments of small molecule complexes to macromolecules, a peptide bond has been the preferred method; however, there are many other strategies that can be employed, such as a thiol-gold bond onto the surface of a nanoparticle; a labile bond such as an acyl hydrazone to release the CA for excretion if bioaccumulation of the macromolecule is a potential issue, enzymatically cleaved linkages,[21] and a malemide-thiol coupling as a more rigid linker.[36]

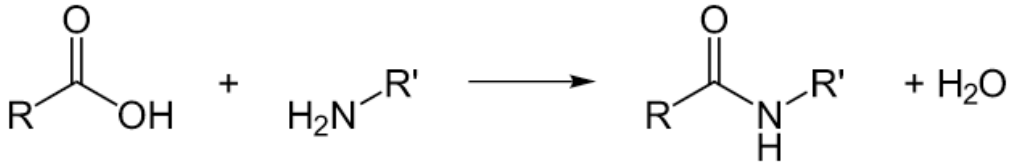

Figure 4. Peptide bond formation used in a variety of macromolecular conjugations to form a stable covalent bond between e.g. Gd-TREN-*bis*-(1-Me)-3,2-HOPO-TAM (Figure 3) and the Esteramide Dendrimer.

Macromolecules Employed as MRI-CA

While macromolecules seem to answer many of the current deficiencies of MRI-CA, the future of CA is somewhat uncertain. The most recent generation of approaches have yet to be well investigated in clinical studies. The clinical environment is rapidly changing for MRI: as clinical instruments have larger and larger magnets (from 10-20 MHz a decade ago to 60-125 MHz common now), they have less use for traditional CA, and traditional CA are less effective and require larger doses at larger field strengths.[37] As the field changes, imaging agents that not only have more imaging modes, but also the potential for therapeutics (termed 'theranostic' agents) and targeted imaging are more widely sought.

Small molecules have dominated the MRI-CA scene for a long time; as a result, an arms race formed to create the molecule with the largest per-Gd(III) relaxivity. When macromolecules are involved that can hold anywhere between one and several hundred million Gd(III) complexes, the per-Gd value becomes increasingly irrelevant. If a nanoparticle, for example, only has an average per-Gd relaxivity, but can delivery several thousand of Gd(III) centers to one location, that could prove clinically to be more powerful than an exceptional per-Gd(III) relaxivity. As a field-wide consensus to these questions has not been attained *in vivo* and in the clinic, both approaches have been pursued with equal veracity and intent. As changes in temperature and field strength do not have generalized formulas to define their impact on a given system, Chapter 2 tells

the story of reevaluating compounds from previous Raymond Laboratory contributions to see their effect at the higher field strengths and physiological temperatures. Some compounds that had been discounted at prior conditions, such as the Gd-TREN-*tris*-1,2-HOPO, performed at the superlatively at conditions applicable to the clinic in 2012. As a fluid science to keep relevant to the clinic, development of CA must be at least in-step with the clinic, if not several steps ahead.

The Approach

To obtain the most elite of macromolecules as scaffolds for MRI-CA, many collaborations from different laboratories that specializes in specific macromolecules around the world have worked toward specific goals of better diagnosis. Chapters 3 and 4 cover dendrimer conjugation in collaboration with the Fréchet Group. The dendrimers evaluated are 40 kDa in molecular weight and hold eight Gd-HOPO complexes. Using other Ln-HOPO complexes with properties to enhance optical imaging and MRI, multimodal-imaging agents were developed, and evaluated for efficiency in imaging and cytotoxicity in cells.

Chapter 5 describes the use of silica mesoparticles in the hunt for the maximum per-particle relaxivity possible. Using porous particles over a micron in diameter, vast surface areas allow loading of up to several hundred million small molecule Gd-complex contrast agents. As kinetic stability has become a larger and larger concern in recent years, a new approach toward achieving high kinetic stability through protein incorporation is explored in Chapter 6. Noble metal and semiconductor Nanoparticles are another potential for multimodal imaging and potential therapeutics, which are the topic of Chapters 7 and 8.

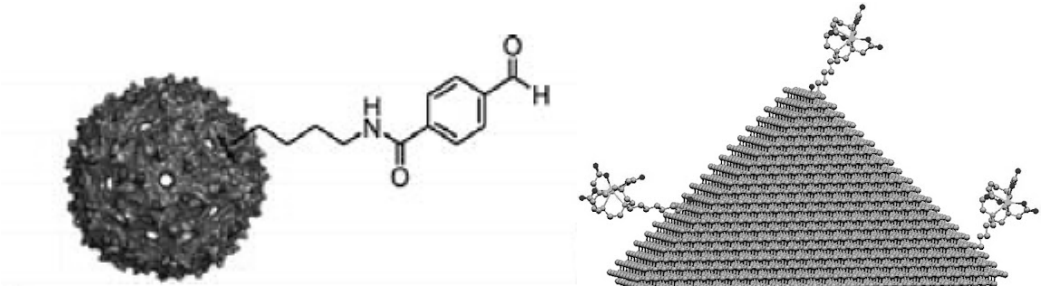

Figure 5. Macromolecules employed to decrease the rotational correlation time and increase relaxivity, solubility, and biocompatibility of MRI-CA. Left: MS2 Viral Capsid, Right: Nanodiamond.

Conclusions

To increase the efficacy and biocompatibility of MRI-CA, major modifications from current agents are required. This can be done through conjugation of an inorganic complex to a well-selected macromolecule that possesses the pharmacokinetic properties desired in the MRI-CA, multimodal diagnostic, or theranostic of interest. In this and upcoming chapters, attention is particularly focused on accomplishing this through

conjugation of Gd-HOPO complexes to a variety of macromolecules selected for size, biocompatibility, loading, and kinetic stability. Their design and synthesis are carefully analyzed, including architectural effects, biocompatility, solubility, and renal excretion profiles.

References

1) Baker, M. Whole animal imaging: the whole picture. *Nature*. **2010**, *463,* 977-981.
2) Port, M.; Idee, J. M.; Medina, C.; Robic, C.; Sabatou, M.; Corot, C. Efficiency, thermodynamic and kinetic stability of marketed gadolinium chelates and their possible consequences: a critical review. *Biometals*. **2008**, *21*, 469-490.
3) Lewis, M.; Yanny, S.; Malcolm, P. N. Advantages of blood pool contrast agents in MR angiography: a pictorial review. *J. Med. Imag. Radiat. On.* **2012**, *56,* 187-191.
4) Nishie, A.; Asayama, Y.; Ishigami, K.; Tajima, T.; Kakihara, D.; Nakayama, T.; Takayama, Y.; Okamoto, D.; Taketomi, A.; Shirabe, K.; Fujita, N.; Obara, M.; Yoshimitsu, K.; Honda, H. *J. Magn. Reson. Imag.* **2012**, *36*, 664-671.
5) Bulte, J. W. M. In vivo MRI cell tracking: clinical studies. *Am. J. Roentgenol.* **2009**, *193,* 314-325.
6) Abrikossova, N.; Skoglund, C.; Ahren, M.; Bengtsson, T.; Uvdal, K. Effect of gadolinium oxide nanoparticles on the oxidative burst from human neutrophil granulocytes. *Nanotechnology.* **2012**, *23*, 275101.
7) Shu, C.-Y.; Zhang, E.-Y.; Ziang, J.-F.; Zhu, C.-F.; Wang, C.-R.; Pei, X.-L.; Han, H.-B. Aggregation studies of the water-soluble gadofullerene magnetic resonance imaging contrast agent: [Gd@C82O6(OH)16(NHCH2CH2COOH)8]x. *J. Phys. Chem. B.* **2006**, *110,* 15597-15601.
8) Müller, C. E., Prodrug Approaches for Enhancing the Bioavailability of Drugs with Low Solubility, *Chemistry and Biodiversity*, **2009**, *6*, 2071-2083.
9) Manus, L. M.; Mastarone, D. J.; Zhang, X. Q.; Waters, E. A.; MacRenaris, K. W.; Parigi, G.; Luchinat, C.; Ho, D.; Meade, T. J. Gd(III)-Nanodiamond conjugates for MRI contrast enhancement. *Nano. Lett.* **2010**, *10*, 484-489.
10) Ananta, J. S.; Godin, B.; Sehti, R.; Moriggi, L.; Liu, X.; Serda, R. E.; Krishnamurthy, R.; Bolskar, R. D.; Helm, L.; Ferrari, M.; Wilson, L. J.; Decuzzi, P. Geormetrical confinement of Gd-based agents in nanoporous particles enhances T1 contrast. *Nat. Nanotechnol.* **2010**, *5*, 815-821.
11) Jackson, S. *Anatomy & Physiology for Nurses.* (9th ed.), **1985**, London: Bailiere Tindall.
12) Merbach, A. E.; Toth, E. *The Chemistry of Contrast Agents in Magnetic Resonance Imaging.* **2001**, Switzerland: Wiley & Sons.
13) Caravan, P.; Ellison, J. J.; McMurry, T. J.; Lauffer, R. B. Gadolinium(III) chelates as MRI contrast agents: structure, dynamics, and applications. *Chem. Rev.* **1999**, *99*, 2293-2352.
14) Eliseeva, S. V.; Buenzli, J.-C. G. Lanthanide luminescence for functional materials and bio-sciences. *Chem. Soc. Rev.* **2010**, *39*, 189-227.

15) Zou, Z.; Lin, M. Nephrogenic Systemic Fibrosis/ Nephrogenic Fibrosing Dermopathy: A Decade-old Disease. *Indian J. Dermatol.* **2007,** *52*, 125-130.
16) Xu, J.; Franklin, S. J.; Whisenhunt, Jr., D. W.; Raymond, K. N. Gadolinium complex of tris[(3-hydroxy-1-methyl-2-oxo-1,2-didehydropyridine-4-carboxamido)ethyl]-amine: a new class of gadolinium magnetic resonance relaxation agents. *J. Am. Chem. Soc.* **1995**, *117*, 7245-7246.
17) Nwe, K.; Bryant, Jr., L. H.; Brechbiel, M. W. Poly(amidoamine) dendrimer based MRI contrast agents exhibiting enhanced relaxivities derived via metal preligation techniques. *Bioconjugate Chem.* **2010**, *21*, 1014-1017.
18) Datta, A.; Raymond, K. N. Gd-Hydroxypyridinone (HOPO)-based high-relaxivity magnetic resonance imaging (MRI) contrast agents. *Acc. Chem. Res.* **2009**, *42,* 948-957.
19) Strauch, R. C.; Mastarone, D. J.; Sukerkar, P. A.; Song, Y.; Ipsaro, J. J.; Meade, T. J. Reporter protein-targeted probes for magnetic resonance imaging. *J. Am. Chem. Soc.* **2011***, 133,* 16346-16349.
20) Heta, Y.; Kumaki, K.; Hifumi, J.; Citterio, D.; Tanimoto, A.; Suzuki, K. Gadolinoium containing photochromic micelles as potential magnetic resonance imaging traceable drug carriers. *Photochem. Photobiol.* **2012**, *88*, 876-883.
21) Lee, S.-M.; Song, Y.; Hong, B. J.; MacRenaris, K. W.; Mastarone, D. J.; O'Halloran, T. V.; Meade, T. J.; Nguyen, S. T. Modular polymer-caged nanobins as a theranostic platform with enhanced magnetic resonance relaxivity and pH-responsive drug release. *Angew. Chem. Intl. Ed.* **2010**, *49,* 9960-9964.
22) Song, Y.; Xu, X.; MacRenaris, K. W.; Zhang, X-Q.; Mirkin, C. A.; Meade, T. J. Multimodal gadolinium-enriched DNA-gold nanoparticle conjugates for cellular imaging. *Angew. Chem. Intl. Ed.* **2009**, *48,* 9143-9147.
23) Steinbacher, J. L.; Lathrop, S. A.; Cheng, K.; Hillegass, J. M.; Butnor, K.; Kauppinen, R. A.; Mossman, B. T.; Landry, C. C. Gd-labeled microparticles in MRI: in vivo imaging of microparticles after intraperitoneal injection. *Small.* **2010**, *6,* 2676-2682.
24) Fox, M. E., Szoka, F. C., and Fréchet, J. M. J., Soluble polymer carriers for the treatment of cancer: the importance of molecular architecture. *Acc. Chem. Res.* **2009**, *42*, 1141-1151.
25) Skotland, T. Molecular imaging: challenges of bringing imaging of intracellular targets into common clinical use. *Contrast Media Mol. Imaging.* **2012**, *7*, 1-6.
26) De Leon-Rodriguez, L. M.; Lubag, A. J. M; Malloy, C. R.; Martinez, G. V.; Gillies, R. J.; Sherry, A. D. Responsive MRI agents for sensing metabolism in vivo. *Acc. Chem. Res.* **2009**, *42,* 948-957.
27) Raymond, K. N.; Pierre, V. C. Next generation, high relaxivity gadolinium MRI agents. *Bioconjugate Chem.* **2005**, *16*, 3-8.
28) Xu, J.; Churchill, D. G.; Botta, M.; Raymond, K. N. Gadolinium(III) 1,2-Hydroxypyridonate-based complexes: toward MRI contrast agents of high relaxivity. *Inorg. Chem.* **2004**, *43*, 5492-5494.
29) Werner, E. J.; Kozhukh, J.; Botta, M; Moore, E. G.; Avedano, S.; Aime, S.; Raymond K. N. 1,2-Hydroxypyridonate/Terephthalamide complexes of gadolinium(III): synthesis, stability, relaxivity, and water exchange properties. *Inorg. Chem.* **2009**, *48*, 277-286.

30) Werner, E. J.; Datta, A.; Jocher, C. J.; Raymond, K. N. High-relaxivity MRI contrast agents: where coordination chemistry meets medical imaging. *Angew. Chem. Intl. Ed.* **2008**, *47*, 8568-8580.
31) Hatakeyama, W.; Sanchez, T. J.; Rowe, M. D.; Serkova, N. J.; Liberatore, M. W.; Boyes, S. G. Synthesis of gadolinium nanoscale metal-organic framework with hydrotropes: manipulation of particle size and magnetic resonance imaging capability. *ACS Appl. Mater. Interfaces.* **2011***, 3*, 1502-1510.
32) Klemm, P. J.; Floyd, III, W. C.; Smiles, D. E.; Fréchet, J. M. J.; Raymond, K. N. Improving T1 and T2 magnetic resonance imaging (MRI) contrast agents through the conjugation of an esteramide dendrimer to whigh water coordination Gd(III) hydroxypyridinone (HOPO) complexes. *Contrast Media Mol. Imaging.* **2012**, *7*, 95-99.
33) Chen, B.; van der Poll, D. G.; Jerger, K.; Floyd, III, W. C.; Fréchet, J. M. J.; Szoka, F. C. Synthesis and properties of star-comb polymers and their doxorubicin conjugates. *Bioconjugate Chem.* **2011**, *22*, 617-624.
34) Floyd, III, W. C.; Klemm, P. J.; Smiles, D. E.; Kohngruber, A. C.; Pierre, V. C. Mynar, J. L.; Fréchet, J. M. J.; Raymond, K. N. Conjugation effects of various linkers on Gd(III) MRI contrast agents with dendrimers: optimizing the hydroxypyridinonate (HOPO) ligands with nontoxic, degradable (EA) dendrimers for high relaxivity. *J. Am. Chem. Soc.* **2011**, *133*, 2390-2393.
35) Klemm, P. J.; Floyd, III, W. C.; Andolina, C. M.; Fréchet, J. M. J.; Raymond, K. N. Conjugation to biocompatible dendrimers increases lanthanide T2 relaixivity of hydrosypyridinone (HOPO) complexes for magnetic resonance imaging (MRI). *Eur. J. Inorg. Chem.* **2012**, *2012*, 2108-2114.
36) Love, J. C.; Estroff, L. A.; Kriebel, J. K.; Nuzzo, R. G.; Whitesides, G. M. Self-assembles monolayers of thiolates on metals as a form of nanotechnology. *Chem. Rev.* **2005**, *105,* 1103-1170.
37) Caravan, P. Strategies for increasing the sensitivity of gadolinium based MRI contrast agents, *Chem. Soc. Rev*. **2006**, *35*, 512-523.

Chapter 2- Following the Field, Measuring MRI Complexes in Current Times & Recalibration of Expectations

Abstract

Magnetic resonance imaging (MRI) contrast agents are administered in 45% of clinical scans as a diagnostic aid to differentiate between healthy and pathological tissue. While T_1 imaging currently dominates clinical scans, changes in recent years have lead researchers to look for alternative contrast agents with better relaxivity at higher field strengths, as well as exploring T_2 imaging. Firstly, field strengths in the clinic have been steadily increasing since the advent of diagnostic MRI. While a 10 MHz scanner was the clinical standard when Gd-DTPA was introduced into the market in 1988, field strength has increased to 20 MHz and now many instruments are 60 MHz (with the current FDA limit being 125 MHz.) Most CA decrease in relaxivity with this increase in field strength; however, select CA maintain roughly constant relaxivity, and very few increase. This change in efficacy due to field strength is not understood well enough to predict on a molecule-by-molecule basis, so each molecule must be re-evaluated with each change in field strength. In this chapter, I re-evaluate known compounds at a new field strength (60 MHz) and temperature (many had never been studied at a physiologically relevant 37 °C). I also explore these and novel lanthanide compounds for their viability as T_2 imaging agents, as measured through T_2 relaxivity.

Introduction

MRI signal depends on both the longitudinal ($1/T_1$) and transverse relaxation rates ($1/T_2$) of bulk solvent exchange with the paramagnetic center. T_2 relaxation times see much more influence from outer sphere interactions. Previous research in the Raymond group had exclusively focused on gadolinium and the longitudinal relaxation ($1/T_1$) relaxation rates. Previously studied HOPO moieties bound to Gd(III) varied in terms of cap and chelator arrangement. Using the 1,2-HOPO, (1-Me)-3,2-HOPO, 3,4-HOPO, and terephthalamide chelating moieties (Figure 1), changes in coordination chemistry and geometry have been extensively explored to optimize relaxivity.[1-8]

While these HOPO chelating moieties using TREN, TACN, and mesityl capping moieties had been explored in the Raymond group for CA ability and efficiency, there are limitations on the applicability of that data. The majority of analyses were conducted at 20 MHz, which, while a relevant comparison when the data was taken, is no longer as meaningful given current clinical conditions. As behavior between different field strengths is not well enough understood to predict changes in relaxivity based on changes in field strength, all of these complexes are re-measured and re-evaluated in Chapter 2.

Not only are previous studies less relevant due to the shift in clinical field strength, these studies were also performed at 25 ºC; at this temperature, experimental data is a poor indicator for the future clinical performance.[2] This chapter focuses on reviewing many complexes at the same conditions to elucidate which ones offer clear increases in

relaxivity, as well as full analysis at physiological conditions. Following these experiments, the CA were evaluated for cytotoxicity.

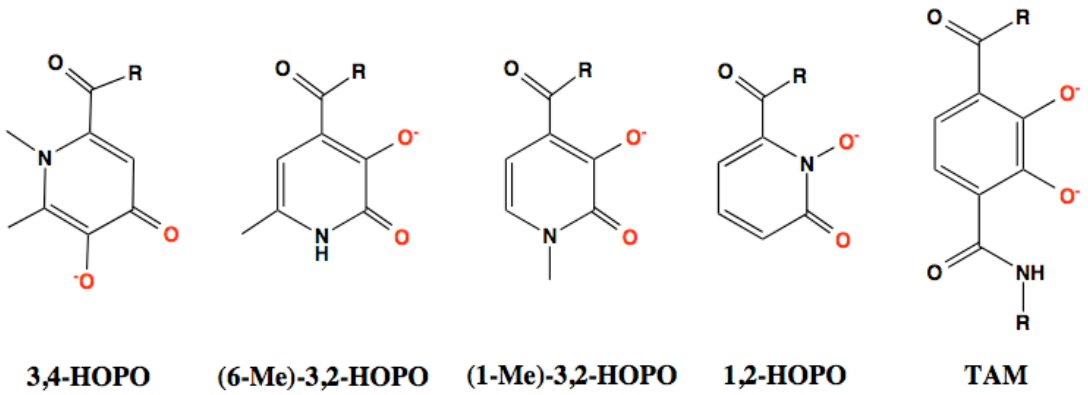

Figure 1. Hydroxypyridinone (HOPO) chelating moieties. Red denotes the oxygen atoms coordinating to the metal center. In these studies, a capping moiety, such as Tris(2-aminoethyl)amine (TREN) is used to form hexadentate ligands, both symmetric and asymmetric.[4-8]

Commercial T_2 contrast agents are iron(III) oxide nanoparticles or iron(III) colloidal suspensions, which are administered orally (as compared to injectable Gd CA). This class of negative mode CA provides an important alternative to Gd(III) for patients with questionable kidney function, and works effectively to image soft tissue with contrast and clarity. However, they are not commercially used in 2012, as fears of toxicity, combined with limited applications, have led to their voluntary reduction from the market. A safe, effective and bioresponsive T_2 CA might yield a large response in the upcoming diagnostic imaging market. Paramagnetic lanthanides, most notably dysprosium(III), have gathered attention recently for their large relaxivities and clinical suitability to become the future of T_2 imaging agents.

A shift in needs for commercial CA has been occurring over the past two decades. While smaller magnets of 10-20 MHz were typical in the early days of MRI, in the last ten years, most clinics in the United States have increased magnets to 60 MHz and to the current FDA limit of 125 MHz. While this is excellent news for patients, as increasing the magnet increases the diagnostic power, it makes the design of CA more difficult. All commercial CA, as well as most CA in the research phase, decrease in efficiency at larger field strengths.[1,3] While there are exceptions of select T_1 agents that do increase in relaxivity with increasing field strength, these are rare and generally have other qualities that will disqualify them for clinical use. T_2 agents are based on the dephasing, which increases at high fields.[3, 10, 11]

In addition to the relaxivity contributions from the inner sphere coordinated water, outer sphere coordination contributes significantly (about 40% of T_1 relaxivity observed) in small molecule monoaqua Gd(III) contrast agents; however, it is difficult to control or modify. This relaxivity is based primarily on the molecule's charge distribution, surface

area, and intermolecular interactions. The outer sphere contribution is strongly effected by random translational diffusion, which is enthalpically favored, as opposed to the inner sphere contribution, which is entropically favored. These are intermolecular interactions, with a different theoretical mechanism. For q = 2 ligands (like some hexadentate HOPO chelators), this effect is somewhat smaller than the inner sphere interactions; however, all paramagnetic activity impacts overall paramagnetic relaxation. Total relaxivity for either T_1 or T_2 is the calculated by adding the inner sphere (IS) and the outer sphere (OS) relaxivity using the equation $r_i = r_i^{IS} + r_i^{OU}$ (i = 1,2).[9-11] Additionally, solvent (water, plasma) molecules can hydrogen bond directly to either the ligand or the Gd(III) ion, contributing to second sphere water coordination. These water exchanges can also account for increases in relaxivity and theoretically behave similarly to the inner sphere.[9] Chapter 2 encompasses all the baseline and comparison data of these small molecule complexes taken at the same biologically and clinically relevant conditions.

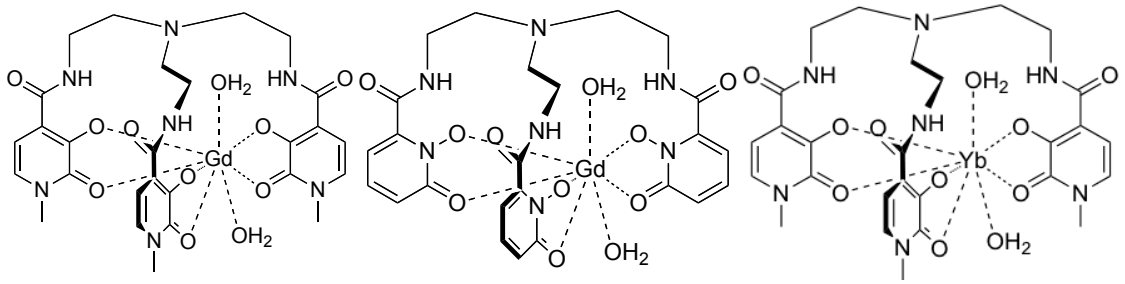

Figure 2. Previously synthesized hexadentate HOPO complexes for T_1 MRI. Left: Gd-TREN-tris(1-Me)-3,2-HOPO, which performs better for longitudinal relaxivity and is more soluble in biological systems. Middle: Gd-TREN-tris-1,2-HOPO. Right: Yb-TREN-tris(1-Me)-3,2-HOPO, synthesized to measure luminescence and q value properties.[12-19]

Experimental Procedure

Synthesis: Many complexes evaluated are previously described synthetically, ligands are from Raymond Group compound storage, presumed to be synthesized by published authors.[12-19]

Tb-TREN-tris(1-Me)-3,2-HOPO: 10.0 mg of TREN-tris(1-Me)-3,2-HOPO (0.0167 mmol, 1 *eq.*) was dissolved in 334 μL of 0.05 M $TbCl_3$ (4.42 mg, 1 *eq.*) in methanol and 1% triethylamine (TEA). This reaction was run for three hours, when it was recrystallized three times in diethyl ether. Excess solvent was removed *in vacuo.* Elemental Analysis: $C_{27}H_{34}N_7O_{11}Tb$ + TEA. Experimental % (Theoretical %). C 45.96 (46.27), H 5.23 (5.29), N 13.18 (13.08). M + H^+ Expected = 756.1423. Actual = 756.1424.

Dy-TREN-tris(1-Me)-3,2-HOPO: 10.0 mg of TREN-tris(1-Me)-3,2-HOPO (0.0167 mmol, 1 *eq.*) was dissolved in 334 μL of 0.05 M $DyCl_3$ (4.48 mg, 1 *eq.*) in methanol and 1% triethylamine (TEA). This reaction was run for three hours, when it was recrystallized three times in diethyl ether. Excess solvent was removed *in vacuo.* Elemental Analysis: $C_{27}H_{34}DyN_7O_{11}$ + TEA + 1.5 H_2O. Experimental % (Theoretical %). C 44.40 (4.67). H 5.28 (5.45). N 13.02 (12.63). M + H^+ Expected = 761.1480. Actual = 761.1477 (ESI-HR).

Gd-tris $(TAM)_3$-$(TREN)_2$: 5.1 mg of tris-TAM-$(TREN)_2$ (6.6 μmol, 1 *eq.*) was dissolved in 2 mL methanol. To this solution was added 130 μL of 0.05 M aqueous $GdCl_3$ (6.6 μmol, 1 *eq.*). The product was dried and recrystallized in methanol-ether and centrifuged. The product was dried to yield 4.2 mg (69%). Ligand+H]$^+$: $C_{46}H_{43}N_8O_{12}$ [M+H$^+$]=779.2969

Dy-tris-$(TAM)_3$-$(TREN)_2$: 4.7 mg of tris-TAM-$(TREN)_2$ (6.0 μm, 1 *eq.*) was dissolved in 2 mL methanol. To this solution was added 12.2 mL of 50 nM $DyCl_3$ in methanol (6.0 μmol, 1 *eq.*). The product was dried and recrystallized in methanol-ether and centrifuged. The product was dried to yield 4.3 mg (77%). $C_{46}H_{43}N_8O_{12}$ [M+H$^+$]=779.2969.

Tb-TREN-bis(1-Me)-3,2-HOPO-TAM-ethanolamine: *m/z* = 830.5 $[M+H]^+$ (FAB-MS). Complex was formed by adding $TbCl_3$ in methanol to TREN-bis(1-Me)-3,2-HOPO-TAM-ethanolamine in a 1:1 ratio. The reaction was run overnight and then was recrystallized three times in ether.

Dy-TREN-bis(1-Me)-3,2-HOPO-TAM-ethanolamine: *m/z* = 834.1 $[M+H]^+$. Complex was formed by adding $DyCl_3$ in methanol to TREN-bis(1-Me)-3,2-HOPO-TAM-ethanolamine in a 1:1 ratio. The reaction was run overnight and then was recrystallized three times in ether.

Yb-TREN-bis(1-Me)-3,2-HOPO-TAM-ethanolamine: *m/z* = 844.6 $[M+H]^+$. Complex was formed by adding $YbCl_3$ in methanol to TREN-bis(1-Me)-3,2-HOPO-TAM-ethanolamine in a 1:1 ratio. The reaction was run overnight and then was recrystallized three times in ether.

Tb-TREN-bis(6-Me)-3,2-HOPO-TAM-TRI: *m/z* = 942.7 $[M-H]^-$. Complex was formed by adding $TbCl_3$ in methanol to TREN-bis(6-Me)-3,2-HOPO-TAM-TRI in a 1:1 ratio. The reaction was run overnight and then was recrystallized three times in ether.

Dy-TREN-bis(6-Me)-3,2-HOPO-TAM-TRI: *m/z* = 945.8 $[M-H]^-$. Complex was formed by adding $DyCl_3$ in methanol to TREN-bis(6-Me)-3,2-HOPO-TAM-TRI in a 1:1 ratio. The reaction was run overnight and then was recrystallized three times in ether.

Yb-TREN-bis(6-Me)-3,2-HOPO-TAM-TRI: *m/z* = 956.8 $[M-H]^-$. Complex was formed by adding $YbCl_3$ in methanol to TREN-bis(6-Me)-3,2-HOPO-TAM-TRI in a 1:1 ratio. The reaction was run overnight and then was recrystallized three times in ether.

Tb-TREN-bis(1-Me)-3,2-HOPO-TAM-dPEG12: *m/z* = 1398.6 $[M+H]^+$. Complex was formed by adding $TbCl_3$ in methanol to TREN-bis(1-Me)-3,2-HOPO-TAM-dPEG12 a 1:1 ratio. The reaction was run overnight and then was recrystallized three times in ether.

Dy-TREN-bis(1-Me)-3,2-HOPO-TAM-dPEG12: *m/z* = 1402.2 $[M+H]^+$. Complex was formed by adding $DyCl_3$ in methanol to TREN-bis(1-Me)-3,2-HOPO-TAM-dPEG12 in a 1:1 ratio. The reaction was run overnight and then was recrystallized three times in ether.

Yb-TREN-bis(1-Me)-3,2-HOPO-TAM-dPEG12: *m/z* =1412.7 $[M+H]^+$. Complex was formed by adding $YbCl_3$ in methanol to TREN-bis(1-Me)-3,2-HOPO-TAM-dPEG12 in a 1:1 ratio. The reaction was run overnight and then was recrystallized three times in ether.

Tb-TREN-bis(6-Me)-3,2-HOPO-TAM-PEG550: *m/z* = 1465.9 $[M+H]^+$. Complex was formed by adding $TbCl_3$ in methanol to TREN-bis(6-Me)-3,2-HOPO-TAM-PEG550 in a 1:1 ratio. The reaction was run overnight and then was recrystallized three times in ether.

Dy-TREN-bis(6-Me)-3,2-HOPO-TAM-PEG550: *m/z* = 1469.5 $[M+H]^+$. Complex was

formed by adding $DyCl_3$ in methanol to TREN-bis(6-Me)-3,2-HOPO-TAM-PEG550 in a 1:1 ratio. The reaction was run overnight and then was recrystallized three times in ether. Yb-TREN-bis(6-Me)-3,2-HOPO-TAM-PEG550: *m/z* = 1480.0 $[M+H]^+$. Complex was formed by adding $YbCl_3$ in methanol to TREN-bis(6-Me)-3,2-HOPO-TAM-PEG550 in a 1:1 ratio. The reaction was run overnight and then was recrystallized three times in ether. Ln-TACN-tris(1,2)HOPO and Ln-TACN-tris(1-Me-3,2)HOPO: To a 0.05 M solution of $LnCl_3*6H_2O$ (1 *eq*.), TACN-trisHOPO was added (15 mg, 1 *eq*.) with one drop 1 M KOH. This solution was stirred for three days when it was evaporated *in vacuo*. The product was washed with methanol and precipitated into 15 mL diethyl ether and centrifuged at 6,000 rpm for 15 minutes. The supernatant was decanted and the precipitation repeated two times. The product was dried *in vacuo* (approximately 10 mg). Chemical Formula: $C_{30}H_{36}DyN_9O_9$ 1,2: Observed Mass: 864.18 (expected 864.18, Neg. Mode). 3,2: Observed Mass 873.08 (expected 873.25, Neg. Mode) Chemical Formula: $C_{33}H_{42}DyN_9O_9$. Nd-TACN-tris(1-Me)-3,2-HOPO Observed Mass: 873.08 (expected 873.25, neg. mode). Tb-TACN-tris(1,2)HOPO and Tb-TACN-tris(1-Me-3,2)HOPO, $C_{30}H_{36}N_9O_9Tb$. Tb-TACN-tris(1,2)HOPO. Observed Mass: 880.17 (expected 880.22, Neg. Mode). Chemical Formula: $C_{33}H_{42}N_9O_9Tb$. Yb-TACN-tris(1,2)HOPO and Yb-TACN-tris(1-Me-3,2)HOPO: MS: Capillary: 2.1 kV; Starting cone 79.0; Extraction Cone: 5.6; Ion Guide: 2.9. 3,2 + 3 NaCl C, 38.49 (38.85); H, 4.89 (4.65); N, 11.54 (11.31); Chemical Formula: $C_{33}H_{42}N_9O_9Yb$.

Relaxivity: Exact Ln(III) concentration was determined by Inductively Coupled Plasma-Optical Emission Spectroscopy (ICP-OES**).** ICP-OES was performed on a Perkin Elmer Optima 7000 DV. Samples for analysis were diluted in 2% (v/v) nitric acid in Millipore water. Gd(III), Dy(III), Tb(III), and Yb(III) standards were prepared in 2% (v/v) nitric acid/Millipore water with concentrations between 0.01 and 10 μg/mL. *Relaxivity Studies:* T_1 and T_2 measurements were performed on a Bruker mq60 minispec relaxometer. T_1 and T_2 were determined at 60 MHz (1.41 T) using an inversion recovery pulse sequence. Temperature controlled at 37 °C using a Julabo F25 circulating water bath. Each sample was analyzed by ICP-OES for exact metal concentration. Relaxivity analyses were performed in triplicate (three samples) and averaged. Samples were vortexed prior to analysis to break up potential aggregation of complexes, 37 °C instrument. For T_1, the inverse of the longitudinal relaxation time of each sample ($1/T_1$, s^{-1}) was plotted against metal concentration (μM) and fit by linear regression ($R^2 > 0.99$). Instrument Parameters: Scans: 4; Recycle Delay: 18.5 s; Gain: 53; Dummy Shots: 0; Detection mode: real; Bandwidth: Broad, 20,000 kHz; Monoexponential Curve Fitting, Phase Cycling. First Pulse Separation: 5 ms; Final Pulse separation: 18,500 ms, Number of data points for fitting: 20; Delay sample window: 0.05 ms; Sampling Window: 0.02 ms; Time for Saturation Curve Display: 6 s. T_2 measurements were performed on a Bruker mq60 minispec relaxometer. T_2 was determined at 60 MHz (1.41 T) using an inversion recovery pulse sequence. Temperature controlled at 37 °C using a Julabo F25 circulating water bath. Relaxivity analyses were performed in triplicate and averaged. Samples were vortexed prior to analysis to break up potential aggregation of complexes. For T_2, the inverse of the longitudinal relaxation time of each sample ($1/T_1$, s^{-1}) was plotted against

metal concentration (μM) and fit by linear regression ($R^2 > 0.99$). Instrument Parameters: Scans: 4; Recycle Delay: 18.5 s; Gain: 53; Dummy Shots: 0; Detection mode: real; Bandwidth: Broad, 20,000 kHz; Monoexponential Curve Fitting, Phase Cycling. Delay sample window: 0.05 ms; Sampling Window: 0.02 ms; Time for Saturation Curve Display: 6 S.Pulse Separation: 1.000 ms. Data Points: 200. Monoexponential Curve Fitting, Phase Cycling.

In vitro cytotoxicity: The cytotoxicity of CA was determined using the MTT assay in HeLa cells. Cells were seeded onto a 96-well plate at a density of 1.0×10^4 cells per well in 100 μL of medium and incubated overnight (37 °C, 5% CO_2, and 80% humidity). An additional 100 μL of new medium (DMEM medium/10% FBS) containing the contrast agents at a concentration of 556 μg/ml to 0.26 μg/ml, was added to the cells. Fresh media (100 μL) or media containing 5% DMSO was used as the positive control. The tests were conducted in triplicate for each concentration. After incubation for 24 h, 40 μL of media containing thiazolyl blue tetrazolium bromide solution (2.5 mg/mL) was added. The cells were incubated for 2 h, after which time the medium was carefully removed. To the resulting purple crystals was added 200 μL of DMSO, followed by 25 μL of pH 10.5 glycine buffer (0.1 M glycine/0.1 M NaCl). The optical densities at 570 nm were measured by using a SpectraMAX 190 microplate reader (Molecular Devices, Sunnyvale, CA). Optical densities measured for wells containing cells that received neither polymer nor drug were considered to represent 100% viability. IC_{50} values were obtained from sigmoidal fits of semilogarithmic plots of the percentage of viability versus metal concentration by using Origin 7 SR4 8.0552 software (OriginLab, Northhampton, MA).

Results and Discussion

TREN-tris-HOPO Ligands:

Novel lanthanide complexes were synthesized and exhibited functional relaxivity trends for T_2 MRI imaging as well as T_1. Relaxivity was calculated by the equation $1/T_2 = 1/T_{2,\ solvent} - r_2[Ln^{3+}]$, to account for the T_2 of the solvent and achieve per-Ln(III) relaxivity. For T_2 relaxivity measured in this study of D_{3H} TREN-trisHOPO complexes, 1,2-HOPO chelators outperformed those of the (1-Me)-3,2-HOPO for all four lanthanides evaluated.

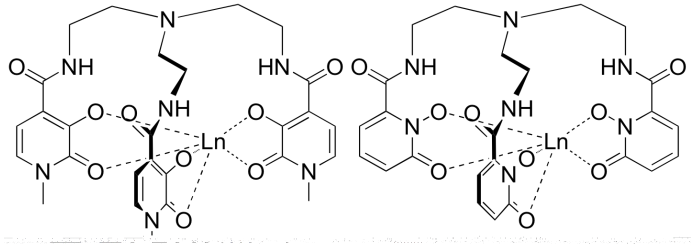

Figure 3. TREN-tris-HOPO ligands. Left is the TREN-tris-(1-Me)-3,2-HOPO and right is the TREN-tris-1,2-HOPO hexadentate chelating ligands for Gd, Yb, Tb, and Dy (synthesized by Dr. Jide Xu). The TREN-tris-(1-Me)-3,2-HOPO was first published by the Raymond Group in 1995[13] and the TREN-tris-1,2-HOPO was published in 2004.[14]

The TREN-tris-1,2-HOPO complexes performed with higher relaxivity for both r_1 and r_2. This is attributed to stability, given that the 1,2-HOPO is more acidic than the (1-Me)-3,2-HOPO.[12-14] Water molecules interacting with both the Gd(III) (inner sphere) and the ligand (outer sphere) are stabilized by hydrogen bonding interactions, which do not destabilize as quickly for the (1-Me)-3,2-HOPO. The rate is increased as the energy to remove a water molecule is lower when the electron density of the metal on the 1,2-HOPO is shifted. such, they have comparatively slower water exchange than the 1,2-HOPO. For both of these hexadentate chelators, with their associative mechanisms of water exchange, q = 2 (coordination number = 8) increasing to q = 3 (coordination number = 9) makes water exchange in both much more rapid than the slow dissociative water exchange for the Gd-DOTA or Gd-DTPA commercial agents. This fast rate of exchange not only improves T_1 and T_2 due to fast inner sphere water exchange, but also provides a more optimal outer sphere and second sphere solvent interactions and rapid bulk solvent exchange. The outer sphere interactions have less effect on T_1; however, they become much more important for T_2. This is caused by the magnetic field fluctuating due to the random motion of molecules. The spin-lattice relaxivity (T_1) is based on stability of the complex, and given that the (1-Me)-3,2-HOPO is more stable, it gets back to equilibrium faster. The TREN-tris-1,2-HOPO complexes have more electron delocalization within the aromatic ring structure, which prefers outer and second sphere interaction,[17] compared to the higher pKa's of the (1-Me)-3,2-HOPO, which prefer inner sphere solvent interaction.

According to the Solomon-Bloembergen-Morgan equations, a small increase in the interatomic distance between proton and metal center causes a reduction in relaxation effects; however, this change can increase relaxivity if it dramatically improves the inner sphere or outer sphere interactions, increasing the T_2 relaxivity of the (1,2)-HOPO far more than that of the (1-Me)-3,2-HOPO.

Among the lanthanides, Gd(III) showed superior performance for T_2 relaxivity, as is expected with seven unpaired electrons. The order of the lanthanides T_2 relaxivity follows paramagnetism. As the number of unpaired electrons decreases, the T_2 relaxivity decreases (Gd > Tb, Dy > Yb. However, these relaxivity values are only a portion of the requirements of a T_2 contrast agent. Given that T_1 is positive mode MRI imaging, to obtain a usable signal in negative mode T_2 imaging, a sufficient increase of T_2 as compared to T_1 is required. This parameter, expressed as the r_2/r_1 ratio, excludes Gd(III) from being a successful T_2 MRI contrast agent. Given its low paramagnetic character, Yb(III) has low T_1 relaxivities, but has sufficient inner and outer sphere bulk solvent to achieve a sufficient T_2 contrast ratio. Compared to the 6.6 r_2/r_1 ratio of Ferridex, a commercial iron oxide nanoparticle MRI contrast agent,[3] only Yb and Tb show sufficient distinction between T_1 and T_2 relaxivity values. Although Dy(III) is the focus of much research toward a lanthanide T_2 contrast agent, its higher T_1 values will likely invalidate it, like Gd(III), to show the required difference in positive and negative mode imaging.

Table 1. Comparison of T_1 relaxivities with different coordinating ligands at 37 °C, pH 7.2-7.5, 1.5 T (60 MHz). Gd-DOTA has a T_1 relaxivity of 3.0 ± 0.3 $mM^{-1}s^{-1}$ under identical conditions.[2] Gd-TREN-tris-1,2-HOPO was previously measured to be 9.5 $mM^{-1}s^{-1}$ at 25 °C and 20 MHz and Gd-TREN-tris(1-Me)-3,2-HOPO was previously measured to be 8.5 $mM^{-1}s^{-1}$at 37 °C and 20 MHz.

Complex	TREN-tris1,2-HOPO r_1 ($mM^{-1}s^{-1}$)	r_2/r_1	TREN-tris(1-Me)-3,2-HOPO r_2 ($mM^{-1}s^{-1}$)	r_2/r_1
Gd(III)	8.9(1)	1.60	8.03(2)	1.49
Yb(III)	0.22(3)	15.91	0.09(2)	4.11
Tb(III)	1.04(9)	5.48	0.11(3)	5.82
Dy(III)	2.15(2)	1.81	1.42(6)	1.83

Cytotoxicity: Complexes were evaluated for cytotoxicity and suitability for MRI contrast agents (Table 3). Solubility at these concentrations was sufficient in buffer and media. No complex in this study exhibited cytotoxicity up to 1.0 mg/mL in HeLa cells over 72 h (all greater than 97% viability). Small molecule contrast agents should be fully excreted from patients within 24 h, however, with the recent emergence of Nephrogenic Systemic Fibrosis (NSF) in patients with renal failure, more rigorous and longer toxicity studies are required for future contrast CA.

Table 2. Cytotoxicity against HeLa cells with 1.0 mg/mL complex over 72 h.

Ln^{3+}	TREN-1,2-HOPO Viability (%)	TREN-(1-Me)-3,2-HOPO Viability (%)
Gd^{3+}	98.2(4)	98.1(2)
Yb^{3+}	97.8(4)	98.1(3)
Tb^{3+}	97.1(3)	97.9(1)
Dy^{3+}	97.7(3)	97.2(3)
Gd-DTPA control	[98.3(2)]	

TREN-3,2-HOPO-TAM Mixed Ligands:

TREN-3,2-HOPO mixed ligand complexes were synthesized and evaluated in this study for T_1 relaxivity, T_2 relaxivity, and cytotoxicity (Figure 4). At 37 °C and 60 MHz, some of the Gd(III) species have markedly shifted relaxivities, indicating changes in q values. The PEG chains and ethanolamine have the ability to double back and coordinate to the Gd(III), using up an inner coordination water site. If this should happen, the decline in q value directly correlates with a decline in relaxivity. Of these compounds, this

phenomenon has previously been noted at 25 °C and 20 MHz in the TRI, dPEG 12, and PEG550 functionalizing and solubilizing moieties.

At physiological and clinical conditions, this loss of relaxivity was only observed in the dPEG12 functionality. The other five Gd(III) complexes had high per Gd(III) relaxivities (9-14 $mM^{-1}s^{-1}$), among the largest observed for thermodynamically stable small molecule MRI contrast agents. As the field strength increased, these complexes show increased relaxivity, thus benefitting from the clinic moving toward 60 and 100 MHz MRI instruments. The opposite is true of commercial contrast agents, which have an inverse relationship with field strength. Additionally, at higher temperatures, the water exchange becomes more rapid, which is often hampered by a faster molecular tumbling time. In these complexes, the molecular weight of the dendritic and PEG chains aid in slowing the tumbling time to increase relaxivity. As expected, the dendritic Gd-TREN-bis(1-Me)-3,2-HOPO-TAM-Asp-Asp_2-12OH has the highest T_1 relaxivity, as it is the most rigid molecule, which limits the local motion of the Gd(III) atom.

For T_2 relaxivity, Yb-TREN-bis(1-Me)-3,2-HOPO-TAM-ethanolamine has the largest r_2/r_1 of 8.62. In comparison, the commercial iron oxide contrast agents Ferodoxen-10 has a ratio of 6.6.[3] Although the Gd(III) complexes, high r_2 values, the equally high r_1 values indicate that the T_1 signal would dominate *in vivo*, which disqualifies them as T_2 agents. The lower T_2 value for PEG12 (6.03) versus PEG4 (10.9) further confirms that a water coordination site is being occupied by the PEG chain. Given its higher molecular weight and more surface area where outer sphere water exchange is occurring, the PEG12 should certainly be higher than the PEG4, unless it was losing an inner sphere water coordination site (q), which would also cause it to lose surface area. Other lanthanides performed with low T_1 values, which was expected for their fewer unpaired electrons. Their T_2 values, although not yet sufficient in most cases for the clinic, demonstrated the possibilities of modifying a small molecule lanthanide system for T_2 imaging, which would not only have fast renal clearance and avoid the use of Gd(III), but may also have different distribution patterns than particle based T_2 agents.

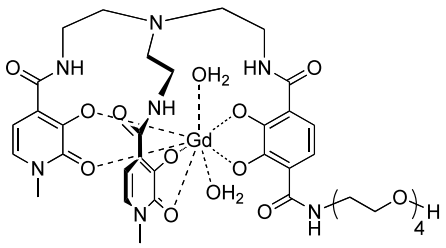

1: Gd-TREN-bis(1-Me)-3,2-HOPO-TAM-dPEG4

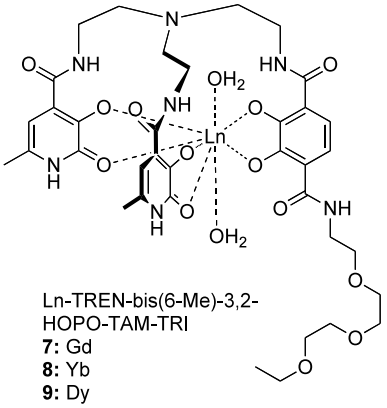

Ln-TREN-bis(6-Me)-3,2-HOPO-TAM-TRI
7: Gd
8: Yb
9: Dy
10: Tb

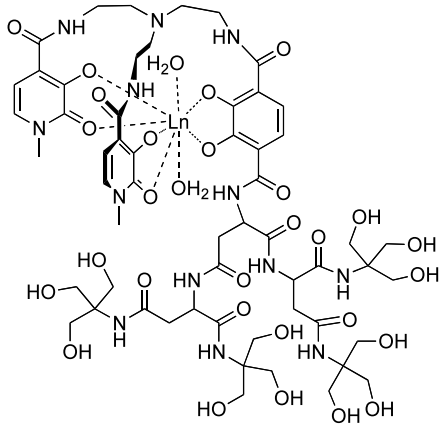

2: Gd-TREN-bis(1-Me)-3,2-HOPO-TAM-Asp-Asp2-12OH

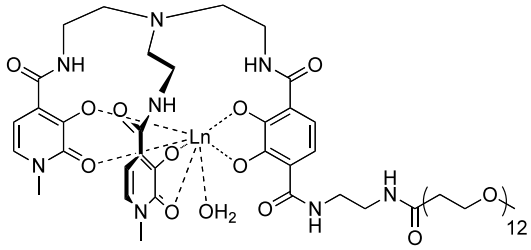

Ln-TREN-bis(1-Me)-3,2-HOPO-TAM-dPEG12
11: Gd
12: Yb
13: Dy
14: Tb

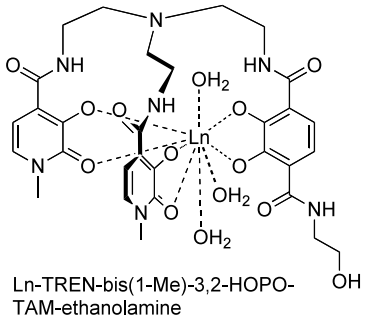

Ln-TREN-bis(1-Me)-3,2-HOPO-TAM-ethanolamine
3: Gd
4: Yb
5: Dy
6: Tb

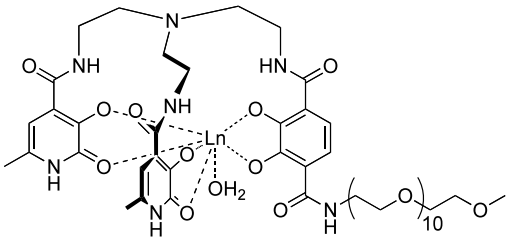

Ln-TREN-bis-6-Me-3,2-HOPO-TAM-PEG550
15: Gd
16: Yb
17: Dy
18: Tb

Figure 4. TREN-HOPO-TAM mixed ligands evaluated for their r_1, r_2, and cytotoxicity.

Table 3. T_1 and T_2 relaxivities for complexes at clinically relevant conditions for TREN complexes.

Ligand	Ln^{3+}	r_1	r_2	r_2/r_1
DTPA[2]	Gd	3.3(3)	3.9(3)	1.18
DOTA[2]	Gd	3.0(3)	3.5(3)	1.17
TREN-dPEG4	Gd	10.9(1)	16.9(3)	1.55
TREN-Asp	Gd	14.1(2)	18.4(3)	1.31
TREN-bisCAM-1,2-HOPO	Gd	8.9(9)	12.7(2)	1.42
TREN-bis(1-3,2-HOPO-Ethanolamine	Gd	9.2(3)	11.1(2)	1.21
	Yb	0.23(1)	2.0(1)	8.62
	Dy	0.88(1)	2.44(1)	2.77
	Tb	0.58(1)	0.99(1)	1.70
TREN-bis-(6-Me-3,2-HOPO-TAM-TRI	Gd	9.33(4)	10.9(2)	1.17
	Yb	0.13(1)	0.29(2)	2.13
	Dy	0.84(1)	1.60(2)	1.91
	Tb	0.52(1)	0.96(2)	1.87
TREN-bis-(1-3,2-HOPO-PEG12	Gd	6.03(7)	13.37(1)	2.21
	Yb	1.00(1)	1.58(1)	1.63
	Dy	1.23(1)	1.81(1)	1.47
	Tb	1.33(1)	1.58(1)	1.19
TREN-bis-(6-3,2-HOPO-PEG-550	Gd	9.09(4)	13.3(7)	1.46
	Yb	0.41(1)	0.71(1)	1.71
	Dy	1.05(1)_	1.43(5)	1.37
	Tb	1.31(1)	2.62(4)	2.00

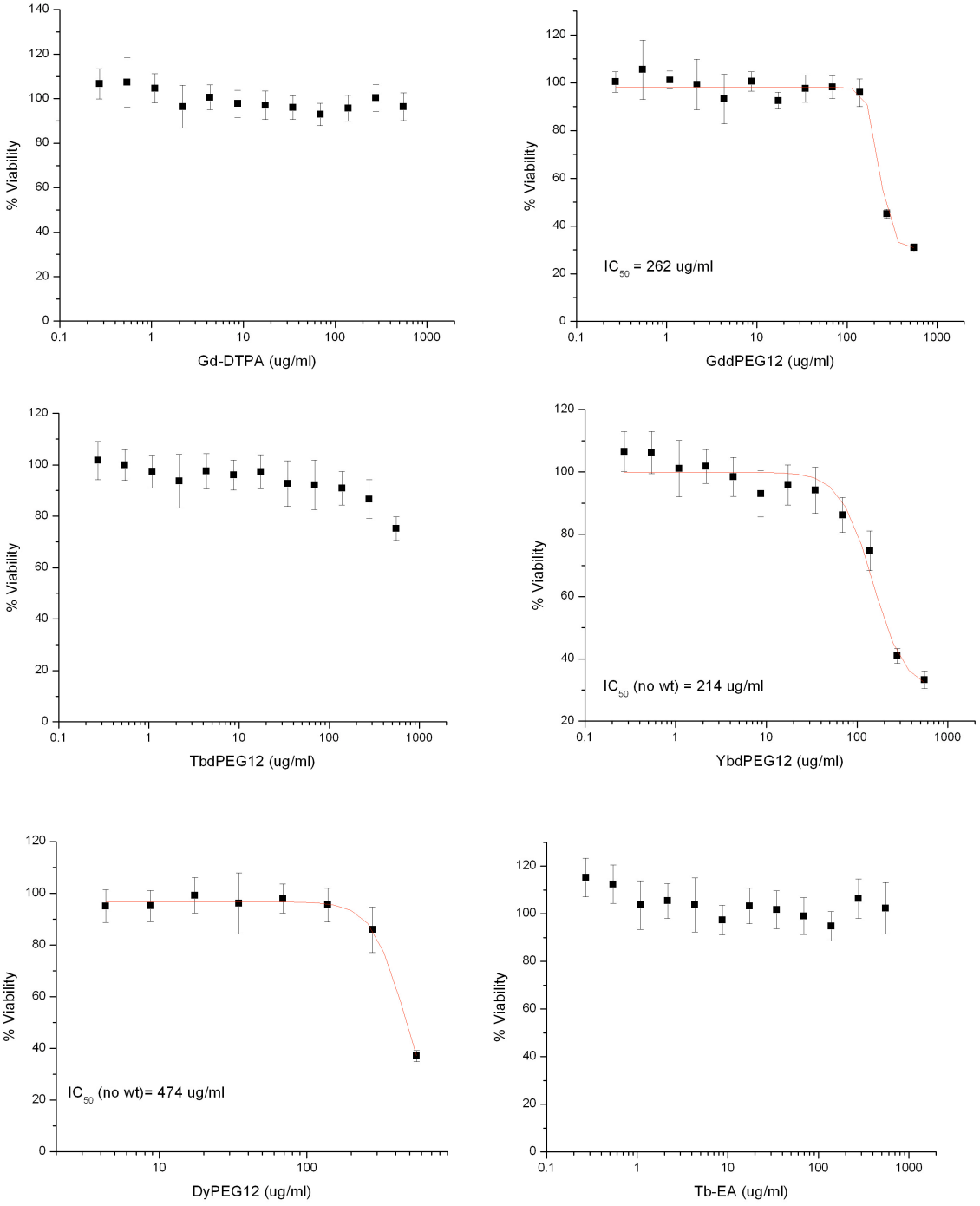

Figure 5. Representative cytotoxicity of several lanthanide TREN-HOPO-TAM mixed complexes against HeLa cells.

TREN-Modified Cap Ligands:

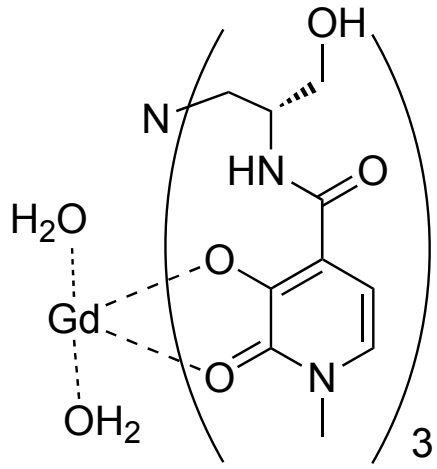

Figure 6. A modified TREN cap Gd(III) complex for use as an MRI contrast agent. The synthesis was originally published in 2000 by the Raymond Group.[19]

As the 1,2-HOPO chelator had a higher relaxivity than the (1-Me)-3,2-HOPO chelator, the TREN-capped HOPO modified with a serine (Ser) moiety was explored further. The Gd-Ser-TREN-tris-HOPO was previously described to have high relaxivity at physiologically irrelevant conditions[13,16] and field strengths far below the modern standard of the field. An NMRD profile was constructed; however, at 25 °C, this profile was not definitive as trends shift from a change to physiological temperatures. Using modern clinical conditions, the Gd(III) complex of these ligands followed the same trends as the TREN-tris-HOPO parent compounds. A higher relaxivity was seen for these daughter compounds, which is consistent theory: the alcohol functional moiety adds to outer sphere hydrogen bonding and bulk solvent exchange interactions, resulting in more paramagnetic character of the bulk solvent and higher relaxivity. Additionally, these compounds have slightly higher molecular weight than their parent compounds, slowing molecular tumbling time and increasing possible solvent exchange interactions and increasing the relaxivity.

The Ser-TREN-tris-HOPO complexes were also compared to previous data at 20 MHz and 25 °C. Due to faster tumbling times, relaxivity decreases from 25 °C to 37 °C. Although water exchange rates increase, their overall effect on relaxivity pales in comparison to that of tumbling times and every system studied from commercial agents to current research stage complexes shows lower relaxivity as the temperature increases. The effect of field strength, however, impacts every compound differently. While the current commercial agents suffer from the clinical increase in field strength and all lose relaxivity from 20 MHz to 60 MHz to 100 MHz, complexes in the Raymond group have been shown to increase relaxivity in a direct relationship with field strength at 25 °C in data from NMRD profiles. Field strength impacts the Ser-TREN-tris(1,2)-HOPO positively (Table 4), as it loses almost no relaxivity as it is negatively impacted by temperature and positively impacted by field strength. However, the Ser-TREN-tris(1-Me)-3,2-HOPO loses a quarter of its relaxivity, as it is negatively impacted by temperature as well as field strength. Between these ligands, the 1,2-HOPO complex is more consistent with the current and future directions of the clinic.

Table 4. Comparison of modified SerTREN capped 1,2 and 3,2 HOPO Gd(III) complexes.

Conditions	Ser-TREN-tris1,2-HOPO r_1 ($mM^{-1}s^{-1}$)	Ser-TREN-tris1,2-HOPO r_2 ($mM^{-1}s^{-1}$) (r_2/r_1)	Ser-TREN-tris(1-Me)-3,2-HOPO r_1 ($mM^{-1}s^{-1}$)	Ser-TREN-tris(1-Me)-3,2-HOPO r_2 ($mM^{-1}s^{-1}$) (r_2/r_1)
20 MHz, 25 °C	10.5(0.1)[12]	--	9.0(0.1)[16]	--
60 MHz, 37 °C	10.44(0.1)	13.6(5) (1.30)	6.84(6)	9.3(5) (1.36)

TACN-tris-HOPO Ligands:

A paramagnetic series of Ln(III) with the TACN-tris-1,2-HOPO and TACN-tris-(1-Me)-3,2-HOPO have been synthesized. The NMRD profile of Gd-TACN-HOPO indicated that its relaxivity increases with increasing field strength, so relaxivity is expected to either be maintained or higher, a positive attribute that separates these molecules from commercial agents. Structures of these complexes are seen in the following figure and cytotoxicity of these complexes is seen in the following table.

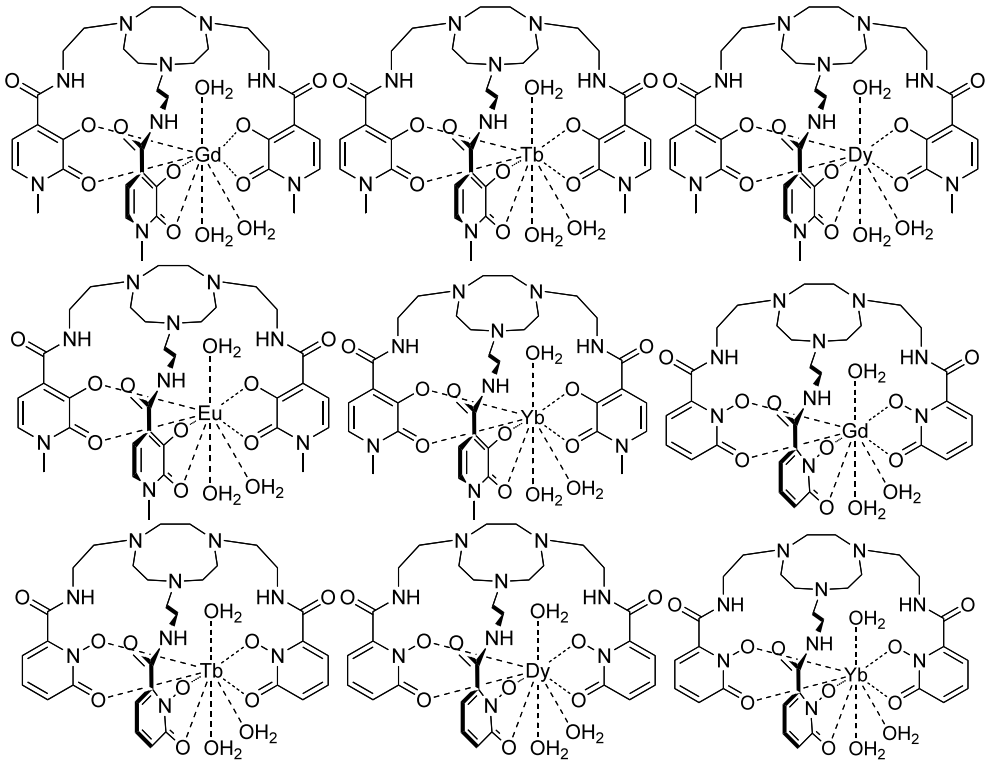

Figure 7. TACN-capped HOPO MRI Contrast agents. The Gd(III) complexes were published by the Raymond Group in 2007.[5]

Table 5. Relaxivities of TACN-capped HOPO CA at 60 MHz and 37 ºC.

Metal	1,2 HOPO r_1	1,2 HOPO r_2	1-Me-(3,2)-HOPO r_1	1-Me-(3,2)-HOPO r_2
Gd	7.7(4)	11.0(1)	7.9(4)	8.5(1)
Dy	0.21(3)	1.5(1)	0.21(4)	0.63(3)
Tb	0.14(2)	0.61(2)	0.39(7)	2.0(3)
Yb	0.08(2)	0.51(2)	0.39(4)	1.74(9)

Table 6. Cytotoxicity data by MTT assay over 72 h of TACN-capped complexes.

Complex (0.5 mg/mL, unless otherwise noted)	% Viability (72 h)
Gd-DTPA (Commercial MRI Contrast Agent) Control	99.6 ± 0.1
Gd-TACN-tris(1-Me-3,2)HOPO	100.0(1)
Gd-TACN-tris(1-Me-3,2)HOPO + $CuCl_2$	99.5(2)
Gd-TACN-tris(1-Me-3,2)HOPO + $ZnCl_2$	99.6(1)
Gd-TACN-tris(1,2)HOPO	100.0(4)
Gd-TACN-tris(1,2)HOPO + $ZnCl_2$	99.6(9)
Gd-TACN-tris(1,2)HOPO + $CuCl_2$	99.7(2)
Nd-TACN-tris(1,2)HOPO	99.7(2)
Sm-TACN-tris(1,2)HOPO	99.6(3)
Eu-TACN-tris(1,2)HOPO	99.4(2)
Dy-TACN-tris(1,2)HOPO	99.7(1)
Yb-TACN-tris(1,2)HOPO	99.5(2)
Dy-TACN-tris(1-Me-3,2)HOPO	99.6(2)
Yb-TACN-tris(1-Me-3,2)HOPO	99.6(2)

TACN-3,2-HOPO-TAM Mixed Ligands:

Previously synthesized TACN-capped HOPO ligands lacked a synthetic handle to which a dendritic macromolecule could be attached.[5] A TACN capped complex was synthesized with two (1-Me)-3,2-HOPO ligands and a functionalized terephthalamide (TAM) ligand, for a hexadentate all-oxygen donor Gd(III) complex. Since the amine functionalized complex differed significantly than the tris-(1-Me)-3,2-HOPO ligands previously described,[5] an analogue of this with an ethyl functionality, Gd-TACN-bis(1-Me)-3,2-HOPO-TAM-ethyl, was synthesized for relaxivity and cytotoxicity comparison to the novel complex and conjugated macromolecule. Relaxivity measurements are also included below.

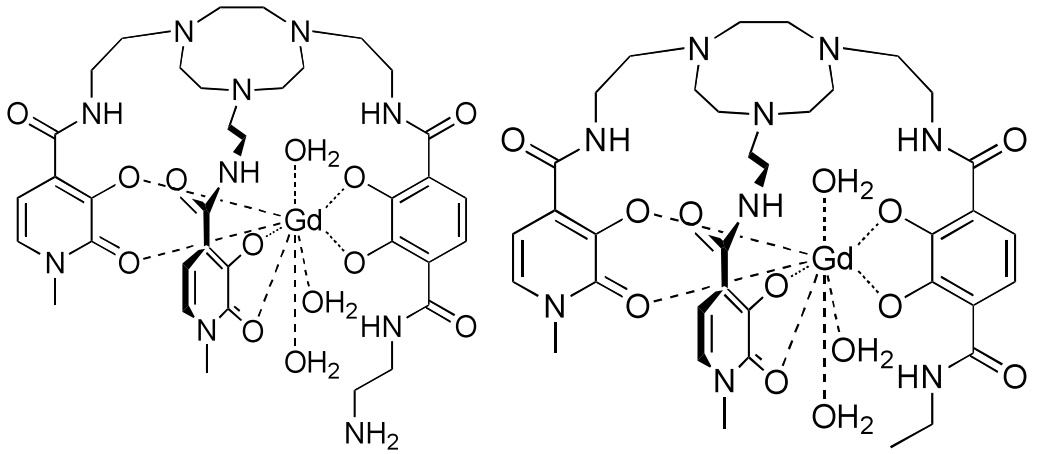

Figure 8. TACN capped complexes to increase T_1 and T_2 relaxivity based on Gd-TACN-tris-HOPO having a q = 3.[5] Gd-TACN-*bis*-(1-Me)-3,2-HOPO-TAM-ethylamine (left) and Gd-TACN-*bis*-(1-Me)-3,2-HOPO-TAM-ethyl (right, synthesized by Danil E. Smiles) was used as a small molecule analogue to compare relaxivity and cytotoxicity.

Table 7. Relaxivities of TACN-3,2-HOPO-TAM Mixed Ligands at 60 MHz and 37 ºC.

Complex	r_1 Complex ($mM^{-1}s^{-1}$)	r_2 Complex ($mM^{-1}s^{-1}$)
Mn-DPDP (Teslascan™)	1.88*at 20 MHz	2.18 *at 20 MHz
Gd-TACN-*bis*-(1-Me)-3,2-HOPO-TAM-ethylamine	9.89(3)	16.0(5)
Gd-TACN-*bis*-(1-Me)-3,2-HOPO-TAM-ethyl	7.27(9)	11.2(2)

Table 8. Cytotoxicity of TACN-3,2-HOPO-TAM Mixed Ligands.

Complex	% Viability (72 h)
Esteramide Control	99.4(4)
Gd-DTPA (Commercial MRI Contrast Agent) Control	99.6(1)
Gd-TACN-bis(1-Me)-3,2-HOPO-TAM-ethyl	99.5(2)
Gd-TACN-bis(1-Me)-3,2-HOPO-TAM-ethyl + $ZnCl_2$	99.5(1)
Gd-TACN-bis(1-Me)-3,2-HOPO-TAM-ethyl + $CuCl_2$	99.4(1)

Mesityl-Capped Ligands:

Previously synthesized mesityl-capped HOPO ligands had high q values of 2-3, but lacked the solubility (<100 μM in water) required for clinical use.[20] Gd-Mes-bis(1-Me)-3,2-HOPO-TAM-ethylamine and Gd-Mes-bis(1-Me)-3,2-HOPO-TAM-ethylamine-bis-ethylamine were re-evaluated for clinically relevant conditions.

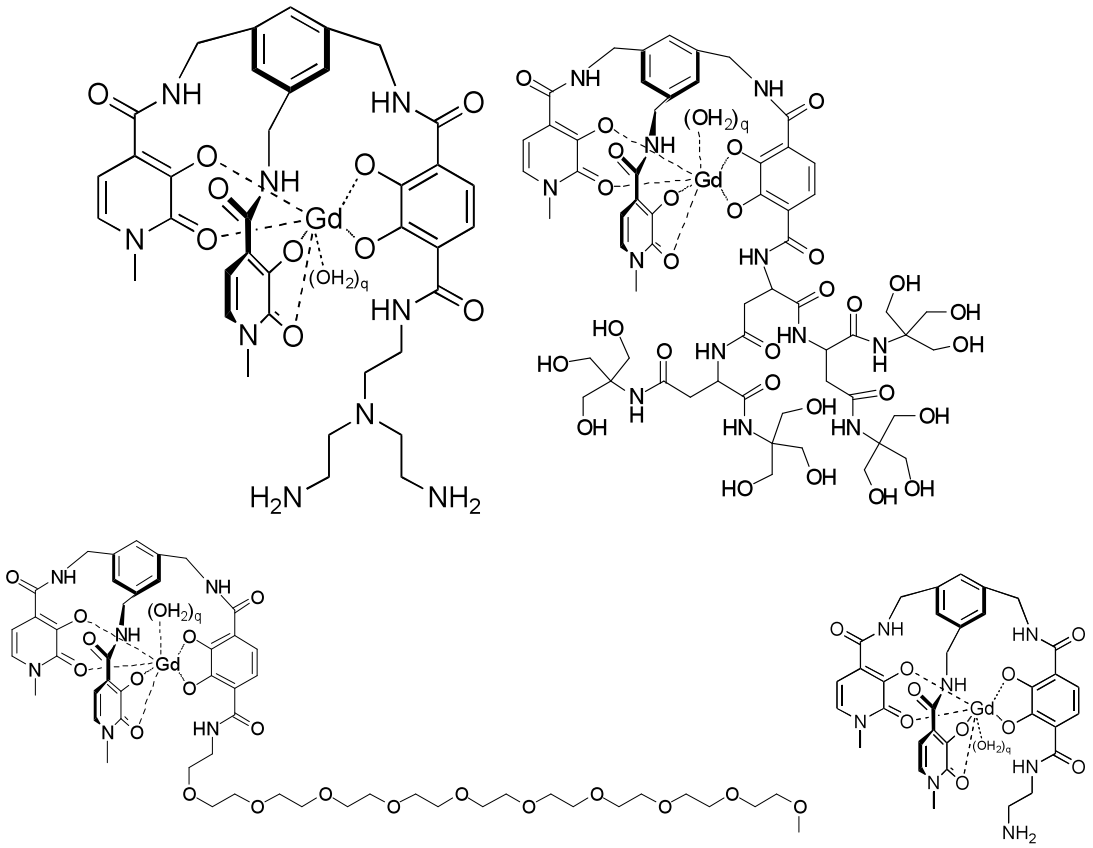

Figure 9. Mesityl capped- Gd-HOPO complexes synthesized to capitalize on a high *q* value. Gd-Mes-bis(1-Me)-3,2-HOPO-TAM-ethylamine-bisethylamine (top right), Gd-Mes-bis(1-Me)-3,2-HOPO-TAM-Asp-Asp$_2$-12OH (top right), Gd-Mes-bis(1-Me)-3,2-HOPO-TAMPEG450 (bottom left) and Gd-Mes-bis(1-Me)-3,2-HOPO-TAM-ethylamine (bottom right). However, these amines were not suitable for MRI contrast agents due to their low solubility (<10 μM in water) and subsequent aggregation.[20] The branched and PEG chains were appended to increase solubility and biocompatibility of the CA. Although solubility of these complexes was increased significantly (> 1 mM) over their small molecule counterparts, the large doses required for MRI imaging would still exclude these complexes due to solubility.

The mesityl-capped HOPO complexes display the resulting relaxivity changes as the molecular weight and the shape of molecules are modified. The Gd-Mesityl-PEG450 complex has a similar molecular weight to that of the branched dendrimer Gd-Mes-Asp-Asp$_2$-12OH. However, despite their chelation and structural similarities, both their T_1 and T_2 relaxivities vary significantly from one another. While the more dendritic branched mesityl (Asp-Asp$_2$-12OH) had a larger T_1 relaxivity than the small molecule, the mesityl with a PEG450 chain obtained a much larger increase in its T_2 relaxivity, and therefore exhibits a much larger r_2/r_1 relaxivity ratio. This was attributed to the much larger surface area of the PEG450 molecule as compared to the ASP-ASP$_2$-12OH molecule. The larger surface area allowed for many more outer sphere solvent interactions, significantly

increasing the r_2 relaxivity. The branched dendrimer slows the tumbling of the gadolinium complex through its high molecular weight and steric restrictions, but coordinates fewer outer sphere water molecules due to its much lower hydrodynamic volume, leading to a larger increase in T_1 relaxivity than T_2.

Table 9. Mesityl-capped Gd(III) complex relaxivities at 60 MHz and 37 °C.

Complex	r_1 ($mM^{-1}s^{-1}$)	r_2 ($mM^{-1}s^{-1}$)
Gd-Mes-bis(1-Me)-3,2-HOPO-TAM-ethylamine	9.3(2)	16.0(2)
Gd-Mes-bis(1-Me)-3,2-HOPO-TAM-ethylamine-bisethylamine	7.2(2)	12.6(4)
Gd-Mes-bis(1-Me)-3,2-HOPO-TAM- Asp- Asp_2-12OH	14.8(4)	17.4(1)
Gd-Mes-bis(1-Me)-3,2-HOPO-TAM-PEG450	12.01(5)	21.3(3)

TAM Bicapped Ligands:

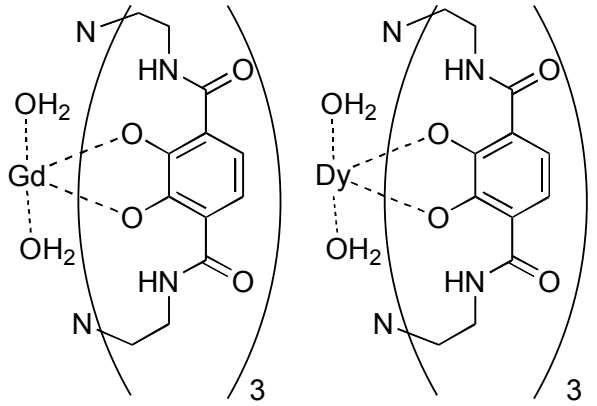

Figure 10. Bicapped TAM complexes, Gd(III), right and Dy(III), right.

The observed r_1 at 37 °C and 60 MHz for Gd-BCTRTAM was 9.9 $mM^{-1}s^{-1}$, which is consistent with previous q = 2 complexes. The r_2 of 11.2 $mM^{-1}s^{-1}$ for the Gd(III) complex is a high value compared to those of Gd-DOTA and Gd-DTPA. The ratio r_2/r_1 is comparable to the T_2 agent Fe-EFPG indicating that it would be competitive for soft tissue imaging.

Although the Dy(III) complex has low r_1 and r_2 values compared to Gd(III), it has shown promise as a cerebral perfusion imaging agent due to its capacity to transiently influence lingering magnetic susceptibility of tissue as it travels through the body.

Table 10. Relaxivities of Bicapped TAM complexes at 37 °C and 60 MHz.

Complex	r_1 ($mM^{-1}s^{-1}$)	r_2 ($mM^{-1}s^{-1}$) [r_2/r_1]
Gd-BCTRTAM	9.9(2)	11.2(4) [1.1]
Dy-BCTRTAM	0.72(2)	3.94(6) [5.5]
Fe-EHPG (*10.7 MHz)[3]	0.9	1.2[1.3]

These two new macrocycles were evaluated for toxicity by MTT assay over one week. No cytotoxicity was visible up to 1.0 mg/mL in HeLa cells over one week.

Table 11. Cytotoxicity by MTT assay.

Complex	% Viabiltiy
Gd-TREN-bicapped-TAM	98.3(4)
Dy-TREN-bicapped-TAM	98.2(5)
Gd-DTPA (Magnevist^{TM})	98.3(2)

Pyridine Macrocycle & DPA:

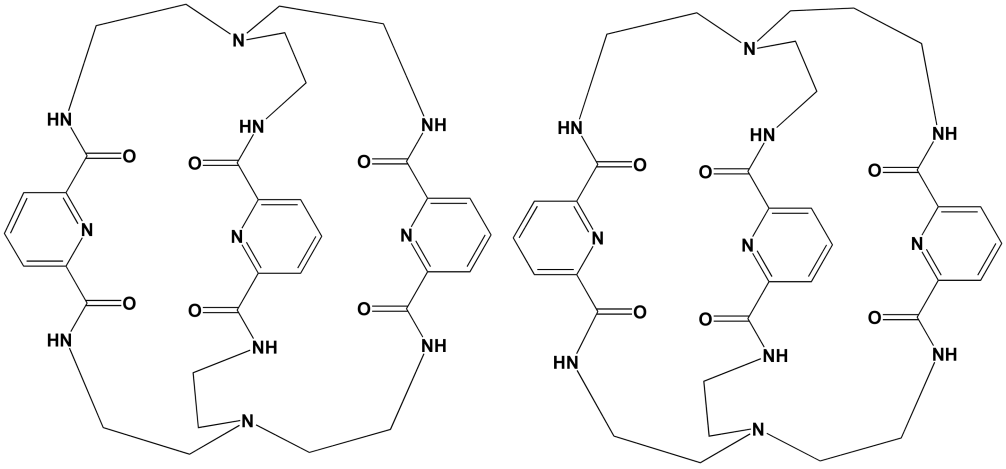

Figure 11. Pyridine macrocycle symmetric (left) and asymmetric (right). Synthesized by Dr. Jide Xu as a lanthanide luminescence agent, the pyridine macrocycle allows us to explore the relaxivity of $q = 0$ complexes.

Table 12. Relaxivities of the symmetric and asymmetric pyridine macrocycle compounds, as well as DPA $q = 0$ complexes for comparison.

Complex	*PYR, PYR* (asymmetric), (DPA*)* r_1	*PYR, PYR* (asymmetric), (DPA*)* r_2
Gd	4.8(2), 6.2(2), 1.36(3)	8.7(3), 9.7(1), 2.2(1)
Yb	(0.01)	(0.09)
Tb	0.18(1), 0.03, (0.05)	4.54(1), 3.0(1), (0.06)
Dy	(0.01)	(0.01)
Eu	0, (0)	0, (0)

Octadentate Ligands:

Table 13. Relaxivities of octadentate complexes.

Complex	r_1	r_2	r_2/r_1
Gd-H5O2-3,2-HOPO	7.4	11.9(1)	1.6
Yb-H22-3,2-HOPO	0.15	2.27	14.9
Yb-H22-1,2-HOPO	0.89	8.8(6)	9.9
Yb-H5O2-3,2-HOPO	0.2	1.44 (6)	8.4
Yb-H5O2-1,2-HOPO	0.3	6.4(2)	22
Yb-H42-1,2-HOPO	0.06	1.22(3)	19
Yb-H8O22-1,2-HOPO	0.06	7.9(5)	125
Yb-H22-TAM	0.04	1.95	47
Yb-H22-IAM	1.14	7.10(7)	6.2

Conclusions

During these studies, it is evident that the 1,2-HOPO complexes merit further evaluation, due to their T_1 and T_2 relaxivities. For a successful T_2 MRI contrast agent, Yb(III)-tris(1,2)-HOPO shows the most positive combination of results- a large T_2 value for a small molecule complex, a small T_1 for this complex and a ratio r_2/r_1 of sufficient magnitude for successful T_2 negative imaging. Additionally, due to the nonionic nature of this complex, it is suitable for injection (no osmolatic shock) and has the potential to cross the blood brain barrier for intercranial T_2 imaging.

References

1) Caravan, P. Strategies for increasing the sensitivity of gadolinium based MRI contrast agents, *Chem. Soc. Rev*. **2006**, *35*, 512-523.

2) Port, M.; Idee, J. M.; Medina, C.; Robic, C.; Sabatou, M.; Corot, C. Efficiency, thermodynamic and kinetic stability of marketed gadolinium chelates and their possible consequences: a critical review. *Biometals*. **2008**, *21*, 469-490.

3) Laurent, S.; Forge, D.; Port, M.; Roch, A.; Robic, C.; Elst, L. V.; Muller, R. N. Magnetic iron oxide nanoparticles: synthesis, stabilization, vectorization, physicochemical characterizations, and biological applications. *Chem Rev.* **2008**, *108*, 2064–2110.

4) Bulte, J. W. M.; Wu, C. C.; Brechbiel, M. W.; Brooks, R. A.; Vymazal, J.; Holla, M.; Frank, J. A. Dysprosium-DOTA-PAMAM dendrimers as macromolecular T2 contrast agents- preparation and relaxometry. *Invest. Radiol.* **1998**, *33*, 841-845.

5) Werner, E. J.; Avedano, S.; Botta, M.; Hay, B. P.; Moore, E. G.; Aime, S.; Raymond, K. N. Highly soluble tris-hydroxypyridonate Gd(III) complexes with increased hydration number, fast water exchange, slow electronic relaxation, and high relaxivity. *J. Am. Chem. Soc*. **2007**, *129*, 1870-1871.

6) Pierre, V. C.; Botta, M.; Aime, S.; Raymond, K. N. Substituent effects on Gd(III)-based MRI contrast agents : optmizing the stability and selectivity of the complex and the

number of coordinated water molecules. *Inorg. Chem.* **2006**, *45*, 8355-8364.
7) Datta, A.; Raymond, K. N. Gd-Hydroxypyridinone (HOPO)-based high-relaxivity magnetic resonance imaging (MRI) contrast agents. *Acc. Chem. Res.* **2009,** *42,* 938–9474.
8) Raymond K. N.; Pierre, V. C. Next generation, high relaxivity gadolinium MRI agents. *Bioconjugate Chem.* **2005**, *16*, 3-8.
9) Botta, M. Second coordination sphere water molecules and relaxivity of gadolinium(III) complexes: implications for MRI contrast agents. *Eur. J. Inorg. Chem*. **2000,** *3,* 399-407.
10) Caravan, P. Strategies for increasing the sensitivity of gadolinium based MRI contrast agents, *Chem. Soc. Rev*. **2006**, *35*, 512-523.
11) Major, J. L.; Meade, T. J. Bioresponsive, cell-penetrating, and multimeric MR contrast agents. *Acc. Chem. Res.* **2009,** *42,* 893-903.
12) Werner, E. J.; Kozhukh, J.; Botta, M; Moore, E. G.; Avedano, S.; Aime, S.; Raymond K. N. 1,2-Hydroxypyridonate/Terephthalamide complexes of gadolinium(III): synthesis, stability, relaxivity, and water exchange properties. *Inorg. Chem.* **2009**, *48*, 277-286.
13) Xu, J.; Churchill, D. G.; Botta, M.; Raymond, K. N. Gadolinium(III) 1,2-hydroxypyridonate-based complexes: toward MRI contrast agents of high relaxivity. *Inorg. Chem.* **2004,** *43,* 5492-5494.
14) Xu, J.; Franklin, S. J.; Whisenhunt, Jr., D. W.; Raymond, K. N. Gadolinium complex tris[(3-hydroxy-1-methyl-2-oxo-1,2-didehydropyridine-4 carboxamido)ethyl]-amine: a new class of gadolinium magnetic resonance relaxation agents. *J. Am. Chem. Soc.* **1995**, *117*, 7245-7246.
15) Moore, E. G.; Seitz, M.; Raymond, K. N. Use of Yb^{III}-centered near infrared (NIR) luminescence to determine the hydration state of a 3,2-HOPO-based MRI contrast agent. *Inorg. Chem.* **2008,** *47,* 8571-8573.
16) Hajela, S.; Botta, M.; Giraudo, S.; Xu, J.; Raymond, K. N.; Aime, S. A tris-hydroxymethyl-substituted derivative of Gd-TREN-Me-3,2-HOPO: an MRI relaxation agent with improved efficiency. *J. Am. Chem. Soc.* **2000**, *122*, 11228-11229.
17) Thompson, M. K.; Botta, M.; Nicolle, G.; Helm, L.; Aime, S.; Merbach, A. E.; Raymond, K. N. A highly stable gadolinium complex with a fast, associative mechanism of water exchange. *J. Am. Chem. Soc.* **2003**, *125,* 14274-14275.
18) Thompson, M. K.; Misselwitz, B.; Tso, L. S.; Doble, D. M. J.; Schmitt-Willich, H.; Raymond, K. N. In vivo evaluation of gadolinium hydroxypyridonate chelates: initial experience as contrast media in magnetic resonance imaging. *J. Med. Chem.* **2005**, *48*, 3874-3877.
19) Pierre, V. C.; Botta, M.; Raymond, K. N. Dendrimeric gadolinium chelate with fast water exchange and high relaxivity at high magnetic field strength. *J. Am. Chem. Soc*. **2005**, *127,* 504-505.
20) Werner, E. J.; Botta, M.; Aime, S.; Raymond, K. N. Effect of a Mesitylene-Based Ligand Cap on the Relaxometric Properties of Hydroxypyridonate Gd(III) MRI Contrast Agents. *Contrast Media Mole Imaging.* **2009,** *4,* 220-229.

Chapter 3 – Improved Relaxivity through Dendrimer Conjugation

Abstract

One essential requirement for more sensitive gadolinium-based MRI contrast agents is to slow the molecular tumbling of the gadolinium(III) ion, which increases the gadolinium's relaxivity, or the ability to speed up the NMR relaxation of nearby water molecules. One route to this is through conjugation to high-molecular weight polymers such as dendrimers. In this work, amine functionalized TREN-bis(1,2-HOPO)-TAM-ethylamine and TREN-bis(1-Me-3,2-HOPO)-TAM-ethylamine ligands have been synthesized and attached to biocompatible 40 kDa esteramide (**EA**) and poly-L-lysine based (**PLL**) dendrimers capable of binding up to eight gadolinium complexes. These conjugates have T_1 relaxivities of up to 38.14 ± 0.02 $mM^{-1}s^{-1}$ per gadolinium at 37 °C, corresponding to relaxivities of up to 228 $mM^{-1}s^{-1}$ per dendrimer molecule. This relaxivity expressed on a "per Gd" basis is several times that of the small molecule complexes, and an order of magnitude higher than that of current commercial agents. Due to their high performance and low toxicity these macromolecules may constitute an attractive complement to currently available gadolinium(III) based contrast agents.

Introduction

MRI contrast agents can be further optimized for larger relaxivity and solubility through conjugation to a biocompatible macromolecule[1,2] such as a protein,[3] polypeptide,[8] dendrimer,[9-14] or nanoparticle,[15,16] which lowers the molecular tumbling time of the gadolinium due to the reduced degrees of freedom of large molecules in solution. Previously reported[17] ester-amide (**EA**) and branched poly-L-lysine (**PLL**) based dendrimers looked promising, as these degradable dendrimers offer a synthetically straightforward route to high molecular weight conjugates with facile renal clearance and low toxicity. We also anticipated that the densely packed core of the dendrimers would sterically inhibit the motion of the gadolinium complex, further increasing its relaxivity. The **EA** and **PLL** dendrimers developed by the Fréchet group have exhibited low toxicity *in vivo*, favorable degradation profiles, and can be decorated with up to eight gadolinium complexes per dendrimer.[17,18] These dendrimers have also been shown to increase half-life in blood serum and residence time of small molecule drugs, allowing for their improved drug delivery *in vivo.*[19] In addition to enhancing the relaxivity and blood half-life of contrast agents, polymeric carriers are also expected to significantly reduce the toxicity of these agents due to the much slower rates of endocytosis for macromolecules compared to lipophilic small molecule compounds such as non polymeric gadolinium complexes. This should reduce the amount required for injection, therefore reduce the amount of gadolinium entering cells, and thereby facilitate its eventual excretion through the renal system.These complexes exhibit high T_1 relaxivities and thermodynamic complex stabilities (pGd ~ 17-18). The 1-Me-3,2-HOPO based ligands used in this study

vary by the nature of the amine pendant to the TAM ring. Complex **1** has a short, rigid linker and a known *q* value of two.[2] Complex **2** has a longer, more flexible linkage incorporating a second ethylamine moiety, and complex **3** has a branched linkage with a third ethylamine group. Complex 4, containing the 1,2-HOPO moiety varies from these by its nitrogen substitution within the HOPO rings.

Experimental Procedure

General Considerations: Unless otherwise noted, starting materials were obtained from commercial suppliers and used without further purification. All solvents were stored over 4 Å molecular sieves. Water was distilled and further purified by a Millipore cartridge system (resistivity 18.2 x 10^6 Ω). All organic extracts were dried over anhydrous $MgSO_4$ and solvents removed *in vacuo* by a rotory evaporator or vacuum pump evacuation. Flash chromatography was performed on Merck Silica Gel (40-7 Mesh). ^1H and ^{13}C NMR spectra were recorded on a Bruker AVQ600 at 600 MHz, AVQ 400 at 400 MHz and 100 MHz or a Bruker AVB 400 at 400 MHz and 100 MHz, respectively; the residual solvent peak was used as an internal reference. Elemental analysis and mass spectra (LR = low resolution; HR = high resolution; FAB MS = fast atom bombardment mass spectrometry; EI MS = electron ionization mass spectrometry; ES MS = electrospray mass spectrometry) were performed by the Microanalytical Laboratory and Mass Spectrometry Laboratory, respectively, at the College of Chemistry at the University of California at Berkeley. Matrix Assisted Laser Desorption Ionization mass spectra (MALDI-MS) were recorded on an Applied Biosystems Voyager System 6322. Applied Biosystems, USA). MALDI measurements were recorded using a 25:1 α-cyano-hydroxycinnamic acid: sample ratio, using positive linear ion detection, with accelerating voltage = 20kV, grid voltage = 94%, and delay time of 100ns. Prep-HPLC was done on a Varian Prep HPLC system using a Varian super-prep C18 column (Dynamax C18, 41.4 x 250 mm, 10 μm particle size). Electrospray LC/MS analysis was performed using an API 150EX system (Applied Biosystems, USA) at standard instrument settings equipped with a Turbospray source and an Agilent 1100 series LC pump. All synthetic reactions were performed in an atmosphere of nitrogen, unless otherwise noted. The esteramide (EA) and PLLG2(Asp(COOH)PEO)$_8$ Polylysine (PLL) dendrimers were synthesized as was previously reported by Dr. Willam C. Floyd, III.[17]

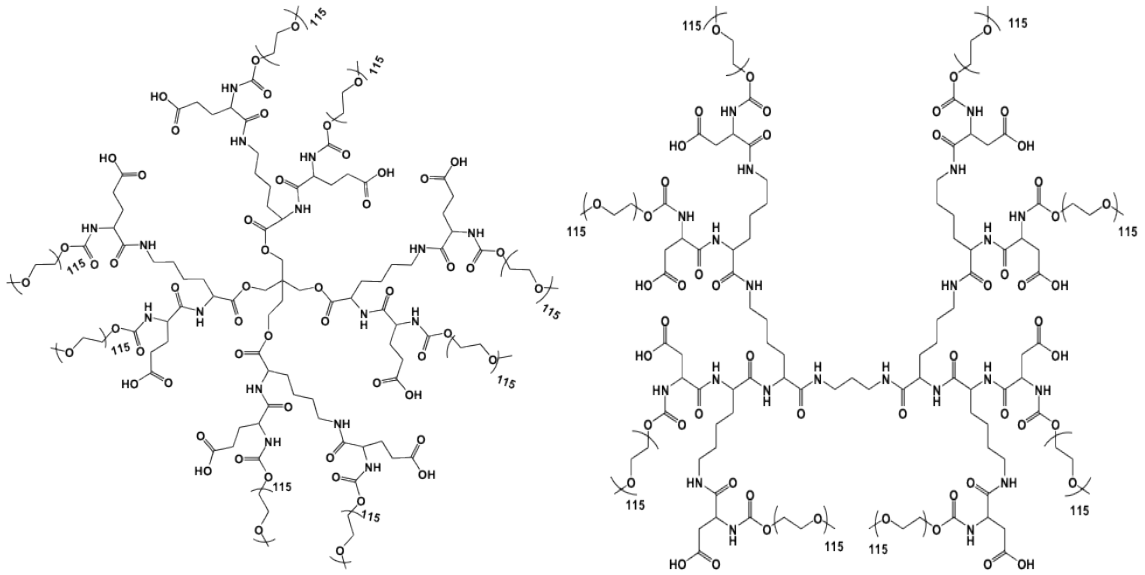

Figure 1. The esteramide (**EA**) dendrimer (left) and polylysine dendrimer (**PLL**) (right).

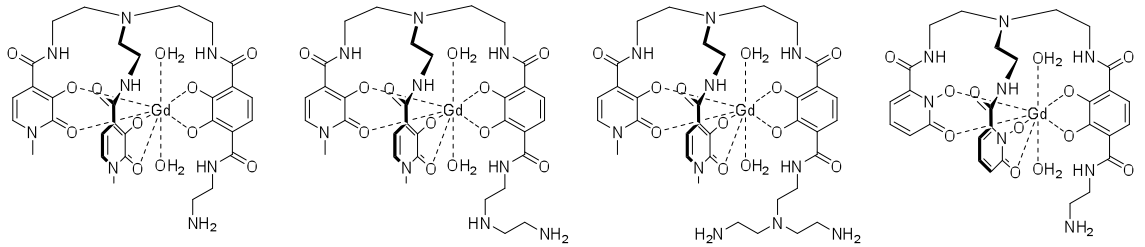

Figure 2. The gadolinium chelators used for macromolecular conjugation.

Size Exclusion Chromatography (SEC) (by Dr. William C. Floyd, III)*:* The SEC system consisted of two SDV Linear S (5 μm) columns (Polymer Standards Service, 300 x 8 mm) using DMF with 0.2% LiBr as the mobile phase (1 mL/min) in series with a Waters 515 pump, 717 autosampler, 996 Photodiode Array Detector (210-600 nm), and 2414 differential refractive index (RI) detector. Sample volumes were 100 μL and UV spectra were viewed at 350 nm. Molecular weight calibrations for RI spectra were made using linear polyethylene glycol standards with toluene as a reference peak. Gadolinium loading was quantified by comparing polymer peak integrals in UV spectra with a calibration curve obtained from spectra of known concentrations of gadolinium complexes run under identical conditions.

Inductively Coupled Plasma- Optical Emission Spectroscopy (ICP-OES): ICP-OES was performed on a Perkin Elmer Optima 700 DV. Samples for analysis were diluted in 2% (v/v) nitric acid in Millipore water. Gd(III) standards were prepared in 2% (v/v) nitric acid/Millipore water with concentrations between 0.01 and 40.0 μg/mL. Using a weighed

sample, a percentage Gd (III) of the sample could be calculated and therefore quantify Gd (III) per dendrimer (μm).

Table 1. Complex loadings of conjugates as measured by ICP. The theoretical maximum loading is eight Gd complexes per dendrimer.

Conjugate	Complex loading (Gd/dendrimer)
5	6.0
6	2.9
7	8.0
8	4.5
9	3.0

Dynamic light scattering (DLS): DLS determined hydrodynamic size and was performed at 25 °C by dissolving samples in 1X PBS buffer to a concentration of approximately 0.5-1 mg/mL. After brief vortexing the samples were filtered over 0.45 μm PTFE filters to remove dust and added to a 0.45 μL quartz cuvette and analyzed using a Zetasizer Nanoseries ZS (Malvern Instruments, UK). Results were repeated in triplicate with averages reported.

Dendrimer-Complex Conjugation (by Dr. William C. Floyd, III)
5: To a 25mL scintillation vial containing 7.5 mg (0.0090 mmol, 1.7 eq.) of complex **1** was added 27 mg (0.005 mmol by carboxylic acid) of **EA** dendrimer. To this was added 4 mg (0.03 mmol, 5 eq.) each of HOBt and DMAP. The solids were dissolved in 1 mL DMSO and 8 mg (0.04 mmol, 8 eq.) of EDC were added and the reaction was allowed to stir overnight at room temperature under nitrogen atmosphere. After 14 hours the solvent was removed *in vacuo* and solids were taken into 5 mL DCM. After filtering solids through a 0.45 μm PTFE filter the red solution was precipitated with the addition of 100 mL ether to give a pink fluffy solid. The solids were isolated by centrifugation and residual ligand was removed using a PD-10 size exclusion column to give 20 mg (70%) of conjugate **5** as a pink solid. SEC: Mn = 44,000 Da, PDI = 1.36.

6: To a 25mL scintillation vial containing 5.9 mg (0.0070 mmol, 1.7 eq.) of complex **2** was added 20 mg (0.004 mmol by carboxylic acid) of **EA** dendrimer. To this was added 3 mg (0.02 mmol, 5 eq.) each of HOBt and DMAP. The solids were dissolved in 0.5 mL of a 1:1 mixture of DMSO and 2.6 mg (0.013 mmol, 3 eq.) of EDC were added and the reaction was allowed to stir overnight at room temperature under nitrogen atmosphere. After 14 hours the reaction was precipitated with the addition of 100 mL ether to give a brown solid. The solids were isolated by centrifugation and taken into 5 mL DCM and filtered over a 0.45 μm PTFE filter. After evaporation residual ligand was removed using a PD-10 size exclusion column to give 18 mg (85%) of conjugate **6** as a pale yellow solid. SEC: Mn: 30,900 Da, PDI: 1.18.

7: To a 2 mL vial containing 2.0 mg (0.0024 mmol, 2.2 eq) of **4** was added 5.5 mg **EA** dendrimer (0.0011 mmol COOH), 0.75mg DMAP (0.0058 mmol, 5.3 eq), and 0.75mg HOBt (0.0065 mmol, 6.9 eq) in 200 µL DMF. This was stirred and vortexed until a homogeneous solution was obtained, and 1.9 mg EDC (0.0099 mmol, 9.0 eq.) was added in 200 µL DMF and the reaction was allowed to stir overnight at room temperature under nitrogen atmosphere. After 14 hours the solvent was removed *in vacuo* and the solids were purified by precipitation in ether from DCM followed by PD-10 size exclusion columns and filtration of the product fraction over 0.45 µm PTFE filters. Lyophilizing gave 7 (6.3 mg, 98%) as a white fluffy solid. SEC: Mn: 38,400 Da, PDI: 1.22

8: To a 25mL scintillation vial containing 15 mg (0.017 mmol, 1.3 *eq.)* of gadolinium complex **1** was added 70 mg (0.014 mmol by carboxylic acid assay) of **PLL** dendrimer. To this was added 11 mg (0.11 mmol, 7 eq.) each of N-hydroxysuccinimide (NHS) and hydroxybenzotriazole (HOBt). The solids were dissolved in 0.5 mL DMSO and 3.5 mg (0.018 mmol, 1.3 eq.) of EDC (EDAC or EDCI, 1-ethyl-3-(3-dimethylaminopropyl) carbodiimide) were added and the reaction was allowed to stir overnight at room temperature under nitrogen atmosphere. After overnight stirring, the solvent was removed *in vacuo* and solids were taken into 5 mL DCM. After filtering solids through a 0.45 µm PTFE (polytetrafluoroethylene) filter the precipitate by addition to 100 mL diethyl ether (anhydrous) to give a light yellow solid. The solids were isolated by centrifugation and residual impurities were removed using a PD-10 size exclusion column to give 35 mg (50.%) of conjugate **8** as a yellow solid. SEC: Mn = 38,000 Da, PDI = 1.11. ^{1}H NMR (D_2O, 500 MHz): δ (ppm) = 0.97 (br s 4), 1.20 (br s, 10), 1.36 (br s, 10), 1.56 (br s, 10), 1.74 (br s, 3), 2.4-2.7 (br m, 20), 2.73 (s, 7), 2.79 (br s, 7), 3.01 (br s, 25), 3.23 (s, 24), 3.4-3.8 (br m, ~3500), 4.24 (br s, 25).

9: To a 25mL scintillation vial containing 10.5 mg (0.00197 mmol by carboxylic acid) of **EA** dendrimer was added 3 mg (0.03 mmol, 10 eq.) of NHS. To this was added 0.5 mL of DMF and the solution was vortexed briefly to dissolve solids. To this was added 2 mg (0.01 mmol, 5 eq.) of EDC and the reaction was stirred for 5 minutes. To this solution was then added 3.5 mg (0.0041 mmol, 2 eq.) of complex **3** and the reaction was allowed to stir overnight at room temperature under nitrogen atmosphere. After 14 hours the reaction was precipitated with the addition of 15 mL ether and centrifuged to give a brown solid. The solids were then taken into 5 mL DCM and filtered over a 0.45 µm PTFE filter. Solvent was removed under reduced pressure to give 9.5 mg (86%) of conjugate **9** as a clear film. SEC: Mn: 37,400 Da, PDI: 1.12

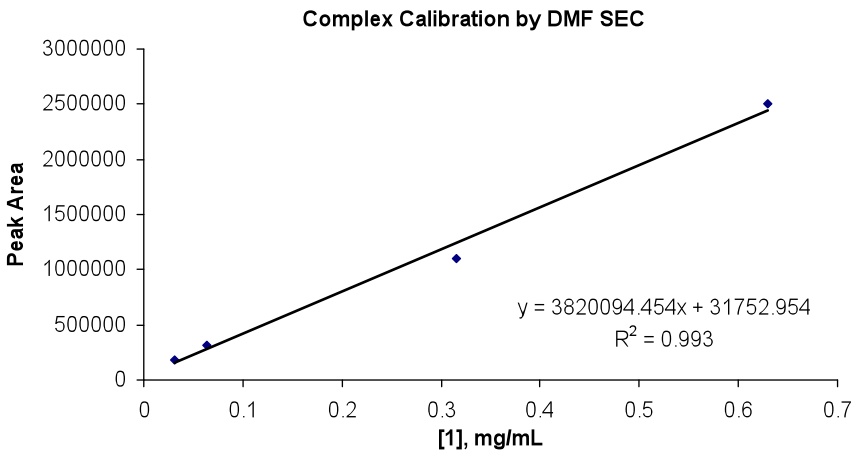

Figure 3. SEC-UV data calibration plot. Plotting peak area versus complex **1** concentration, a sample's Gd concentration could be determined from the SEC's peak area. A preliminary loading of 4.5 gadolinium complexes/dendrimer (55% of theoretical max) for **8** was calculated in this way.

Relaxivity Studies: T_1 measurements were performed on a Bruker mq60 minispec relaxometer. T_1 was determined at 60 MHz (1.41 T) using an inversion recovery pulse sequence. Temperature controlled at 37 °C using a Julabo F25 circulating water bath. Each sample was analyzed by ICP-OES for exact Gd(III) concentration. The inverse of the longitudinal relaxation time of each sample ($1/T_1$, s^{-1}) was plotted against Gd(III) concentration (μM) and fit by linear regression ($R^2 > 0.99$). Relaxivity analyses were performed in triplicate (three samples). Samples vortexed prior to analysis to break up potential aggregation of complexes. 37 °C instrument. Instrument Parameters: Scans: 4; Recycle Delay: 18.5 s; Gain: 53; Dummy Shots: 0; Detection mode: real; Bandwidth: Broad, 20,000 kHz; Monoexponential Curve Fitting, Phase Cycling. First Pulse Separation: 5 ms; Final Pulse separation: 18,500 ms, Number of data points for fitting: 20; Delay sample window: 0.05 ms; Sampling Window: 0.02 ms; Time for Saturation Curve Display: 6 s.

Cell Culture by MTT Assay for Conjugates: HeLa cells were purchased from American Type Culture Collection (ATTC) and plated by the Molecular and Cell Biology Cell Culture Facility at University of California, Berkeley, to 10,000 cells per well. All conjugates were evaluated, as well as control samples used were the esteramide dendrimer, the polylysine dendrimer, and Gd-DTPA, a commercial MRI contrast agent.

Solutions were made in the concentration of 1.0 mg/mL in Dulbecco's modification of Eagle's Media (DMEM, with glucose and 10% fetal bovine serum (FBS). Dilutions were made on one plate at the rate of two-fold per well, for eight total dilutions and a final concentration of 0.05 mg/mL of sample. These solutions were transferred in 100 μL dilutions onto HeLa cells, which were already in 100 μL of media. These samples were incubated for 72 h at 37 °C and 5% CO_2. After 24 hours, 40 μL of thiazolyl blue tetrazolium bromide (98% TLC) was added for a MTT assay at 2.9 mg/mL. These samples were incubate for 30 min at 37 °C and 5% CO_2. After 30 min, the cells were

aspirated and 200 µL of DMSO added, followed by 25 µL of pH 10.5 glycine buffer (100 mmol glycine and 100 mmol salt). Absorbance was measured at 570 nm on a Molecular Devices plate reader and cytotoxicity determined based on blank live cells and starved cells (terminated by denying media). All results repeated in triplicate and averaged reported.

Results and Discussion

The syntheses of the **PLL** and **EA** dendrimers,[17] complexes **1**-**3**[2] and complex **4**[20] have been reported previously. Conjugates were obtained by coupling the carboxylic acid functionalities of the dendrimer to the amine moiety of a Gd-TREN-bis-HOPO-TAM complex using carbodiimide as the coupling agent (Scheme 1). Because the gadolinium introduced into the reaction is already tightly bound as a highly stable complex, this pre-complexation of the metal before conjugation reduces the possibility that free gadolinium ions might bind to non-specific coordination sites. Conjugates were purified by precipitation into ether followed by aqueous size exclusion chromatography using PD-10 columns.

When **1** was coupled to the **EA** dendrimer, (Scheme 1) ICP and SEC measurements suggest a loading of six gadolinium complexes per dendrimer. This conjugate, **5**, has a relaxivity of 38.14 ± 0.02 mM-1s-1 per gadolinium, or 228 $mM^{-1}s^{-1}$ per dendrimer, at 37 ^{o}C. This value compares very favorably to other relaxivities measured under clinically relevant conditions, which are typically in the range of 3-5 $mM^{-1}s^{-1}$ for current commercial agents (Figure 2).

We further investigated **2** as a conjugate with the **EA** dendrimer (**6**) due to its high thermodynamic stability. This small molecule complex has a thermodynamic stability value three orders of magnitude larger than that of **1** or **3**.[2] This increased complex stability should reduce the amount of free gadolinium that can be leached from the conjugate *in vivo*, which may reduce toxicity concerns. However, due to the longer and more flexible linker, the molecular tumbling time and relaxivity were decreased compared to conjugate **5**, giving conjugate **6** a relaxivity of 31.9 ± 0.1 $s^{-1}mM^{-1}$ per gadolinium. Although a lower complex loading per dendrimer was observed by ICP and SEC (2.8 complexes/dendrimer), conjugate **6** has the potential to be a safer option due to the higher thermodynamic stability of the gadolinium-chelate binding.

Given the success of the 1-Me-3,2-HOPO chelator, a variation on this moiety, a 1,2-HOPO chelator was evaluated. When conjugated to the **EA** dendrimer, relaxivity values of 20.2 ± 0.6 $mM^{-1}s^{-1}$ were obtained for conjugate **7**. In general the 1,2-HOPO complexes show lower relaxivity than their 1-Me-3,2-HOPO counterparts,[4,21] and this trend appears to be conserved upon conjugation to the dendrimer.

The **PLL** dendrimer was evalutated as a scaffoldto further test the versatility of this approach. Conjugate **8** has a relaxivity of 21.0 ± 0.6 mM-1s-1 per gadolinium. While this constitutes a significant increase over the small molecule complex, it is still significantly lower than that obtained with the **EA** dendrimer. I attribute this decrease to greater internal hydrogen bonding between the inner-sphere water coordination sites of the gadolinium and the more hydrophilic amide based **PLL** dendrimer core, or to

increased tumbling of the gadolinium(III) complexes caused by the less branched and sterically crowded core of this dendrimer. The decreased relaxivity observed with the **PLL** dendrimer, combined to the more favorable biodegradability of the **EA** dendrimer, suggests that the **EA** dendrimer is a superior platform for this application.

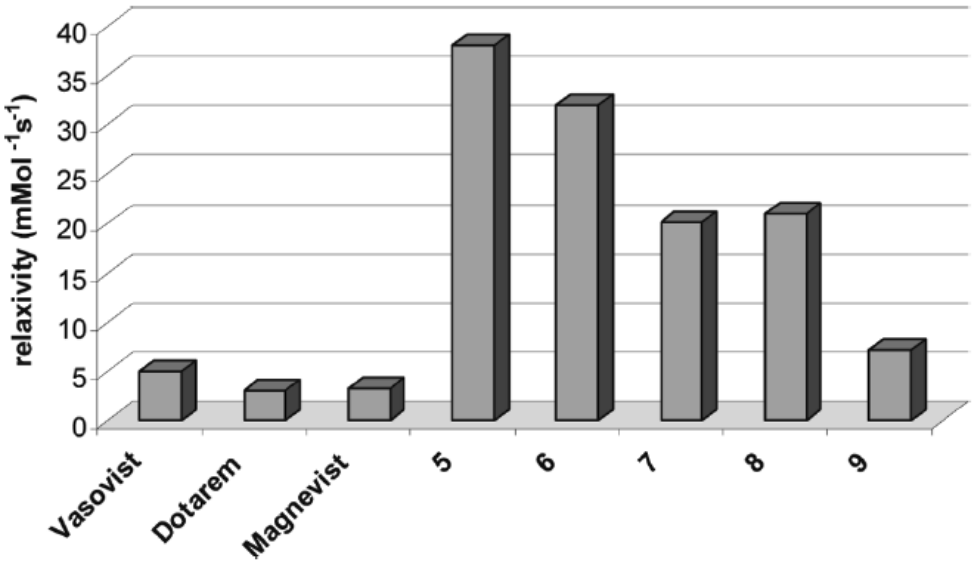

Figure 4. A comparison of the per gadolinium relaxivities of several clinical Gd(III) contrast agents and the dendrimer contrast agents investigated. Values measured at 37 ^{o}C at 60 MHz.

Finally, I investigated complex **3** with the **EA** dendrimer, but found that the extended linker and extra primary amine resulted in a conjugate, **9**, with a relatively low relaxivity of 7.19 ± 0.07 $s^{-1}mM^{-1}$. To evaluate the toxicity of these conjugates, cytotoxicity studies were carried out for 72 h to determine their effect on cell viability using Gd-DTPA, **PLL**, and **EA** dendrimers as controls. While most MRI contrast agents are excreted within 24 h, the macromolecules may be excreted more slowly, and cytotoxicity testing was performed over a period of 72 h to reflect this increased residence time. Each of the conjugates exhibited no evidence of cytotoxicity at 1.0 mg/mL concentrations of conjugates **5-9**, indicating that these contrast agents have not acquired short term toxicity through their macromolecular conjugation.

Conclusions

Through conjugation to highly biocompatible and readily synthesized dendrimers, the relaxivity of HOPO-based TREN capped Gd(III) complexes was improved over commercial agents without compromising clinical conditions. The conjugates presented here contain tightly bound gadolinium and give relaxivities of up to 38 $mM^{-1}s^{-1}$ under the clinically relevant conditions of 60 MHz and 37 ^{o}C, and were shown to be nontoxic to cells at mM concentrations.[22,23]

References

1) Caravan, P. Strategies for increasing the sensitivity of gadolinium based MRI contrast agents. *Chem. Soc. Rev*. **2006**, *35*, 512-523.

2) Pierre, V. C.; Botta, M.; Aime, S.; Raymond, K. N. Substituent effects on Gd(III)-based MRI contrast agents : optmizing the stability and selectivity of the complex and the number of coordinated water molecules. *Inorg. Chem.* **2006**, *45*, 8355-8364.

3) Datta, A.; Raymond, K. N. Gd-Hydroxypyridinone (HOPO)-based high-relaxivity magnetic resonance imaging (MRI) contrast agents. *Acc. Chem. Res.* **2009**, *7*, 938-947.

4) Werner, E. J.; Avedano, S.; Botta, M.; Hay, B. P.; Moore, E. G.; Aime, S.; Raymond, K. N. Highly soluble tris-hydroxypyridonate Gd(III) complexes with increased hydration number, fast water exchange, slow electronic relaxation, and high relaxivity *J. Am. Chem. Soc*. **2007**, *129*, 1870-1871.

5) Doble, D. M. J.; Botta, M.; Wang, J.; Aime, S.; Barge, A.; Raymond, K. N. Optimization of the relaxivity of MRI contrast agents: effect of poly(ethylene) glycol chains on the water-exchange rates of Gd(III) complexes. *J. Am. Chem. Soc.* **2001**, *123*, 10758-10759.

6) Cohen, S. M.; O'Sullivan, B.; Raymond, K. N. Mixed hydroxypyridinonate ligands as iron chelators. *Inorg. Chem.* **2000**, *39*, 4339-4346.

7) Raymond K. N.; Pierre, V. C. Next generation, high relaxivity gadolinium MRI agents. *Bioconj. Chem*. **2005**, *16*, 3-8.

8) Mishra, R.; Su, W.; Pohmann, R.; Pfeuffer, J.; Sauer, M. G.; Ugurbil, K.; Engelmann, J. Cell-penetrating peptides and peptide nucleic acid-coupled MRI contrast agents: evaluation of cellular delivery and target binding. *Bioconj. Chem.* **2009**, *20,* 1860-1868.

9) Pierre, V. C.; Botta, M.; Raymond, K. N. Dendrimeric gadolinium chelate with fast water exchange and high relaxivity at high magnetic field strength. *J. Am. Chem. Soc*. **2005**, *127*, 504-505.

10) Ali, M. M.; Woods, M.; Caravan, P.; Opina, A. C. L.; Spiller, M.; Fettinger, J. C.; Sherry, A. D. Synthesis and relaxometric studies of a dendrimer-based pH-responsive MRI contrast agent. *Chem.- Eur. J.* **2008**, *14,* 7250-7258.

11) Bulte, J. W. M.; Wu, C. C.; Brechbiel, M. W.; Brooks, R. A.; Vymazal, J.; Holla, M.; Frank, J. A. Dysprosium-DOTA-PAMAM dendrimers as macromolecular T2 contrast agents- preparation and relaxometry. *Invest. Radiol.* **1998**, *33*, 841-845.

12) Cheng, Z.; Thorek, D. L. J.; Tsourkas, A. Gadolinium-conjugated dendrimer nanoclusters as tumor-targeted T1 magnetid resonance imaging contrast agent. *Angew. Chem. Int. Ed*., **2010**, *49*, 346-350

13) Nwe, K.; Bernardo, M.; Regino, C. A. S.; Williams, M.; Brechbiel, M. W. Comparison of MRI properties between derivatized DTPA and DOTA gadolinium-dendrimer conjugates. *Bioorg Med Chem*, **2010**, *18*, 5925-5931.

14) Bumb, A., Brechbeil, M. W., Choyke, P. Macromolecular and dendrimer based magnetic resonance imaging contrast agents. *Acta Radiol*, **2010**, *51*, 751-767.

15) Manus, L. M,; Mastarone, D. J.; Waters, E. A.; Zhang, X-Q.; Schultz-Sikma, E. A.; MacRenaris, K. W.; Ho, D.; Meade, T. J. Gd(III)-Nanodiamond conjugates for MRI contrast enhancement. *Nano Lett.* **2010**, *10,* 484-489.
16) Song, Y.; Xu, X.; MacRenaris, K. W.; Zhang, X-Q.; Mirkin, C. A.; Meade, T. J. Multimodal gadolinium-enriched DNA-gold nanoparticle conjugates for cellular imaging. *Angew. Chem. Intl. Ed.* **2009**, *48,* 9143-9147.
17) van der Poll, D. G.; Kieler-Ferguson, H. M.; Floyd, W. C.; Guillaudeu, S. J.; Jerger, K,; Szoka, F. C.; Fréchet, J. M. J. Design, synthesis, and biological evaluation of a robust, biodegradable dendrimer. *Bioconj. Chem.* **2010**, *21,* 764-773.
18) Fox, M. E.; Szoka, F. C.; Fréchet, J. M. J. Soluble polymer carriers for the treatment of cancer: the importance of molecular architecture *Acc Chem Res.* **2009**, *42*, 1141-1151.
19) Lee, C. C.; Gillies, E. R.; Fox, M. E.; Guillaudeu, S. J.; Fréchet, J. M. J.; Dy, E. E.; Szoka, F.C. A single dose of doxorubicin-functionalized bow-tie dendrimer cures mice bearing C-26 colon carcinomas. *Proc. Nat. Acad. Sci.*, **2006**, *103*, 16649-16654.
20) Werner, E. J.; Kozhukh, J.; Botta, M.; Moore, E. G.; Avedano, S.; Aime, S. Raymond, K. N. 1,2-hydroxypyridonate/terephthalamide complexes of gadolinium(III): synthesis, stability, relaxivity, and water exchage properties. *Inorg. Chem.* **2009,** *48,* 277-286.
21) Xu, J.; Franklin, S. J.; Whisenhunt, Jr., D. W.; Raymond, K. N. Gadolinium complex of tris[(3-hydroxy-1-methyl-2-oxo-1,2-didehydropyridine-4-carboxamido)ethyl]-amine: a new class of gadolinium magnetic resonance relaxation agents. *J. Am. Chem. Soc.* **1995**, *117*, 7245-7246.
22) Floyd, III, W. C.; Klemm, P. J.; Smiles, D. E.; Kohngruber, A. C.; Pierre, V. C. Mynar, J. L.; Fréchet, J. M. J.; Raymond, K. N. Conjugation effects of various linkers on Gd(III) MRI contrast agents with dendrimers: optimizing the hydroxypyridinonate (HOPO) ligands with nontoxic, degradable (EA) dendrimers for high relaxivity. *J. Am. Chem. Soc.* **2011**, *133*, 2390-2393.
23) Klemm, P. J.; Floyd, III, W. C.; Smiles, D. E.; Fréchet, J. M. J.; Raymond, K. N. Improving T1 and T2 magnetic resonance imaging (MRI) contrast agents through the conjugation of an esteramide dendrimer to whigh water coordination Gd(III) hydroxypyridinone (HOPO) complexes. *Contrast Media Mol. Imaging.* **2012**, *7*, 95-99.

Chapter 4 – Improved Function through Dendrimer Conjugation

Abstract

Magnetic resonance imaging (MRI) contrast agents represent a worldwide billion-dollar market annually. While T_1 relaxivity enhancement contrast agents receive greater attention and a significantly larger market share, the commercial potential for T_2 relaxivity enhancing contrast agents remains a viable diagnostic option due to their increased relaxivity at high field strengths. Improving the contrast and biocompatibility of T_2 MRI probes may enable new diagnostic prospects for MRI. Paramagnetic lanthanides have the potential to decrease T_1 and T_2 proton relaxation times, but are not commercially used in MRI diagnostics as T_2 agents. In this article, oxygen donor chelates (hydroxypyridinone, HOPO, and terephthalamide, TAM) of various lanthanides are demonstrated as biocompatible macromolecular dendrimer conjugates for the development of T_2 MRI probes. These conjugates have relaxivities up to 374 $mM^{-1}s^{-1}$ per dendrimer, high bioavailability, and low *in vitro* toxicity.

Introduction

All T_1 commercial contrast agents suffer a decrease in efficiency at higher field strengths,[1-4] which is a liability as clinical instruments increase in magnetic field strength to enhance inherent instrument contrast. Many MRI's in the clinic have reached 60 to 125 MHz to increase resolution, but at the cost of diminishing the efficacy of the contrast agent injected.[2,3] To counteract the increase in field strength, increasing dosage is required to maintain current levels of contrast, however, gram quantities of T_1 contrast agents must already be injected to overcome low sensitivity. Therefore, alternative options need to be explored and developed, both improving T_1 relaxivity and providing an alternative such as an effective T_2 CA.[2]

In contrast to T_1 imaging agents, the T_2 agents exhibit a direct correlation between increasing field strength and relaxivity,[1] and as a result they improve contrast at the larger field strengths now seen in the clinic. This relationship, combined with increasingly powerful magnets used for MRIs, suggests that over time T_2 agents may emerge as a more thoroughly studied and highly developed class of MRI-CAs. The development of T_2 targeted imaging for MRI will require higher relaxivities than are currently attained if this approach is to be realized for diagnostic medicine.[3] High relaxivity at physiological conditions and 60 – 100 MHz, combined with adequate synthetic functionality and versatility, would allow conjugation of various targeting molecules such as antibodies, proteins or targeting ligands and enable the development of a new generation of MRI agents capable of site selective delivery.[1]

Currently, T_2 commercial contrast agents are primarily superparamagnetic iron oxide nanoparticles (SPION). Current SPION's are unsuitable for targeted imaging and

bioresponsive mechanisms. In addition, SPION's have not responded to investigations into advanced applications such as tumor targeting and the tracking of stem cells.[1]

In Chapter 2, Gd^{III} complexes were reported for enhanced T_1 relaxivities compared to current commercial agents.[5,6] These include Gd-TREN-bis(1-methyl-3,2-HOPO)-TAM-ethylamine (**1**), Gd-TREN-bis(1-methyl-3,2-HOPO)-TAM-N2 (**2**), Gd-TREN-bis(1-methyl-3,2-HOPO)-TAM-N3 (**3**), and Gd-TREN-bis(1,2-HOPO)-TAM-ethylamine (**4**) (Figure 1). To investigate the feasibility of using alternate lanthanides for T_2 imaging, Yb^{III} and Dy^{III} based agents, Dy-TREN-bis(1-methyl-3,2-HOPO)-TAM-ethylamine (**5**), Yb-TREN-bis(1-methyl-3,2-HOPO)-TAM-ethylamine (**6**), Dy-TREN-bis(1-methyl-3,2-HOPO)-TAM-N2 (**7**), Yb-TREN-bis(1-methyl-3,2-HOPO)-TAM-N2 (**8**), Dy-TREN-bis(1-methyl-3,2-HOPO)-TAM-N3 (**9**), and Yb-TREN-bis(1-methyl-3,2-HOPO)-TAM-N3 (**10**), were also synthesized and evaluated as dendrimer conjugates. Yb^{III} has potential as a bimodal imaging agent as a T_2 MRI contrast agent and a near infrared probe in biological systems. Dy^{III} has been shown to be a prospective cerebral perfusion agent, superior to Gd^{III} and therefore should be explored as a specific MRI diagnostic analysis. In addition to varying the lanthanide used in these complexes, they were also varied by the amine linking appendage used to attach the complex to the dendrimer. These linkers vary in length and rigidity, as well as the potential coordinating environment surrounding the lanthanide.

The poly-L-lysine (PLL) based dendrimer (Figure 2, bottom structure) contains a moderately branched hydrophilic amide core, and provides a highly resilient platform for agent delivery. The esteramide (EA) dendrimer (Figure 2, top structure) contains a highly compact core with both ester and amide bonds. The ester bonds are incorporated to allow for more rapid biodegradability and expedite the synthesis. The PEG chains radiating out from the core increase solubility of these conjugates *in vivo* and prevent the agent from interacting with the surrounding biological environment.[18] Due to a phenomenon known as the enhanced permeation and retention (EPR) effect,[19] which takes advantage of the increased permeability of the vasculature and decreased efficiency of the lymphatic system in well formed tumors, these macromolecules can also passively accumulate in tumors at levels up to 10-15% of the dose per gram of tumor tissue.[20] This may enable these conjugates to outperform small (< 1000 Da) molecules in the imaging of tumors, and prove valuable in the imaging and diagnosis of some cancers. These macromolecules also remain in the blood at high levels for much longer than small molecules, enabling more time for MRI scans to be carried out.[16-17] In Chapter 4, T_2 MRI probes with no observed cultured cell toxicity, high biocompatibility, and high T_2 relaxivity were synthesized.

Experimental Procedure

General Considerations: Unless otherwise noted, starting materials were obtained from commercial suppliers and used without further purification. All organic solvents were stored over 4 Å molecular sieves. Water was distilled and further purified by a Millipore cartridge system. All organic extracts were dried over anhydrous $MgSO_4$ and solvents removed *in vacuo*. Flash chromatography was performed on Merck Silica Gel (40-7

Mesh). Ion exchange chromatography was done on Phenomenex Strata X-C prepacked columns (pore size 85 Å, particle size 33 μm). ^{1}H and ^{13}C NMR spectra were recorded on a Bruker AVQ 400 at 400 MHz and 100 MHz, respectively or a DRX 500 at 500 MHz; the residual solvent peak was used as an internal reference. Elemental analysis and mass spectra (HR = high resolution; ESI-MS = electrospray ionization mass spectrometry) were performed by the Microanalytical Laboratory and Mass Spectrometry Laboratory, respectively, at the College of Chemistry at the University of California at Berkeley. Prep-HPLC was done on a Varian Prep HPLC system using a Varian super-prep C18 column (Dynamax C18, 41.4 x 250 mm, 10 μm particle size). All synthetic reactions were performed in an atmosphere of nitrogen, unless otherwise noted.

Esteramide (EA) and PLLG2(Asp(COOH)PEO)$_8$ Polylysine (PLL) Dendrimer Synthesis: (Figure 2) Synthesized by Dr. William C. Floyd, III as was previously reported.[16]

5 (by Dr. Christopher M. Andolina):10. mg of TREN-bis(1-Me)-3,2-HOPO-TAM-ethylamine (0.0615 mmol, 1 *eq.*) was dissolved in 0.308 mL of 0.05 M $DyCl_3$ (1 *eq.*) in methanol and 1% TEA. This reaction was refluxed for three h, and was recrystallized three times in diethyl ether. Excess solvent was removed *in vacuo*. $[DyC_{30}H_{33}N_8O_{10}]^-$. Charge -1. Neg. Mode MS-ESI *m/z* = 829.1613 (Calc. 829.1612).

6 (by Dr. Christopher M. Andolina):10. mg of TREN-bis(1-Me)-3,2-HOPO-TAM-ethylamine (0.0578 mmol, 1 *eq.*) was dissolved in 0.290 mL of 0.05 M $YbCl_3$ (1 *eq.*) in methanol and 1% triethylamine (TEA). This reaction was refluxed for three h, and was recrystallized three times in diethyl ether. Excess solvent was removed *in vacuo*. $[C_{30}H_{33}N_8O_{10}Yb]^-$ Charge: -1. Neg. Mode ESI-MS *m/z* = 839.1716 (calc. 839.1711).

7 (by Dr. Christopher M. Andolina):10. mg of TREN-bis(1-Me)-3,2-HOPO-TAM-ethylamine-ethylamine (0.0615 mmol, 1 *eq.*) was dissolved in 0.308 mL of 0.05 M $DyCl_3$ (1 *eq.*) in methanol and 1% TEA. This reaction was refluxed for 3 h, and was recrystallized three times in diethyl ether. Excess solvent was removed *in vacuo*. $[DyC_{32}H_{38}N_9O_{10}]^-$. Charge -1. Neg. Mode MS-ESI *m/z* = 872.2032 (Calc. 872.2033).

Dynamic light scattering (DLS) (by Dr. William C. Floyd, III): DLS determined hydrodynamic size and was performed at 25 °C by dissolving samples in 1X PBS buffer to a concentration of approximately 1 mg/mL. After brief vortexing the samples were filtered over 0.45 μm PTFE filters to remove dust and added to a 0.45 μL quartz cuvette and analyzed using a Zetasizer Nanoseries ZS (Malvern Instruments, UK). Results were repeated in triplicate with averages reported.

Size Exclusion Chromatography (SEC) (by Dr. William C. Floyd, III): The SEC system consisted of two SDV Linear S (5 μm) columns (Polymer Standards Service, 300 x 8 mm) using DMF with 0.2 % LiBr as the mobile phase (1 mL/min) in series with a Waters 515 pump, 717 autosampler, 996 Photodiode Array Detector (210-600 nm), and 2414 differential refractive index detector. Sample volumes were 100 μL and UV spectra were viewed at 350 nm. Molecular weight calibrations for RI spectra were made using linear polyethylene glycol standards with toluene as a reference peak. Complex loading was quantified by comparing polymer peak integrals in UV spectra with a calibration curve obtained from spectra of known quantities of ligand dissolved in DMF and run under identical conditions.

1:EA and 1:PLL, 2:EA and 4:EA conjugates were synthesized as reported (by Dr. William C. Floyd, III).[12]

Yb-TREN-Dendrimer Conjugation Synthesis (by Dr. William C. Floyd, III):

6:EA: To a 25 mL scintillation vial containing 1 mg (0.011 mmol, 1.1 *eq.*) of metal complex 6 was added 5 mg (0.001 mmol by carboxylic acid) of EA dendrimer. To this was added 1 mg (0.008 mmol, 9 *eq.*) each of N-hydroxysuccinimide (NHS) and hydroxybenzotriazole (HOBt). The solids were dissolved in 0.5 mL DMSO and 1 mg (0.005 mmol, 5 *eq.*) of EDC (EDAC or EDCI, 1-ethyl-3-(3-dimethylaminopropyl) carbodiimide) was added and the reaction was allowed to stir overnight at room temperature . After overnight stirring, the solvent was removed *in vacuo* and solids were taken into 5 mL DCM. After filtering solids through a 0.45 μm PTFE (polytetrafluoroethylene) filter the solution was precipitated by addition to 100 mL diethyl ether (anhydrous) to give a light yellow solid. The solids were isolated by centrifugation and residual impurities were removed using a PD-10 size exclusion column to give 3 mg (60 %) of conjugate 6:EA as a yellow solid.

8:EA: To a 25 mL scintillation vial containing 1.4 mg (0.0015 mmol, 1.4 *eq.*) of metal complex 8 was added 5.5 mg (0.0011 mmol by carboxylic acid) of EA dendrimer. To this was added 0.75 mg (0.0065 mmol, 6.5 *eq.*) each of NHS and HOBt. The solids were dissolved in 0.5 mL DMSO and 1.5 mg (0.0078 mmol, 7.8 *eq.*) of EDC was added and the reaction was allowed to stir overnight at room temperature. After overnight stirring, the solvent was removed *in vacuo* and solids were taken into 5 mL DCM. After filtering solids through a 0.45 μm PTFE filter the solution was precipitated by addition to 100 mL diethyl ether (anhydrous) to give a light yellow solid. The solids were isolated by centrifugation and residual impurities were removed using a PD-10 size exclusion column to give 5.2 mg (91 %) of conjugate 8:EA as a yellow solid.

10:EA: To a 25 mL scintillation vial containing 2.6 mg (0.0028 mmol, 1.2 *eq.*) of metal complex 10 was added 11.5 mg (0.0023 mmol by carboxylic acid) of EA dendrimer. To this was added 1.5 mg (0.005 mmol, 5 *eq.*) each of NHS and HOBt. The solids were dissolved in 0.5 mL DMSO and 2.4 mg (0.005 mmol, 5 *eq.*) of EDC was added and the reaction was allowed to stir overnight at room temperature. After overnight stirring, the solvent was removed *in vacuo* and solids were taken into 5 mL DCM. After filtering solids through a 0.45 μm PTFE filter the solution was precipitated by addition to 100 mL diethyl ether (anhydrous) to give a light yellow solid. The solids were isolated by centrifugation and residual impurities were removed using a PD-10 size exclusion column to give 3.9 mg (31 %) of conjugate 10 as a yellow solid.

Dy-TREN-Dendrimer Conjugation Synthesis (by Dr. William C. Floyd, III):

5:EA: To a 25 mL scintillation vial containing 3.2 mg (0.0039 mmol, 3.5 *eq.*) of metal complex 5 was added 5.5 mg (0.0011 mmol by carboxylic acid) of EA dendrimer. To this was added 0.75 mg (0.065 mmol, 5.9 *eq.*) each of NHS and HOBt. The solids were dissolved in 0.5 mL DMSO and 1.5 mg (0.0078 mmol, 7.1 *eq.*) of EDC was added and the reaction was allowed to stir overnight at room temperature. After overnight stirring, the solvent was removed *in vacuo* and solids were taken into 5 mL DCM. After filtering solids through a 0.45 μm PTFE filter the solution was precipitated by addition to 100 mL diethyl ether (anhydrous) to give a light yellow solid. The solids were isolated by

centrifugation and residual impurities were removed using a PD-10 size exclusion column to give 4.2 mg (76 %) of conjugate 5:EA as a yellow solid.
7:EA: To a 25 mL scintillation vial containing 2.8 mg (0.003 mmol, 1.3 *eq.*) of metal complex 7 was added 12.5 mg (0.0025 mmol by carboxylic acid) of EA dendrimer. To this was added 1.5 mg (0.013 mmol, 5 *eq.*) each of NHS and HOBt. The solids were dissolved in 0.5 mL DMSO and 2.4 mg (0.0125 mmol, 5 *eq.*) of EDC was added and the reaction was allowed to stir overnight at room temperature. After overnight stirring, the solvent was removed *in vacuo* and solids were taken into 5 mL DCM. After filtering solids through a 0.45 μm PTFE filter the solution was precipitated by addition to 100 mL diethyl ether (anhydrous) to give a light yellow solid. The solids were isolated by centrifugation and residual impurities were removed using a PD-10 size exclusion column to give 6.1 mg (49 %) of conjugate 7:EA as a yellow solid.
9:EA: To a 25 mL scintillation vial containing 2.0 mg (0.002 mmol, 1.8 *eq*.) of metal complex 9 was added 5.5 mg (0.0011 mmol by carboxylic acid) of EA dendrimer. To this was added 0.75 mg (0.065 mmol, 5.9 *eq.*) each of NHS and HOBt. The solids were dissolved in 0.5 mL DMSO and 1.5 mg (0.0078 mmol, 7.1 *eq.*) of EDC was added and the reaction was allowed to stir overnight at room temperature. After overnight stirring, the solvent was removed *in vacuo* and solids were taken into 5 mL DCM. After filtering solids through a 0.45 μm PTFE filter the solution was precipitated by addition to 100 mL diethyl ether (anhydrous) to give a light yellow solid. The solids were isolated by centrifugation and residual impurities were removed using a PD-10 size exclusion column to give 4.6 mg (83 %) of conjugate 9. Although repeated many times conjugation higher than one complex per dendrimer was never achieved due to low solubility.
Cell Culture for Dendrimer Conjugates: HeLa cells were purchased from American Type Culture Collection (ATTC) and plated by the Molecular and Cell Biology Cell Culture Facility at University of California, Berkeley, to 10,000 cells per well. Control samples used were the live and dead cells on each plate, the esteramide dendrimer, the polylysine dendrimer, and Gd-DTPA, a commercial MRI contrast agent. Lanthanide MRI samples tested with dendrimers were 5-10:EA. The Gd^{III} conjugates were previously studied and determined to be nontoxic at similar concentrations. Solutions were made in the concentration of 1.0 mg/mL in Dulbecco's modification of Eagle's Media (DMEM, with glucose and 10% fetal bovine serum (FBS). Dilutions were made on one plate at the rate of two-fold per well, for eight total dilutions and a final concentration of 0.05 mg/mL of sample. These solutions were transferred in 100 μL dilutions onto HeLa cells, which were already in 100 μL of media. These samples were incubated for 72 h at 37 °C and 5% CO_2. After 72 h, 40 μL of thiazolyl blue tetrazolium bromide (98%) was added for a MTT assay at 2.9 mg/mL. These samples were incubated for 30 min at 37 °C and 5% CO_2. After 30 min, the cells were aspirated and 200 μL of DMSO added, followed by 25 μL of pH 10.5 glycine buffer (100 mmol glycine and 100 mmol salt). Absorbance was measured at 570 nm on a Molecular Devices plate reader and cytotoxicity determined based on blank live cells and starved cells (terminated by denying media). All results were repeated in triplicate and the average reported.
Inductively Coupled Plasma- Optical Emission Spectroscopy (ICP-OES): ICP-OES was performed on a Perkin Elmer Optima 7000 DV. Samples for analysis were diluted in 2%

(v/v) nitric acid in Millipore water using plastic or EDTA washed glassware. Gd^{III}, Yb^{III}, and Dy^{III} standards were prepared in 2% (v/v) nitric acid/Millipore water (in plastic or EDTA washed glassware) with concentrations between 0.01 μg/mL and 10 μg/mL.

Relaxivity Studies: T_2 measurements were performed on a Bruker mq60 minispec relaxometer. T_2 was determined at 60 MHz (1.41 T) using an inversion recovery pulse sequence. Temperature controlled at 37 °C using a Julabo F25 circulating water bath. Each sample was analyzed by ICP-OES for exact Gd^{III}, Yb^{III}, and Dy^{III} concentration. The inverse of the transverse relaxation time of each sample ($1/T_2$, s^{-1}) was plotted against Gd^{III}, Yb^{III}, and Dy^{III} concentration and fit by linear regression ($R^2 > 0.99$). Relaxivity analyses were performed in triplicate. Samples were vortexed prior to analysis to break up potential aggregation of complexes. Instrument Parameters: 37.0 °C; Scans: 4; Recycle Delay: 18.5 s; Gain: 53; Dummy Shots: 0; Detection mode: real; Bandwidth: Broad, 20,000 kHz; Monoexponential Curve Fitting, Phase Cycling. First Pulse Separation: 5 ms; Number of data points for fitting: 200; Delay sample window: 0.05 ms; Sampling Window: 0.02 ms; Time for Saturation Curve Display: 6 s.

Results and Discussion

Synthesis: Ligands of complexes 5-10 (Figure 1) were synthesized according to preparation of previously reported ligands.[5] The trichloride salts of the lanthanide metals were used for complexation. Metallated complexes were conjugated through their amine side chains to the acid functionalities of the dendrimers using carbodiimide-coupling chemistry (Scheme 1). Due to differences in the amine side chains and solubilities of the complexes, coupling yields to the dendrimer (Table 1) vary substantially between the complexes. Fortunately, coupling yields for higher performing complexes tend to be closer to or at the theoretical maximum of eight complexes per dendrimer, although a strict correlation is not observed. Coupling yields also appear to be dependent on complex solubility, as some of these are sparingly soluble even in DMSO. It is also possible that some of these complexes possess metal-amine or other intermolecular bonding, which could attenuate the nucleophilicity of the side chain amines.

Conjugates were characterized by size exclusion chromatography (SEC), DLS, relaxivity measurements and inductively coupled plasma optical emission spectroscopy (ICP-OES). SEC showed that while the dendrimer itself has no UV activity, after conjugation to metal complexes UV peaks corresponding to a 40 kDa polymer are observed. The UV peaks of the complexes are also observed to migrate from the small molecule region (22-28 minutes, data not shown) to a region corresponding to a 40 kDa macromolecule (15 minutes) upon conjugation to the polymer, although an oscillating system peak (21-24 min) and toluene reference peak (26 minutes) are still observed. The UV-active polymer peak also corresponds to the refractive index (RI) trace of the polymer (Figures 4 and 5). A peak observed at 18 minutes corresponding to a 5 kDa polymer can also be observed in the RI traces, and this corresponds to a small amount of linear PEG remaining from dendrimer synthesis. The end groups of this PEG are capped with an methyl group (to render it inert) before introduction of the metal chelates, which prohibits the PEG from interfering with coupling reactions.

Relaxivity: T_2 relaxivity was evaluated in a 1.41 T (60 MHz) relaxometer at 37.0 °C to ensure clinically relevant conditions were used for analysis. Accounting for diamagnetic solvent character, per Ln^{III} relaxivity was determined by the equation $1/T_{i,obs} = 1/T_{i,d} + r_i$ [M] (i = 1, 2). From the relaxation time (T_1 or T_2) observed (s^{-1}) via water relaxivity, the relaxation time of the solvent (s^{-1}) was subtracted. The concentration of the metal (μmol) was determined precisely by inductively coupled plasma- optical emission spectroscopy (ICP-OES) on each sample. Relaxivity (r_1 for T_1 relaxivity; r_2 for T_2 relaxivity) is therefore reported in $mM^{-1}s^{-1}$.

While high relaxivities are reported for T_2 (Table 1), trends for T_2 relaxivity did not follow those for T_1 relaxivity. The HOPO – esteramide dendrimer conjugates show remarkably short T_2 relaxation times. The r_2 of the Gd-TREN-bis-1,2-HOPO-TAM-ethylamine esteramide dendrimer complex (4:EA) was the largest reported in this study, with per dendrimer relaxivity of 374 $mM^{-1}s^{-1}$. In previous work, the 1,2-HOPO complexes have been inferior to the (1-Me)-3,2-HOPO for T_1 imaging regardless of the chelator linking cap, other functionalizing, or solubilizing moieties attached.[5-10] However, T_2 is more dependent on the outer-sphere water molecule interactions than T_1,[1,3] favoring the 1,2-HOPO complex. This is because, due to changes in pK_a values between the 1,2-HOPO and the (1-Me)-3,2-HOPO, outer-sphere water interactions are more favorable in the 1,2-HOPO as opposed to the (1-Me)-3,2-HOPO. A similar phenomenon, the impact of pK_a on outer-sphere interactions, has been observed by measuring entropic considerations of proline by infrared photodissociation (IRPD) spectroscopy and kinetics.[18]

Due to their decreased paramagnetism, Dy^{III} and Yb^{III} TREN-bis-(1-Methyl-3,2)-HOPO-TAM complexes (5:EA, 7:EA, 9:EA and 6:EA, 8:EA, 10:EA) conjugated to the EA dendrimer did not produce r_2 values as high as those obtained from comparable Gd^{III} complexes. The HOPO agents developed in this study are still of interest for alternative imaging properties as Dy^{III} has potential as a cerebral perfusion imaging agent[21,22] and Yb^{III} has potential as a bimodal T_2 and near infrared imaging agent, allowing for the simultaneous imaging of tissue by two independent methods. Dy^{III} has the ability to transiently influence lingering magnetic susceptibility of tissues as it travels through the body, which could provide an interesting alternative to using iron oxide nanoparticles as agents of magnetic susceptibility. Generally Yb^{III}-HOPO agents preformed better than Dy^{III}-HOPO MRI-CAs (Table 1). Due to its near IR imaging capabilities,[23-24] Yb^{III} has potential for imaging of tumors being surgically removed, as these are often close to the tissue surface during this process. Additionally, with low r_1 values, these complexes have a much larger r_2/r_1 ratio, than that of Gd^{III} complexes.

Cytotoxicity: Suitability of conjugates for further testing as potential contrast agents was determined by cultured cell cytotoxicity studies by MTT assay. Up to 5.0 mg/mL (0.2 mM Gd^{III}), the highest concentration evaluated, cytotoxicity was not observed to HeLa cells over 72 h at 37.0 °C and 5 % CO_2. The esteramide and polylysine dendrimers have exhibited low toxicity in mice[22] and have excellent biocompatibility and high solubility. Biodistribution has been conducted on Gd-TREN-bis-3,2-HOPO-TAM moieties with similar functionalities.[25]

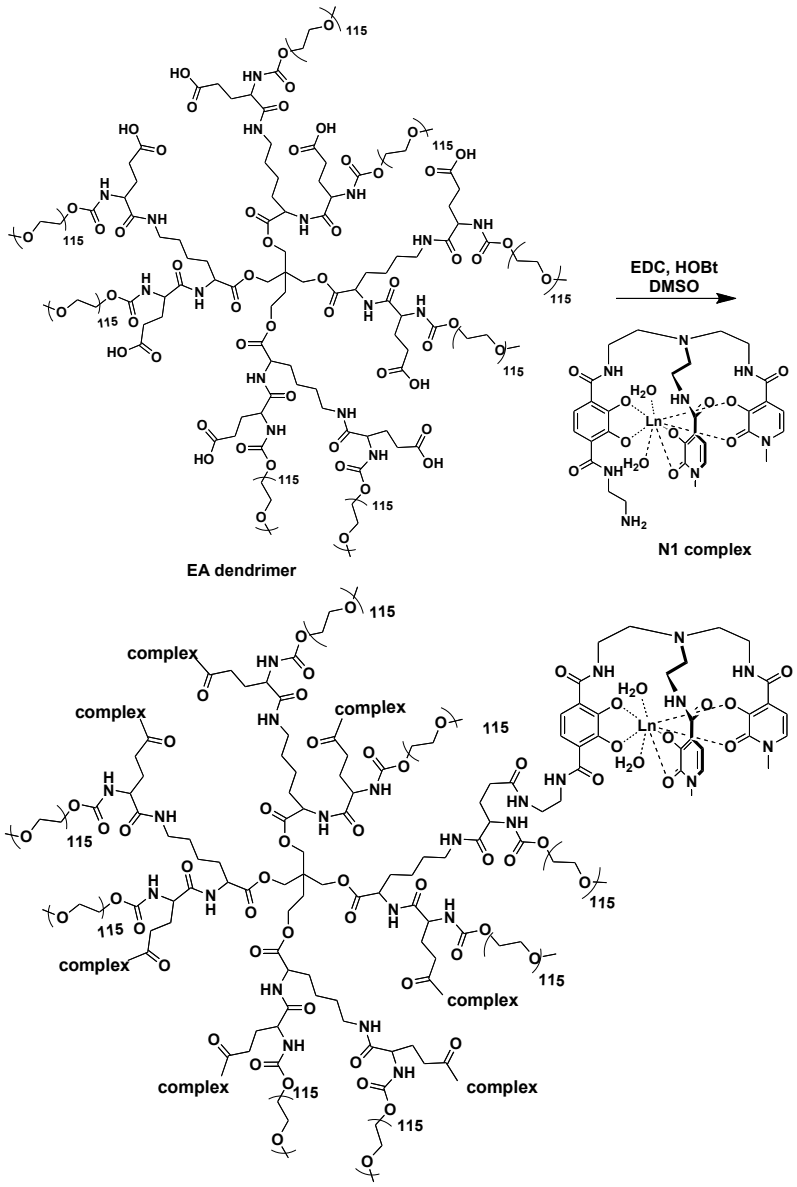

Figure 1. Metalated EA dendrimer conjugates were synthesized through carbodiimide coupling with the precomplexed ligand in DMSO. Coupling to the PLL dendrimer was carried out similarly.

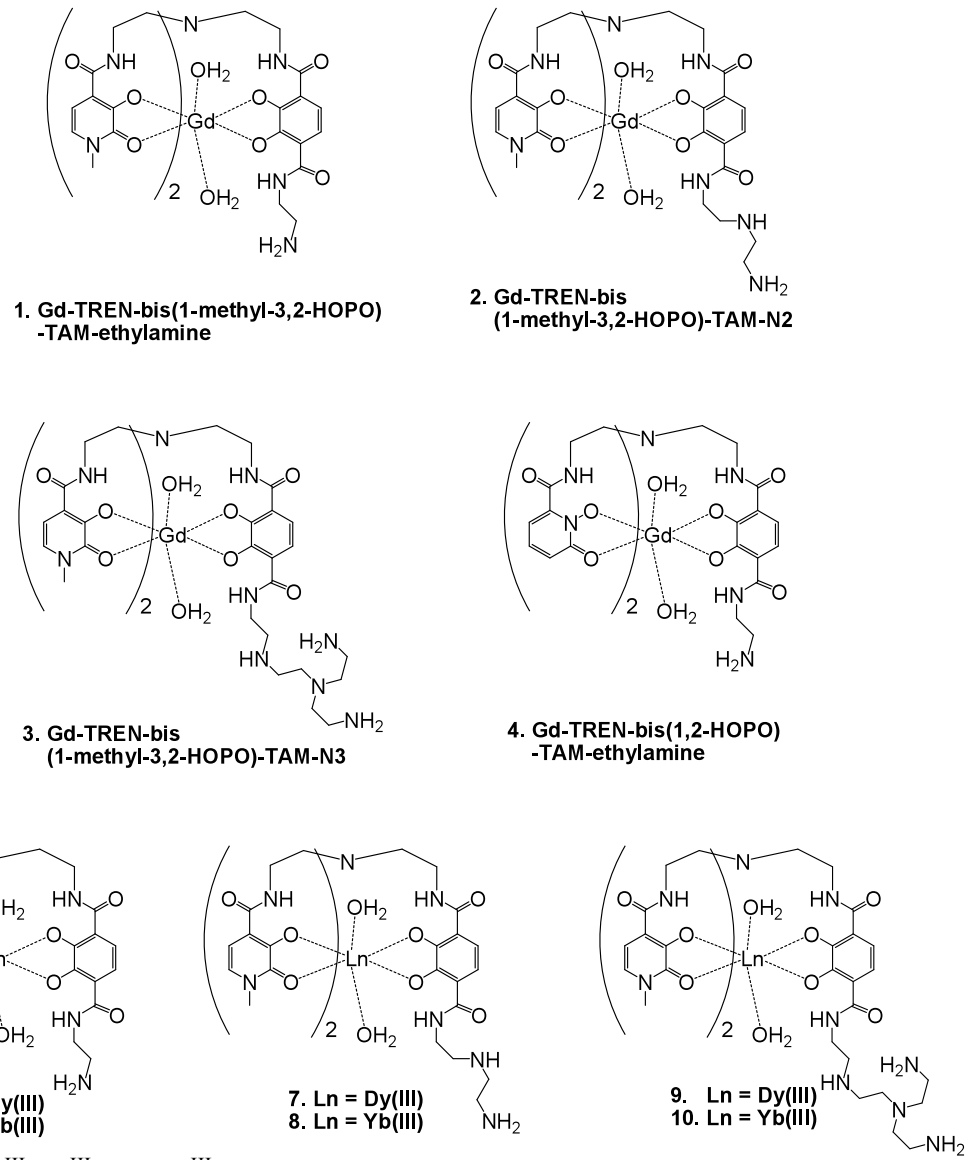

Figure 2. Gd^{III} Dy^{III} and Yb^{III} contrast agents with fast water exchange, high *q* values, and high thermodynamic stability.

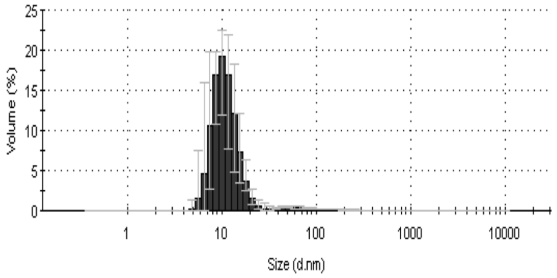

Figure 3. DLS of 8:EA in PBS buffer, showing an average dendrimer diameter of 10 nm. Aggregation is low or not present.

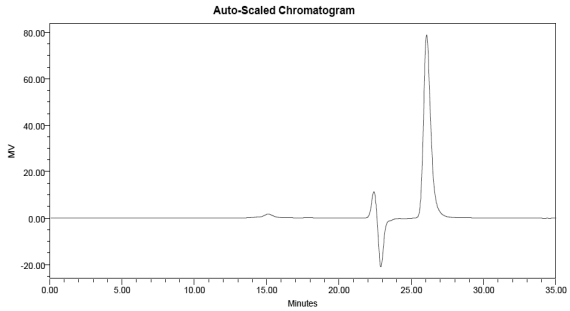

Figure 4. RI Trace of 8:EA. The polymeric conjugate appears at 15 minutes. The toluene reference peak (26 minutes) and system peak oscillation (22-24 min.) are also visible.

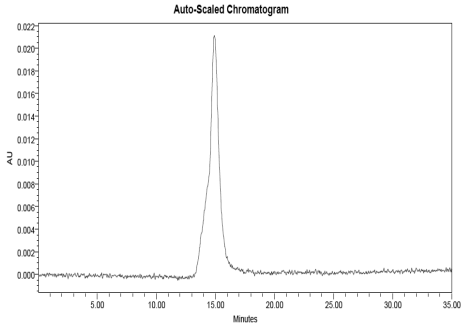

Figure 5. UV-Vis trace of 8:EA. A large molecular weight molecule (15 minutes, corresponding to 40 kDa) is UV active, indicating conjugation of the HOPO-TAM ligands to the non-UV active dendrimer. Given the binding affinity of the N2 ligand to Yb^{III}, this serves as a strong indication that the multiple N1 complexes are bound to the dendrimer, which can be quantified by peak area and separately confirmed by ICP-OES.

Table 1. Comparison of the per lanthanide T_2 relaxivity ($mM^{-1}s^{-1}$) of the prototypes measured in this study at physiological conditions (37.0 °C, 60 MHz) with associated error (in parentheses), as well as the average complex loading per dendrimer and resulting total relaxivity per dendrimer.

Conjugate	T_2 relaxivity/ ionic ($mM^{-1}s^{-1}$)	Complexes/Dendrimer	T_2 relaxivity/ dendrimer
1:EA	42.4(16)	6	254.4
2:EA	35.1(4)	2.9	101.79
3:EA	23.4(4)	3	70.2
4:EA	46.8(8)	8	374.4
5:EA	14.1(4)	6	84.6
6:EA	23.0(2)	2	46
7:EA	5.5(4)	5	27.5
8:EA	12.2(12)	7	85.4
9:EA	2.2(1)	<1	<2.2
10:EA	5.6(8)	6	33.6
1:PLL	38.1(6)	4.5	171.45

Conclusions

T_1 MRI is currently a more commonly employed imaging modality than T_2 in medicine. However, due to changes in field strength and toxicity concerns, T_2 contrast agents are a viable alternative. In this work we have described the synthesis of dendrimer based T_2 lanthanide MRI probes with high biocompatibility and relaxivity values. Due to the high relaxivities obtained, these agents may be promising candidates for future investigation into lanthanide T_2 imaging.[26]

References

1) Laurent, S.; Forge, D.; Port, M.; Roch, A.; Robic, C.; Elst, L. V.; Muller, R. N. Magnetic iron oxide nanoparticles: synthesis, stabilization, vectorization, physicochemical characterizations, and biological applications. *Chem Rev.* **2008**, *108*, 2064–2110.

2) Port, M.; Idee, J. M.; Medina, C.; Robic, C.; Sabatou, M.; Corot, C. Efficiency, thermodynamic and kinetic stability of marketed gadolinium chelates and their possible consequences: a critical review. *Biometals*. **2008**, *21*, 469-490.

3) Caravan, P. Protein-targeted gadolinium-based magnetic resonance imaging (MRI) contrast agents: design and mechanism of action. *Acc. Chem. Res*. **2009**, *42*, 851-862.

4) Bulte, J. W. M.; Kraitchman, D. L. Iron oxide MR contrast agents for molecular and cellular imaging. *NMR Biomed.* **2004,** *17*, 484–499.

5) Pierre, V. C.; Botta, M.; Aime, S.; Raymond, K. N. Substituent effects on Gd(III)-based MRI contrast agents : optmizing the stability and selectivity of the complex and the number of coordinated water molecules. *Inorg. Chem.* **2006**, *45,* 8355-8364.

6) Werner, E. J.; Kozhukh, J.; Botta, M; Moore, E. G.; Avedano, S.; Aime, S.; Raymond K. N. 1,2-Hydroxypyridonate/Terephthalamide complexes of gadolinium(III): synthesis, stability, relaxivity, and water exchange properties. *Inorg. Chem.* **2009**, *48*, 277-286.

7) Werner, E. J.; Avedano, S.; Botta, M.; Hay, B. P.; Moore, E. G.; Aime, S.; Raymond, K. N. Highly soluble tris-hydroxypyridonate Gd(III) complexes with increased hydration number, fast water exchange, slow electronic relaxation, and high relaxivity. *J. Am. Chem. Soc*. **2007**, *129*, 1870-1871.

8) Hooker, J. M.; Kovacs, E. W.; Francis, M. B. Interior surface modification of bacteriophage MS2. *J. Am. Chem. Soc.* **2004**, *126*, 3718-3719.

9) Xu, J.; Franklin, S. J.; Whisenhunt, Jr., D. W.; Raymond, K. N. Gadolinium complex of tris[(3-hydroxy-1-methyl-2-oxo-1,2-didehydropyridine-4-carboxamido)ethyl]-amine: a new class of gadolinium magnetic resonance relaxation agents. *J. Am. Chem. Soc.* **1995**, *117*, 7245-7246.

10) Werner, E. J.; Datta, A.; Jocher, C. J.; Raymond, K. N. High-relaxivity MRI contrast agents: where coordination chemistry meets medical imaging. *Angew. Chem. Intl. Ed.* **2008**, *47*, 8568-8580.

11) Ali, M.; Woods, M.; Caravan, P.; Opina, A. C. L.; Spiller, M.; Fettinger, J. C.; Sherry, A. D. Synthesis and relaxometric studies of a dendrimer-based pH-responsive MRI contrast agent. *Chem.-Eur. J.* **2008,** *14,* 7250-7258.
12) Floyd, III, W. C.; Klemm, P. J.; Smiles, D. E.; Kohngruber, A. C.; Pierre, V. C. Mynar, J. L.; Fréchet, J. M. J.; Raymond, K. N. Conjugation effects of various linkers on Gd(III) MRI contrast agents with dendrimers: optimizing the hydroxypyridinonate (HOPO) ligands with nontoxic, degradable (EA) dendrimers for high relaxivity. *J. Am. Chem. Soc.* **2011**, *133*, 2390-2393.
13) Datta, A.; Hooker, J. M.; Botta, M.; Francis, M. B.; Aime, S.; Raymond, K. N. High relaxivity gadolinium hydroxypyridonate-viral capsid conjugates: nanosized MRI contrast agents. *J. Am. Chem. Soc.* **2008,** *130,* 2546-2552..
14) Song, Y.; Xu, X.; MacRenaris, K. W.; Zhang, X-Q.; Mirkin, C. A.; Meade, T. J. Multimodal gadolinium-enriched DNA-gold nanoparticle conjugates for cellular imaging. *Angew. Chem. Intl. Ed.* **2009**, *48,* 9143-9147.
15) Manus, L. M.; Mastarone, D. J.; Zhang, X. Q.; Waters, E. A.; MacRenaris, K. W.; Parigi, G.; Luchinat, C.; Ho, D.; Meade, T. J. Gd(III)-Nanodiamond conjugates for MRI contrast enhancement.*Nano Lett.* **2010**, *10*, 484-489.
16) van der Poll, D. G.; Kieler-Ferguson, H. M.; Floyd III, W. C.; Guillaudeu, S. J.; Jerger, K.; Szoka, F. C.; Fréchet, J. M. J. Design, synthesis, and biological evaluation of a robust, biodegradable dendrimer. *Bioconj. Chem.* **2010**, *21,* 764-773.
17) Fox, M. E.; Szoka, F. C.; Fréchet, J. M. J. Soluble polymer carriers for the treatment of cancer : the importance of molecular architecture. *Acc. Chem. Res.* **2009**, *42*, 1141-1151.
18) Greenwald, R. B.; Conover, C. D.; Choe, Y. H. Poly(ethylene glycol) conjugated drugs and prodrugs: a comprehensive review. *Crit. Rev. Ther. Drug. Carrier. Syst.* **2000**, *17*, 101-161.
19) Matsumura, Y.; Maeda, H. A new concept for macromolecular therapeutics in cancer chemotherapy: mechanism of tumoritropic accumulation of proteins and the antitumor agent smancs *Cancer Res*. **1986**, *46*, 6387-6392.
20) Lee, C. C.; Yoshida, M.; Fréchet, J. M. J.; Dy, E. E.; Szoka, F. C. In vitro and in vivo evaluation of hydrophilic dendrionized linear polymers. *Bioconj. Chem*. **2005,** *16*, 535-541.
21) Rocklage, S. M.; Watson, A. D. Chelates of gadolinium and dysprosium as contrast agents for MR imaging. *J. Magn. Res. Imaging*. **1993**, *3*, 167-178.
22) Weissleder, R.; Ntziachristos V. Shedding light onto live molecular targets. *Nat. Med*. **2003,** *9*, 123–128.
23) Faulkner, S.; Pope S. J. A.; Burton-Pye, B. P. Lanthanide complexes for luminescence imaging applications. *Appl. Spectrosc. Rev.* **2005**, *40*, 1–31.
24) Moore, E. G.; Xu, J.; Dodani, S. C.; Jocher, C. J.; D'Aleo, A.; Seitz, M.; Raymond, K. N. 1-Methyl-3-hydroxy-pyridin-2-one complexes of near infra-red emitting lanthanides: efficient sensitization of Yb(III) and Nd(III) in aqueous solution.*Inorg Chem.* **2010,** *49,* 4156-4166.
25) Thompson, M. K.; Misselwitz, B.; Tso, L. S.; Doble, D. M. J.; Schmitt-Willich, H.; Raymond, K. N. In vivo evaluation of the gadolinium hydroxypyridonate chelates:

initial experience as contrast media in magnetic resonance imaging. *J. Med. Chem*. **2005**, *48*, 3874-3877.
26) Klemm, P. J.; Floyd, III, W. C.; Andolina, C. M.; Fréchet, J. M. J.; Raymond, K. N. Conjugation to biocompatible dendrimers increases lanthanide T2 relaixivity of hydrosypyridinone (HOPO) complexes for magnetic resonance imaging (MRI). *Eur. J. Inorg. Chem.* **2012**, *2012*, 2108-2114.

Chapter 5 – Improved Per-Particle Relaxivity through Silica Mesoparticle Conjugation

Abstract

Particle-based magnetic resonance imaging (MRI) contrast agents have been the focus of recent research, primarily due to the possibility of preparing multimodal particles capable of simultaneously targeting, imaging, and treating specific biological tissues in vivo. In addition, particle-based MRI contrast agents often have greater sensitivity than commercially available, soluble agents due to decreased molecular tumbling rates following surface immobilization, leading to increased relaxivities. Mesoporous silica particles are particularly attractive substrates due to their large internal surface areas. In this study, we immobilized a unique phosphonate-containing ligand onto mesoporous silica particles with a range of pore diameters, pore volumes, and surface areas, and Gd(III) ions were then chelated to the particles. Per-Gd(III) ionic relaxivities ranged from ~2 to 10 $mM^{-1}s^{-1}$ (37 °C, 60 MHz), compared to 3.0−3.5 $mM^{-1}s^{-1}$ for commercial agents. The large surface areas allowed many Gd(III) ions to be chelated, leading to per-particle relaxivities of 3.3×10^7 $mM^{-1}s^{-1}$, which is the largest value measured for a biologically suitable particle.

Introduction

Interest in improved MRI resolution and diagnosis[1-8] has motivated research into new ligands and hybrid materials as components in new contrast agents. Gd(III) chelators have been conjugated to a variety of scaffolds,[9] including nanoparticles,[10-12] dendrimers,[13-14] proteins,[15-16] viral capsids,[17] silica particles,[18-21] and zeolites, as well as other hybrid materials[22]. Recent reports have shown that grafting Gd(III) chelates onto a solid support can provide a highly efficient imaging agent with a large per-Gd(III) relaxivity and also delivers large quantities of the contrast agent to a single location through surface modification with tissue-targeting biomolecules.[19-21, 23] Mesoporous materials have shown much promise in the field, as their large surface areas allow many Gd(III) chelators to be functionalized onto each particle. Mesoporous materials have also been shown to increase the sensitivity of MR probes *in vivo*.[19-21] An important feature of these materials is the ability to control water exchange to the metal center, due to the porous nature of the support. Control of water exchange is important because it is directly related to relaxivity. The relaxivities of commercial complexes are often restricted by slow water exchange.

Lanthanide ions readily complex with carboxylates, hydroxypyridinones,[24] and alkoxides.[25] Many studies have illustrated the use of phosphorus-containing ligands to sequester Ln(III) ions,[26-32] and diphosphonate ligands have been shown to be efficient materials for the removal of lanthanide ions over a range of pH values.[29-32] The ligand imidodi(methanediphosphate) (NDP2) has been shown to be a highly efficient Gd(III) chelator, even compared to the diethylenetriamine pentaacetate (DTPA) ligand used in

the commercial agent Magnevist.[29] In designing a solid-based contrast agent, an additional benefit of using NDP2 as a Gd(III) ligand is that it can easily be appended onto silica supports. Our procedure for modifying silica particles was similar to that described by Shkrob et al., who described modifying the surface through reaction of surface silanols with aminopropyl triethoxysilane followed by reaction with methylene bis-(phosphonic dichloride) in the presence of triethylamine (Scheme 1).[29] Recent reports have shown that grafting Gd(III) chelates onto a solid support can provide a highly efficient imaging agent, which has not only increased per Gd(III) relaxivities, but can also deliver large quantities of contrast agents to a single location.

Experimental Procedure

Synthesis and Characterization of Mesoporous Silica Particles (by Alexandra K. Duncan). Cetyltrimethylammonium bromide (CTAB), $GdCl_3 \cdot 6H_2O$, and tetraethyl orthosilicate (TEOS), (3-aminopropyl)triethoxysilane (APTES), and methylene-bis(phosphonic dichloride) were purchased from Sigma Aldrich and used without further purification. N2 Physisorption measurements were obtained on a Micromeritics Tristar 2400. A JEOL JSM 6060 Scanning Electron Microscope (SEM) was used to determine particle size and morphology (Figure 1).

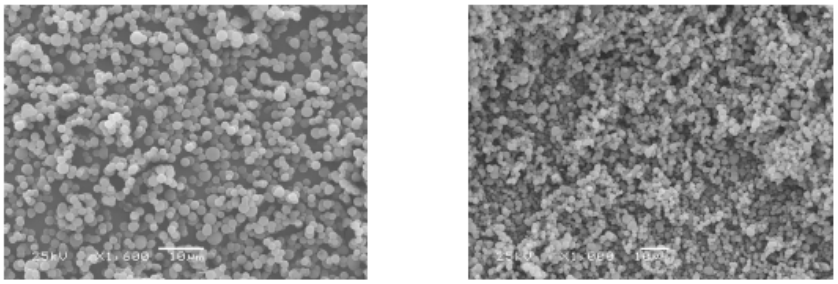

Figure 1. Representative SEM of 1 post-modification (left) and 2 post-modification (right).

Inductively Coupled Plasma. Optical Emission Spectroscopy (ICP-OES) was performed on a Perkin Elmer Optima 7000 DV. Complexed mesoporous silica particles were digested and diluted in 1% (v/v) hydrofluoric acid in Millipore water in EDTA washed glassware for analysis of gadolinium and silica content. Gadolinium standards were prepared (in EDTA washed glassware) in 2% (v/v) nitric acid/Millipore water from commercial ICP standards with concentrations between 0.01 and 10.0 µg/mL. Exact gadolinium concentration was measured in six times and used for relaxivity analysis (µm). Silica standards were prepared (in EDTA washed glassware) in 1% (v/v) hydrofluoric acid/Millipore water from commercial ICP standards.

Synthesis of APMS, (by Alexandra K. Duncan). CTAB (18 g), water (400 mL) concentrated HCl (37.5 mL, 36.5 wt%), and ethanol (140 mL) were vigorously stirred at 0 ˚C until the surfactant was dissolved. TEOS (40 mL) was then added while stirring. After 5 min, NaF (0.5 M in water, 47.5 mL) was added and stirring was continued until

the mixture became turbid (~ 2 min). The mixture was then quickly transferred to a Teflon bottle and heated in a 100 ˚C oven for 42 min. The resulting precipitate was cooled for 15 min in an ice bath, collected by vacuum filtration, and dried under vacuum for subsequent steps. Calcination at 550 ˚C for 6 hrs under air to produce APMS with open pores.

Synthesis of Gd-exchanged APMS (no ligand) (by Alexandra K. Duncan). Unmodified APMS (0.12 g) was suspended in suspended in sodium acetate buffer (10 mL, 10 mM, pH = 6.5). In a separate flask, $GdCl_3$•6 H_2O (100 mg, 0.27 mmol) was dissolved in deionized water, and this solution was then added to the APMS suspension. The resulting suspension was stirred at room temperature overnight, and the particles were isolated by vacuum filtration and repeatedly washed with the same acetate buffer (4 x 5 mL) and deionized water (3 x 5 mL) before being dried under vacuum.

Inductively Coupled Plasma-Optical Emission Spectroscopy (ICP-OES). Gd standards were prepared (in EDTA washed glassware) in 2% (v/v) nitric acid/Millipore water from commercial ICP standards with concentrations between 0.01 and 10.0 μg/mL. Exact Gd concentration was measured in six times and used for relaxivity analysis (μm).

Relaxivity studies. T_1 and T_2 measurements were performed on a Bruker mq60 minispec relaxometer in buffer H (50 mM HEPES, pH 7.4, 50 mM NaCl, 5% glycerol). T_1 and T_2 were determined at 60 MHz (1.41 T) using an inversion recovery pulse sequence. Temperature of the samples, in Millipore water (pH 6), was controlled at 37.0 °C using a Julabo F25 circulating water bath. Each sample was analyzed by ICP-OES for exact Gd concentration. The inverse of the longitudinal relaxation time of each sample ($1/T_1$, s^{-1}) was plotted against Gd, Mn, and Fe concentration (μM) and fit by linear regression ($R^2 >$ 0.99) to determine the relaxivity (r).

Relaxivity analyses were performed in triplicate and averages reported. Instrument Parameters: Scans: 4; Recycle Delay: 18.5 s; Gain: 53; Dummy Shots: 0; Detection mode: real; Bandwidth: Broad, 20,000 kHz; Monoexponential Curve Fitting, Phase Cycling. First Pulse Separation: 5 ms; Final Pulse separation: 18,500 ms, Number of data points for fitting: 20; Delay sample window: 0.05 ms; Sampling Window: 0.02 ms; Time for Saturation Curve Display: 6 s.

Results and Discussion

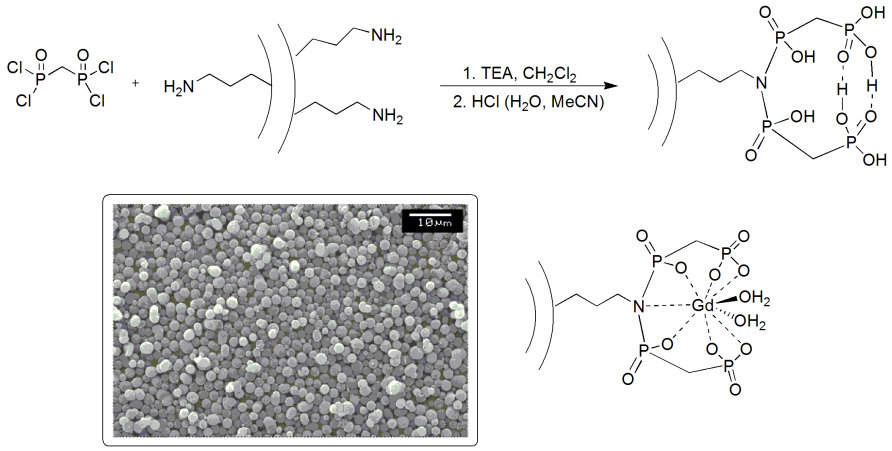

Figure 2. Synthesis and SEM a. Synthesis of surface Functionalized Gd(III)-phosphate on APMS. b. SEM image of surface functionalized APMS.

Mesoporous materials have shown much promise in the future of MRI CA, as their large surface area allows for a loading into the hundreds of millions per particle of Gd(III) chelators. Using increased per Gd(III) relaxivity and higher loading, mesoporous materials have been shown to increase sensitivity of MR probes in vivo. Solvent accessibility to the Gd(III) center is a crucial factor for proton and water exchange with the metal center, which is a property that mesoporous silica particles can capitalize on, allowing solvent access directly to the metal center, regardless of its loading location in the porous particle. Acid-prepared mesoporous silica (APMS) developed in the Landry Laboratory[26] was prepared by polymerization of the silicon alkoxide (TEOS) in the presence of cationic surfactant micelles and additives to control the rates of nucleation and growth (NaF and EtOH). APMS is easily and rapidly synthesized on a multi-gram scale in less than 2 h, has spherical particle morphology, controllable particle size between 1 and 10 µm, and a cost-effective synthesis. Additionally, as with many mesoporous materials, the pore sizes of APMS may also be controlled, either through modification of synthesis conditions or by post-synthetic treatments. APMS has been utilized for a variety of applications including imaging, drug delivery, and catalysis. Through extensive animal studies, APMS has been shown to be a non-toxic material readily taken up by cells, when modified with tetraethylene glycol (TEG) on their external surfaces. These microparticles are also able to deliver chemotherapeutic agents, and can be bifunctionally modified for targeted uptake by cancer cells.

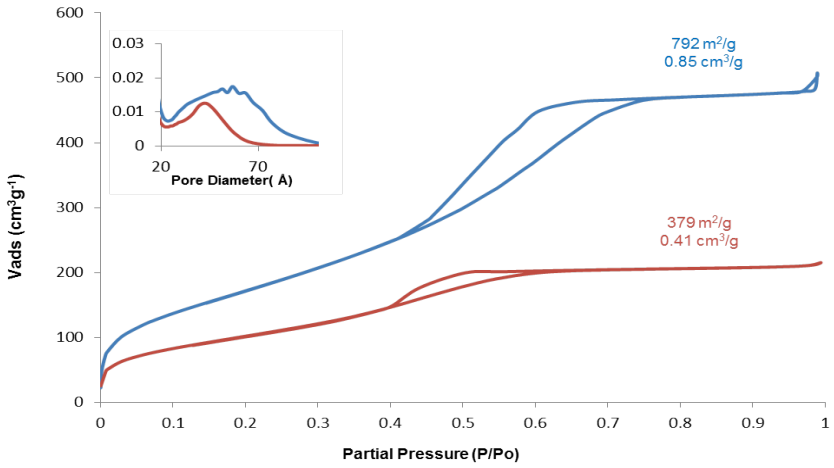

Figure 3. Representative nitrogen physiorption characterization of Conjugate C.

Nitrogen physisorption isotherms indicated that the unmodified APMS was highly porous with average pore diameters ranging from 26 to 45 Å, with Brunauer-Emmett-Teller surface area (SBET) ranging 650 to 800 m^2/g and pore volumes (Vpore) of 0.63 to 0.97 cm^3/g. As expected, a decrease in pore diameter, surface area, and pore volume was observed for the functionalized materials, indicating the ligand was successfully attached to the particle (Figure 2).

The ionic relaxivities of these hybrid materials ranged from 2 to 10 $mM^{-1}s^{-1}$. Variation of pore size, pore volume and surface area offered insight into the design of materials incorporating complexes with tunable relaxivities. The particles exhibited high val-ues for both r_1 and r_2 with relaxivities ranging from 35 million to 130 million $mM^{-1}s^{-1}$.

As many groups have demonstrated,[26-30] relaxivity values for mesoporous silica materials are strongly dependent on pore size. As it is increased in two otherwise indistinguishable systems, relaxivity is increased. Decrease in relaxivity for smaller pore materials are attributed to steric crowding between complexes inside the pores. The increase in steric crowding results in fewer solvent molecules that can be influenced by the paragmagnetic character of the Gd(III) center. Thus, both the inner and outer sphere relaxivity suffer in this scenario causing a decrease in relaxivity.

The rehydroxylation process involves the physical adsorption of water molecules on the silanol groups followed by dissociative chemisorption on the adjacent silanol bridges. The rehydroxylation of the dehydrated siloxane bridges was carried out in attempts to maximally functionalize the complex onto the particles. This process was carried out on the NDP^2 D in comparison to the original material NDP2 C. A decrease in surface area and pore volume was observed upon rehydroxylation, while the pore size retained the original mean value. This observation verified that the number of surface hydroxyls was increased from that of the original sur-face. Increasing the amount of complexes conjugated to the surface could help slow the local motion of the Gd(III) center and thus increase relaxivity by allowing the slowed global motion of the particle to be harnessed more fully by the metal. As expected, an increase in per Gd(III) relaxivity of the rehydroxylated material from 4.6 to 6.0 $mM^{-1}s^{-1}$ was observed. Often, optimal

relaxivities are not obtained, regardless of the size of the macromolecule used due to the flexibility of the complex linker or lack of hydrogen bonding to the metal center, thus the complex still experiences significant local motion.

To ensure that relaxivity measurements were not distorted by any non-specifically associating Gd(III) atoms to the surface of the silica particle, $GdCl_3$ was allowed to non-specifically bind to the particle. Excess Gd(III) in solution (not associated with the particle) was removed through a series of washes. The Gd(III) relaxivities measured in this study had near negligent relaxivities, which were barely over the diamagnetic baseline of the solvent. While not anticipated based on protein studies,[17] this was attributed to the Gd(III) uptake within the surface of the particle. Given this finding, any non-specific binding would negatively affect the results in this study as opposed to enhancing them.

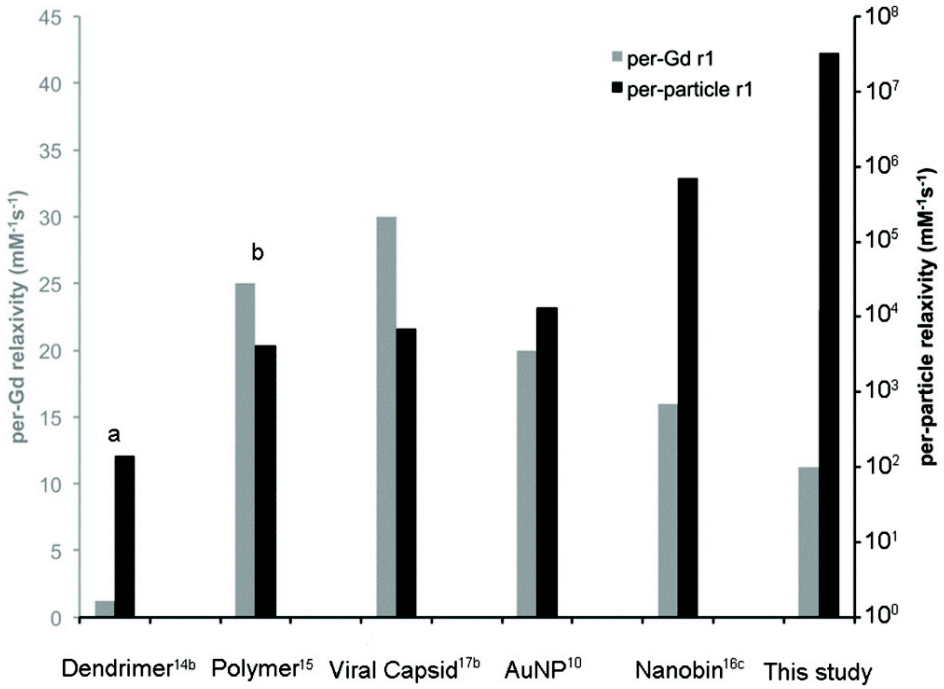

Figure 4. Per-gadoliniuma and per-particle relaxivity (note log scale, conditions at 60 MHz and 37 °C, relaxivities are the highest in their respective publications).

Conclusion

These studies follow the development of new class of biologically suitable mesoporous silica contrast agents. A novel chelating moiety for Gd(III) that capitalizes on the strong binding affinity of phosphate was immobilized onto the silica microparticles surface. These results indicate that an exciting new class of ligands for imaging is inexpensively available for scalable production. APMS are non-toxic, rapidly excreted, and thus serve as an exciting new scaffold for increased MRI applications with per particle relaxivity values up to 130 million $mM^{-1}s^{-1}$.[33]

References

1) Ananta, J.S.; Godin, B.; Sehti, R.; Moriggi, L.; Liu, X.; Serda, R. E.; Krishnamurthy, R,; Bolskar, R. D,; Helm, L.; Ferrari M.; Wilson, L. J.; Decuzzi, P. Geormetrical confinement of Gd-based agents in nanoporous particles enhances T1 contrast. *Nat. Nanotechnol.* **2010***, 5,* 815-821.
2) Wong, W.; Chan, K. W. Gadolinium complexes as MRI contrast agents for diagnosis. In *Rare Earth Coordination Chemistry: Fundamentals and Applications;* Huang, C.; 1st Ed.; Wiley: Asia, **2010**, 407-433. John Wiley & Sons (Asia) **2010**, p. 407-410.
3) Caravan, P.; Ellison, J. J.; McMurry, T. J.; Lauffer, R. B. Gadolinium(III) chelates as MRI contrast agents: structure, dynamics, and applications. *Chem. Rev.* **1999**, *99,* 2293-2352.
4) Major, J. L.; Meade, T. J. Bioresponsive, cell-penetrating, and multimeric MR contast agents. *Acc. Chem. Res.* **2009,** *42,* 893-903.
5) Port, M.; Idee, J. M.; Medina, C.; Robic, C.; Sabatou, M.; Corot, C. Efficiency, thermodynamic and kinetic stability of marketed gadolinium chelates and their possible consequences: a critical review. *Biometals.* **2008,** *21,* 469-490.
6) Raymond, K. N.; Pierre, V. C. Next generation, high relaxivity gadolinium MRI agents. *Bioconj. Chem.* **2005,** *16,* 3–8.
7) Caravan, P. Strategies for increasing the sensitivity of gadolinium based MRI contrast agents. *Chem. Soc. Rev.* **2006,** *35,* 512–523.
8) Werner, E. J.; Datta, A.; Jocher, C. J.; Raymond, K. N. High-relaxivity MRI contrast agents: where coordination chemistry meets medical imaging. *Angew. Chem., Int. Ed.* **2008,** *45,* 8568-8580.
9) Strauch, R. C.; Mastarone, D. J.; Harrison, V. S. R.; Eckermann, A. L.; Parigi, G.; Luchinat, C.; Meade, T. J. Reporter protein-targeted probes for magnetic resonance imaging. *J. Am. Chem. Soc.* **2011,** *133*, 5329-5337.
10) Song, Y.; Xu, X.; MacRenaris, K. W.; Zhang, X.-Q.; Mirkin, C. A.; Meade, T. J. Multimodal gadolinium-enriched DNA-gold nanoparticle conjugates for cellular imaging. *Angew. Chem., Int. Ed.* **2009,** *48,* 9143–9147.
11) Manus, L. M.; Mastarone, D. J.; Waters, E. A.; Zhang, X.-Q.; Schultz-Sikma, E. A.; MacRenaris, K. W.; Ho, D.; Meade, T. J. Gd(III)-Nanodiamond conjugates for MRI contrast enhancement. *Nano Lett.* **2010,** *10,* 484–489.
12) Alric, C.; Taleb, J.; Le Duc, G.; Mandon, C.; Billotey, C.; Meur-Herland, A. L.; Brochard, T.; Vocanson, F.; Janier, M.; Perriat, P.; Roux, S.; Tillement, O. Gadolinium chelate coated gold nanoparticles as contrast agents for both X-ray computed tomography and magnetic resonance imaging. *J. Am. Chem. Soc.* **2008,** *130,* 5908-5915.
13) Reynolds, C. H.; Annan, N.; Beshah, K.; Huber, J. H.; Shaber, S. H.; Lenkinski, R. E.; Wortman, J. A. Gadolinium-loaded nanoparticles: new contrast agents for magnetic resonance imaging. *J. Am. Chem. Soc.* **2000**, *122,* 8940-8945.
14) Floyd, W.C. III; Klemm, P. J.; Smiles, D. E.; Kohlgruber, A. C.; Pierre, V. C.; Mynar, J. L.; Fréchet, J. M. J.; Raymond, K. N. Conjugation effects of various linkers on Gd(III) MRI contrast agents with dendrimers: optimizing the hydroxypyridinonate (HOPO)

ligands with nontoxic, degradable (EA) dendrimers for high relaxivity. *J. Am. Chem. Soc.* **2011,** *133,* 2390-2393.
15) Klemm, P. J.; Floyd, W.C.III; Smiles, D.E.; Fréchet, J. M. J.; Raymond, K. N. Improving T1 and T2 magnetic resonance imaging (MRI) contrast agents through the conjugation of an esteramide dendrimer to whigh water coordination Gd(III) hydroxypyridinone (HOPO) complexes. *Contrast Media & Mol Imaging.* **2012,** *7,* 95-99.
16) Nwe, K.; Diane, M.; Henry, B. L.; Regino, C. A. S.; Brechbiel, M. W. Preparation, characterization, and in vivo assessment of Gd-albumin and Gd-dendrimer conjugates as intravascular contrast-enhancing agents for MRI. *J. Inorg. Biochem.* **2011,** *105*, 722-727.
17) Nwe, K.; Bryant Jr., L. H.; Brechbiel, M. W. Poly(amidoamine) dendrimer based MRI contrast agents exhibiting enhanced relaxivities derived via metal preligation techniques. *Bioconjugate Chem.* **2010,** *21*, 1014-1017.
18) Liepold, L. O.; Abedin, M. J.; Buckhouse, E. D.; Frank, J. A.; Young, M. J.; Doublas, T. Supramolcular protein cage composite MR contrast agents with extremely efficient relaixvity properties. *Nano Lett.* **2009,** *9,* 4520-4526.
19) Shapiro, M. G.; Szablowski, J. O.; Langer, R.; Jasanoff, A. Protein nanoparticles engineered to sense kinase activity in MRI. *J. Am. Chem. Soc.* **2009**, *131,* 2484-2486.
20) Yang, J. J.; Yang, J.; Wei, L.; Zurkiya, O.; Yang, W.; Li, S.; Zou, J.; Zhou, Y.; Wilkins Maniccia, A. L.; Mao, H.; Zhao, F.; Malchow, R.; Zhao, S.; Johnson, J.; Hu, Z.; Krogstad, E.; Liu, Z.-R. Rational design of protein-based MRI contrast agents. *J. Am. Chem. Soc.* **2008,** *130,* 9260-9267.
21) Lee, S.-M.; Song, Y.; Hong, B. J.; MacRenaris, K. W.; Mastarone, D. J.; O'Halloran, T. V.; Meade, T. J.; Nguyen, S. T. Modular polymer-caged nanobins as a theranostic platform with enhanced magnetic resonance relaxivity and pH-responsive drug release. *Angew. Chem. Int. Ed.* **2010,** *49,* 1 – 6.
22) Hooker, J. M.; Datta, A.; Botta, M.; Raymond, K. N.; Francis, M. B. Magnetic resonance contrast agents from viral capsid shells: a comparison of exterior and interior cargo strategies. *Nano Lett.* **2007,** *7,* 2207-2210.
23) Datta, A.; Raymond, K. N. Gd-Hydroxypyridinone (HOPO)-based high-relaxivity magnetic resonance imaging (MRI) contrast agents. *Acc. Chem. Res.* **2009,** *42,* 938–9474.
24) Garimella, P.; Datta, A.; Romanini, D. W.; Raymond, K. N.; Francis, M. B. Multivalent, high-relaxivity, MRI contrast agents using rigid cysteine-reactive gadolinium complexes. *J. Am. Chem. Soc.* **2011,** *133,* 14704-14709.
25) Datta, A.; Hooker, J. M.; Botta, M.; Francis, M. B.; Aime, S.; Raymond, K. N. High relaxivity gadolinium hydroxypyridonate-viral capsid conjugates: nanosized MRI contrast agents. *J. Am. Chem. Soc.* **2008,** *130,* 2546-2552.
26) Steinbacher, J. L.; Lathrop, S. A.; Cheng, K.; Hillegass, J. M.; Kauppinen, R. A.; Mossman, B. T.; Landry, C. C. Gd-labeled microparticles in MRI: in vivo imaging of microparticles after intraperitoneal injection. *Small*. **2010,** *6,* 2678-2682.
27) Liu, G.; Tse, N. M. K.; Hill, M. R.; Kennedy, D. F.; Drummond, C. J. Disordered mesoporous gadolinosilicate nanoparticles prepared using gadolinium based ionic liquid emulsions: potential as magnetic resonance imaging contrast agents. *Aust. J. Chem.* **2011,** *64,* 617-624.
28) Lee, J. E.; Lee, N.; Kim, H.; Kim, J.; Choi, S. H.; Kim, J. H.; Kim, T. Song, I. C.;

Park, S. P.; Moon, W. K.; Hyeon, T. Uniform mesoporous dye-doped silica nanoparticles decorated with multiple magnetite nanocrystals for simultaneous enhanced magnetic resonance imaging, fluorescence imaging, and drug delivery. *J. Am. Chem. Soc.* **2010,** *132,* 552-557.
29) Carniato, F.; Tei, L.; Cossi, M.; Marchese, L.; Botta, M. A chemical strategy for the relaxivity enhancement of Gd-III chelates anchored on mesoporous silica nanoparticles. *Chem.- Eur. J.* **2010,** *16,* 10727-10734.
30) Tu, C.; Ma, X.; Pantazis, P.; Kauzlarich, S. M.; Louie, A. Y. Paramagnetic, silicon quantum dots for magnetic resonance and two-photo imaging of macrophages. *J. Am. Chem. Soc.* **2010,** *132,* 2016-2023.
31) Bridot, J.-L.; Faure, A.-C.; Laurent, S.; Riviere, C.; Billotey, C.; Hiba, B.; Janier, M.; Josserand, V.; Coll, J.-L.; Vander Elst, L.; Muller, R.; Roux, S.; Perriat, P.; Tillement, O. Hybrid gadolinium oxide nanoparticles: multimodal contrast agents for in vivo imaging. *J. Am. Chem. Soc.* **2007,** *129,* 5076-5984.
32) Shao, Y.-Z.; Liu, L.-Z.; Song, S.-Q.; Cao, R.-H.; Liu, H.; Cui, C. Y.; Li, X.; Bie, M. J.; Li, L. *Contrast Media Mol. Imaging.* A novel one-step synthesis of Gd3+-incorporated mesoporous SiO2 nanoparticles for use as an efficient MRI contrast agent. **2011,** *6,* 110-118.
33) Duncan, A. K.; Klemm, P. J.; Raymond, K. N.; Landry, C. C. Silica microparticles as a solid support for gadolinium-phosphonate magnetic resonance imaging (MRI) contrast agents. *J. Am. Chem. Soc.* **2012**, *134*, 8046-8049.

Chapter 6 – Improved Kinetic Stability through *Tt-HNOX* Protoporphyrin IX Incorporation

Abstract

MRI contrast agents are generated using porphyrin substitutions of the H-NOX proteins, proteins typically used as molecular sensors. Heme protein-based MRI contrast agents represent a novel platform to both rationally tune metalloporphyrin properties for unparalleled kinetic stability of metal within the protein, enhanced relaxivities, and provide tightly coordinating frameworks for more effective delivery in biological systems. The proteins described in this chapter display improved properties over commercial small molecule MRI contrast agents and are promising candidates for future biological imaging applications.

Introduction

In Chapter 6, hemoprotein-based scaffolds are used as a platform for the development of novel MRI contrast agents.[1-3] Heme proteins represent readily modifiable frameworks for tuning the properties of metalloporphyrins and enhancing porphyrin bioavailability.[4-5] The Heme Nitric oxide/OXygen-binding (H-NOX) domain from the thermophilic bacterium *Thermoanaerobacter tengcongensis* (*Tt* H-NOX) is an ideal scaffold for hemoprotein-based agents. *Tt* H-NOX is readily modifiable with site-directed mutagenesis and genetically encoded tags.[6,7] Additionally, *Tt* H-NOX is stable under extreme temperatures (>70 °C).[6] Using expression-based method for porphyrin-substitution, the *Tt* H-NOX scaffold was implemented to design a new class of high-relaxivity, high-stability MRI contrast agents.

Experimental Procedure

Porphyrin preparation. All manipulations of the porphyrins were carried out in low light. Mn^{III} protoporphyrin IX (MnPP) was purchased from Frontier Scientific. Initial synthesis attempts of Gd^{III} protoporphyrin IX (GdPP) were carried out through modification of established methods.[8] Briefly, water was removed from a solution of $GdCl_3$ (6 mL, 0.3 mmol, 3 *eq*.) through rotary evaporation. $GdCl_3$ and protoporphyrin IX (50 mg, 0.09 mmol, 1 *eq*.) were refluxed under N_2 in a 2.0 g imidazole melt at 215 °C for 4 h. Reaction progress was monitored by UV-vis spectroscopy.

Plasmids for protein expression (Dr. Michael B. Winter). The gene for *Tt* H-NOX (residues 1-188 of *Tt*Tar4H from *Thermoanaerobacter tengcongensis*) was used in the pCW vector with and without a C-terminal His_6 tag.[7,9]

Protein expression and porphyrin incorporation (Dr. Michael B. Winter). Myoglobin (sperm whale skeletal muscle) was purchased from Sigma. Heme-containing *Tt* H-NOX His_6 was expressed.[7] MnPP and GdPP were incorporated into *Tt* H-NOX constructs during anaerobic protein expression in the RP523 *E. coli* strain[5] with the

following exceptions: Final concentrations of up to 30 μg/mL MnPP and 100 μM $MnCl_2$ were added to *E. coli* cultures to decrease Fe contamination in purified Mn *Tt* H-NOX. A modify recipe for TB media was used for Gd *Tt* H-NOX expression that contained 50 mM HEPES (pH 7.4), instead of phosphate buffer, to prevent metal coordination. The crude GdPP reaction was dissolved in DMSO (~30 mL) and added to the culture immediately prior to induction.

Purification of Mn and Gd Tt H-NOX (Dr. Michael B. Winter). Cell pellets (from 9 L of *E. coli* expression) were slowly thawed using warm water and re-suspended in ~100 mL of buffer A (50 mM TEA or HEPES, pH 7.5, 50 mM NaCl), which also contained 1 mM Pefabloc and DNase I. TEA was used for Mn *Tt* H-NOX, and HEPES was used for Gd *Tt* H-NOX. The resuspended cells were lysed 3 times with an EmulsiFlex-C5 homogenizer (Avestin, Inc.) at 4 ^{o}C between 50,000 and 150,000 psi. The lysate was then heat-denatured at 70 ^{o}C for 30 min using a water bath. All further manipulations were carried out at 4 ^{o}C. The lysate underwent centrifugation with an Optima XL-100K ultracentrifuge (Beckman Coulter, Inc.) for 1 h at 42,000 rpm.

For His_6-tagged Mn and Gd *Tt* H-NOX, the supernatant following ultracentrifugation was applied to a Co column at 1-2 mL/min equilibrated with buffer A. The column was washed with ~10 column volumes of buffer A, followed by ~10 column volumes of buffer A containing 10 mM imidazole at 2 mL/min. The protein was eluted with buffer A containing 150 mM imidazole at 2 mL/min. The flow-through was concentrated using a 5,000 MWCO spin concentrator and stored in small aliquots at –80 ^{o}C. Purity was estimated to be >95% by Coomassie stain following SDS-PAGE.

For non-tagged Mn *Tt* H-NOX, the supernatant was concentrated (~10 mL) and exchanged into buffer B (50 mM HEPES, pH 6.2, 5% glycerol) by gravity using a ~100 mL Sephadex G-25 column. The protein was then applied to a Toyopearl CM-650M cation exchange column (Tosoh Bioscience GmbH) that had been equilibrated with buffer B. The column was washed with 100 mL buffer B, and the protein was eluted with a NaCl gradient from 0% to 100% buffer C (50 mM HEPES, pH 6.2, 500 mM NaCl, 5% glycerol) over 800 mL while 5 mL fractions were collected. The Mn-containing protein was concentrated using a 5,000 MWCO spin concentrator and exchanged into buffer D (50 mM TEA, pH 7.5, 50 mM NaCl, 5% glycerol). Mn *Tt* H-NOX was then stored in small aliquots at –80 ^{o}C. Purity was estimated to be >95% by Coomassie stain following SDS-PAGE.

Mn Tt H-NOX His_6 native nanoelectrospray ionization mass spectrometry and tandem mass spectrometry (Dr. Anthony T. Ivarone). Mass spectra were acquired using an orthogonal acceleration quadrupole time-of-flight (Q-Tof) mass spectrometer equipped with a Z-spray electrospray ionization (ESI) source (Q-Tof Premier, Waters, Milford, MA). Ions were formed directly from aqueous solutions containing micromolar analyte and 50 mM ammonium bicarbonate, using positive-ion nanoelectrospray ionization (nanoESI). NanoESI emitters were pulled from borosilicate glass capillary tubes (1.0 mm outer diameter/0.78 mm inner diameter, Sutter Instruments, Novato, CA) using a Flaming/Brown micropipette puller (Model P-87, Sutter). Approximately 10 μL of the sample solution was added into a nanoESI emitter using a 10 μL microsyringe (Hamilton, Reno, NV). The nanoESI tip was positioned approximately 2 mm from the

sample cone aperture. The electrospray was initiated by gradually increasing the DC potential applied to a platinum wire (0.127 mm diameter, Sigma-Aldrich, St. Louis, MO), which was inserted into the nanoESI emitter to within approximately 2 mm of the tip, until the onset of mass spectral signal. No back pressure or cone gas was used. Instrument parameters during data acquisition were as follows: nanoESI voltage 1.8 kV, sample cone voltage 20 V, extraction cone and ion guide voltages both 4.0 V, source block temperature 80 ºC, accelerating voltage into the argon-filled cell 3 V, first pumping stage (backing) pressure 2 mbar, ion transfer stage pressure 6×10^{-3} mbar, argon-filled cell pressure 8×10^{-3} mbar, TOF analyzer pressure 8×10^{-7} mbar. The TOF analyzer was operated in "V" mode. For tandem mass spectrometry (MS/MS) measurements using collisionally activated dissociation (CAD), the precursor ion of interest was mass-selected using the quadrupole filter and the accelerating voltage into the argon-filled cell was gradually increased, to a final value of 25 V, to achieve precursor ion dissociation. Mass spectra and MS/MS spectra were recorded over a period of 3 min using a 0.95 s scan integration and 0.05 s interscan delay. External mass calibration of the TOF analyzer was performed immediately prior to measurements. Mass spectra were processed using MassLynx software (version 4.1, Waters).

Crystallization of Mn Tt H-NOX (Dr. Michael B. Winter). Crystallization experiments were carried out using Mn^{III} *Tt* H-NOX (non-tagged), and all manipulations were carried out in low light. Protein was exchanged into buffer F (20 mM TEA, pH 7.5) using a PD-10 column and then concentrated to 30 mg/mL using a Vivaspin 500 5,000 MWCO PES spin concentrator. Crystals were grown using sitting drop vapor diffusion in which 1 μL of the protein was mixed with 1 μL of reservoir solution and equilibrated against a 500 μL reservoir of 40% to 42.5% (w/v) polypropylene glycol P400 and 0.1 M BIS-TRIS (pH 6.5) at 20 ^{o}C. Crystals appeared within 24 h and were cryoprotected by soaking them in the precipitant solution supplemented with 10% (v/v) glycerol. The crystals were flash frozen in liquid N_2 for storage.

X-ray data collection and structure solution (Dr. Christine M. Phillips-Piro). X-ray data for Mn *Tt* H-NOX were collected using synchrotron radiation at beamline 8.3.1 at the Advanced Light Source (ALS), Lawrence Berkeley National Laboratory (Berkeley, CA). Diffraction images were collected at 100 K with exposure times of 2.5 s to 3 s with 1º oscillations per frame at a wavelength of $\lambda = 0.97$ Å. Data integration and scaling were performed using the HKL2000 (10) suite. Phases were determined by molecular replacement with Phaser (11) using wild-type *Tt* H-NOX (PDB ID 1U55, molecule A), with water molecules and heme removed, as the search model.

X-ray absorption spectroscopy (Dr. Christine M. Phillips-Piro). To confirm the presence of Mn in the *Tt* H-NOX crystals (and lack of Fe contamination), X-ray absorption spectra were collected at the Mn and Fe K-edges (1.90 and 1.74 Å, respectively) at 100 K using synchrotron radiation as described above.

UV-visible spectroscopy (Dr. Michael B. Winter). Steady-state absorbance measurements were carried out at room temperature in buffer G (50 mM HEPES, pH 7.4, 50 mM NaCl) on a Cary 3E 300 spectrophotometer (Varian).

Inductively coupled plasma-optical emission spectroscopy (ICP-OES). ICP-OES was performed on a Perkin Elmer Optima 7000 DV. Proteins for analysis were digested

and diluted in 2% (v/v) nitric acid in Millipore water in plastic or EDTA washed glassware. Gd, Mn, and Fe standards were prepared (in EDTA washed glassware) in 2% (v/v) nitric acid/Millipore water from commercial ICP standards with concentrations between 0.01 and 10.0 μg/mL. Exact Gd, Mn, and Fe concentration was measured in six times and used for relaxivity analysis (μm).

Relaxivity studies. T_1 and T_2 measurements were performed on a Bruker mq60 minispec relaxometer in buffer H (50 mM HEPES, pH 7.4, 50 mM NaCl, 5% glycerol). T_1 and T_2 were determined at 60 MHz (1.41 T) using an inversion recovery pulse sequence. Temperature of the samples, in Millipore water (pH 6), was controlled at 37.0 °C using a Julabo F25 circulating water bath. Each sample was analyzed by ICP-OES for exact Gd, Mn and Fe concentration. The inverse of the longitudinal relaxation time of each sample ($1/T_1$, s^{-1}) was plotted against Gd, Mn, and Fe concentration (μM) and fit by linear regression ($R^2 > 0.99$) to determine the relaxivity (r) according to the following equation:

$$\frac{1}{T_{n=1,2}} = \frac{1}{T_{(solvent)n=1,2}} + r_{n=1,2}[agent]$$

Relaxivity analyses were performed in triplicate (3 samples, 3 times to report experimental and instrument error) and averages reported. Instrument Parameters: Scans: 4; Recycle Delay: 18.5 s; Gain: 53; Dummy Shots: 0; Detection mode: real; Bandwidth: Broad, 20,000 kHz; Monoexponential Curve Fitting, Phase Cycling. First Pulse Separation: 5 ms; Final Pulse separation: 18,500 ms, Number of data points for fitting: 20; Delay sample window: 0.05 ms; Sampling Window: 0.02 ms; Time for Saturation Curve Display: 6 s.

Plasma stability. The stability of Fe^{III}, Mn^{III}, and Gd^{III} *Tt* H-NOX His_6 were measured in plasma at 37 °C over 24 h.[5] Briefly, the proteins were exchanged into DPBS using a PD10 column. An equal volume of protein (~5 mg/mL by A280) and plasma were incubated at 37 °C, and time points were taken after 0, 1, 3, 6, and 24 h. For each time point, the aliquots were centrifuged for 2 min at 3,000 rpm (665 x *g*), and UV-visible spectra were acquired of the supernatant in DPBS.

Results and Discussion

Relaxivities of ferric proteins. Iron is an inexpensive, abundant earth metal.[12] Although Fe displays lower relaxivities compared to lanthanides, the lower cost and environmental impact of Fe make it a promising candidate for more sustainable contrast agent development.[12,13] In an effort to enhance the relaxivity of Fe, we first evaluated native heme-containing *Tt* H-NOX and myoglobin as potential protein scaffolds for MRI.

UV-visible spectral characterization of ferric Mb and *Tt* H-NOX was carried out to probe the influence of the protein scaffolds on heme electronic properties. The ferric proteins were found to have distinct UV-visible spectra. The spectrum of ferric Mb has a sharp Soret band at 408 nm, whereas *Tt* H-NOX has a broad Soret band at 413 nm and distinct splitting in the α/β region (~500-600 nm) (Figure 1). These data suggest that the protein scaffolds provide unique porphyrin coordination environments. Indeed, examination of the crystal structures of both proteins demonstrates that they have diverse

heme pocket architectures, and the heme groups are in different protein-bound conformations (Figure 2).

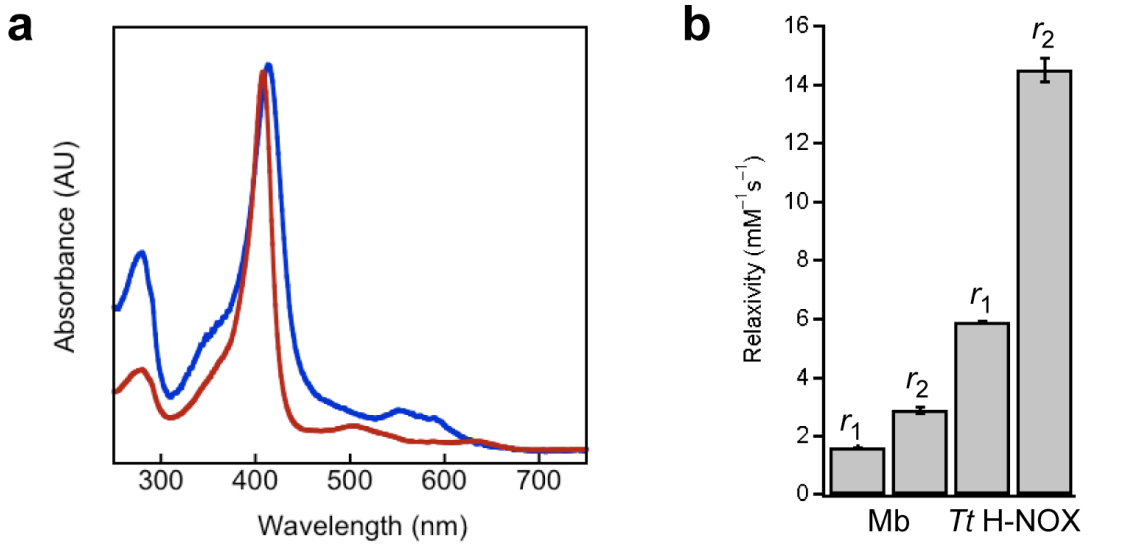

Figure 1. (a) UV-visible spectra of ferric myoglobin (—) and *Tt* H-NOX (—). (b) Relaxivities of ferric myoglobin and *Tt* H-NOX at 37 °C and 60 MHz.

To assess the influence of protein structure on relaxivity, T_1 and T_2 measurements were carried out on the ferric proteins. Mb was found to have T_1 and T_2 relaxivities of 1.6 and 2.9 $mM^{-1}s^{-1}$, respectively. Surprisingly, *Tt* H-NOX displayed much higher T_1 and T_2 relaxivities of 5.9 and 14.5 $mM^{-1}s^{-1}$ (Figure 1 & Table 1). *Tt* H-NOX is a larger protein (~22 kDa vs. ~17 kDa), which could enhance relaxivity by decreasing protein tumbling in solution.[2, 14] Additionally, comparison of reported pK_a values of the heme –OH(H) ligand suggests that it has different protonation states at physiological pH in the proteins (pK_a = 6.8 and 8.95 for *Tt* H-NOX[15] and Mb (16), respectively). In *Tt* H-NOX, the more labile water ligand is favored, which likely enhances relaxivity by undergoing more facile exchange with solvent.

Relaxivities of Mn Tt H-NOX. Due to the enhanced relaxivity of *Tt* H-NOX, we decided to incorporate other metals into the protein scaffold to improve its imaging properties. Mn complexes have been evaluated as potential MRI contrast agents.[17] However, Mn-based complexes have seen only limited clinical use because they suffer from high kinetic lability under physiological conditions.[17,18] Although Mn complexes display lower relaxivities, they have emerged as an important alternative for lanthanide-based agents due to the decreased toxicity of Mn as an endogenous metal ion.[17]

Mn^{III} protoporphyrin IX (MnPP) was incorporated into *Tt* H-NOX during protein expression. Heme contamination was observed by UV-visible spectroscopy following longer induction times, and during expressions with high protein yields (data not shown). However, Mn and Fe-bound protein was readily separated with cation-exchange chromatography using standard protocols (see Experimental Procedures). A UV-visible

spectrum of the purified protein shows two characteristic Mn-based absorption features (376 nm and 474 nm) (Figure 3) that are similar to those reported previously.[19] To further characterize purified Mn *Tt* H-NOX, native ionization mass spectrometry was performed on the intact protein complex. A mass corresponding to the holoprotein was observed (23,695 ± 3 Da; calc: 23,693 Da), and collisionally activated dissociation (CAD) confirmed that the protein was purified MnPP-bound (obs: 615.18 Da; calc: 615.18). Further ICP-OES analysis carried out on the purified protein verified the presence of Mn and no detectible Fe (to pM concentrations).

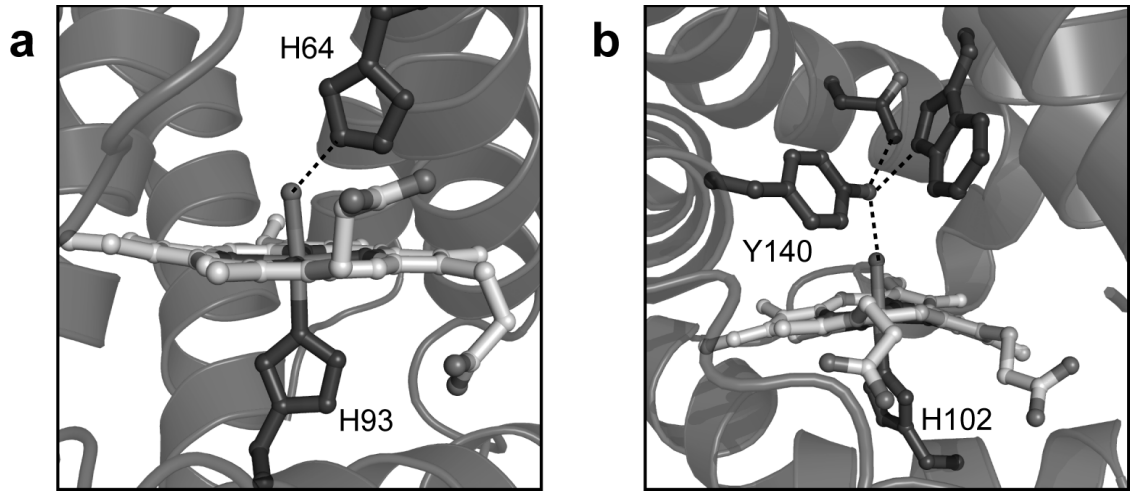

Figure 2. Crystal structures of the ferric forms of **(a)** myoglobin (PDB ID 1A6K) and **(b)** *Tt* H-NOX (PDB ID 1U56). Proximal histidine ligands, –OH(H) ligands, and hydrogen bonding

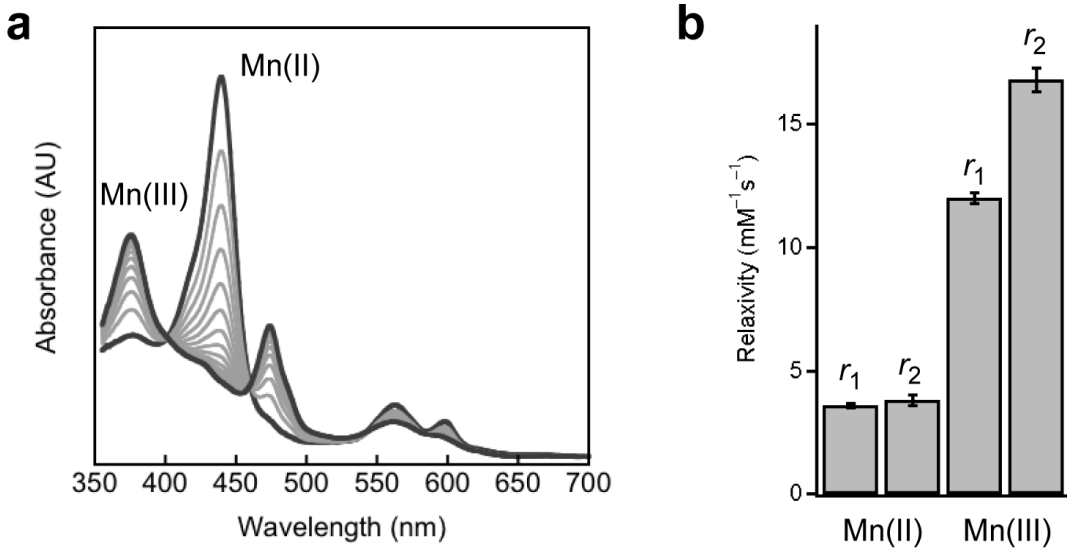

Figure 3. (a) Time-resolved UV-visible spectra of Mn^{II} to Mn^{III} *Tt* H-NOX oxidation in air. (b) Relaxivities of Mn^{II} and Mn^{III} *Tt* H-NOX at 37.0 °C and 60 MHz.

Results and Discussion

T_1 and T_2 relaxivity measurements were performed on Mn *Tt* H-NOX. The Mn^{II} oxidation state was found to not be stable in air (k_{ox} = ~0.069 min^{-1} at 22 °C) (Figure 3), and therefore, relaxivity measurements for Mn^{II} *Tt* H-NOX were conducted under anaerobic conditions. The T_1 and T_2 relaxivities of Mn^{III} *Tt* H-NOX (12.0 and 16.9 $mM^{-1}s^{-1}$, respectively) are much higher than those of the Mn^{II} protein (Figure 3 & Table 1). Notably, the relaxivities of the protein in both oxidation states are higher than MnDPDP, which is the only current clinical Mn-based agent (Table 1).[20]

To provide a molecular understanding for the high relaxivity in Mn^{III} *Tt* H-NOX, a crystal structure of the protein was obtained. Crystals were obtained of Mn^{III} *Tt* H-NOX using sitting-drop vapor diffusion and were found to diffract to 2.15 Å. X-ray absorption spectra collected at the Mn and Fe K-edges confirmed the presence of Mn and no detectable Fe in the protein crystals. Preliminary crystal structure of Mn *Tt* H-NOX was solved in the C_2 space group using molecular replacement with the structure of wild-type *Tt* H-NOX as the search model (PDB ID 1U55). Initial electron density corresponding to Mn was observed in the protein heme pocket.

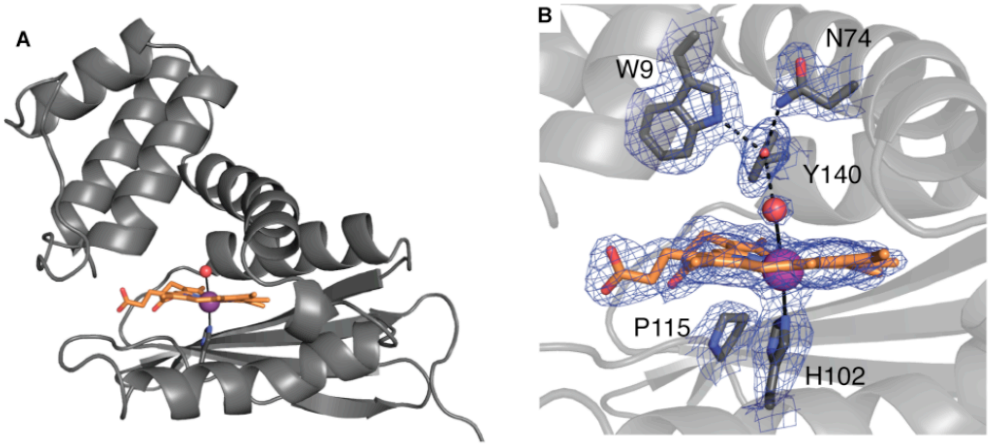

Figure 4. Figure 3. X-ray crystal structure of Mn(III) Tt H-NOX at 2.1 Å resolution. (a) Monomeric Mn(III) Tt H-NOX is shown in gray cartoon with the porphyrin in orange sticks, Mn in purple sphere, H102 in sticks, and coordinating water molecule in red sphere. (b) Mn(III) protoporphyrin IX binds in the heme pocket. H102 coordinates the Mn, and Y140 in the distal pocket forms a hydrogen bond with the water ligand. Blue mesh illustrates $2F_o–F_c$ electron density for the porphyrin and heme pocket residues.

Relaxivities of Gd Tt H-NOX. The high relaxivities displayed by Ln(III) complexes are ideally suited for MRI applications (3). However, as discussed above, Ln complexes are kinetically labile under biological conditions, and aqueous lanthanide(III) ions are highly toxic. To address this issue, we have also sought to incorporate Gd^{III} protoporphyrin IX into the *Tt* H-NOX scaffold in an effort to create a kinetically inert, protein-based contrast agent.

Gd^{III} protoporphyrin IX was synthesized using an imidazole melt in a manner similar to published methods.[8] However, initial mass spectrometry analysis suggests that the porphyrin macrocycle was adducted by imidazole during reflux conditions. To test the feasibility of generating Gd *Tt* H-NOX, initial Gd porphyrin incorporation studies were pursued. UV-visible spectroscopy conducted on the purified protein suggests at least two different species are present (Figure 4). ICP-OES analysis confirmed the presence Gd in the purified protein and absence of Fe contamination. This suggests that the *Tt* H-NOX sample may contain either different Gd-bound species or a mixture of Gd and metal-free porphyrin. Importantly, no significant Gd loss was observed by UV-visible spectroscopy during protein purification, providing initial evidence that Gd is not readily labile when protein-bound. Preliminary T_1 and T_2 relaxivity measurements were performed on the Gd protein. Gd *Tt* H-NOX was found to have relaxivities of 19 and 27 $mM^{-1}s^{-1}$ (Figure 4) which are greatly enhanced compared to small molecule Gd complexes measured under identical conditions (Table 1).

Table 1. Relaxivities of selected complexes acquired at 60 MHz and 37 °C using micromolar concentrations of agent.

Complex[a]	r_1 ($mM^{-1}s^{-1}$)	r_2 ($mM^{-1}s^{-1}$)	***q* value**
Fe^{III} Mb	1.60 ± 0.01	2.9 ± 0.1	1
Fe^{III} *Tt* H-NOX	5.90 ± 0.03	14.5 ± 0.4	1
Mn^{II} *Tt* H-NOX	3.6 ± 0.1	3.8 ± 0.2	N/D
Mn^{III} *Tt* H-NOX	12.0 ± 0.2	16.8 ± 0.5	1
Gd^{III} *Tt* H-NOX	28.7 ± 5.0	39.9 ± 4.9	N/D
MnDPDP[20]	2.8[b]	N/D	N/D
Gd-DTPA (Magnevist)[21]	3.3 ± 0.3	3.9 ± 0.3	1
Gd-DOTA (Dotarem)[21]	3.0 ± 0.3	3.5 ± 0.3	1
Gd-HP-DO3A (Prohance)[21]	2.9 ± 0.3	3.4 ± 0.3	1

[a]This work unless noted. [b] 10 MHz and 25 °C. N/D = not determined.

Plasma stability of H-NOX complexes. To evaluate the stability of the Fe^{III}, Mn^{III}, and Gd^{III} *Tt* H-NOX complexes under biological conditions, stability time courses were conducted in plasma at 37 °C. UV-visible spectra were acquired over 24 h to record any changes in porphyrin absorbance. Importantly, no porphyrin loss or demetalation was observed in any of the protein complexes under the assay conditions (Figure 5). These

data confirm that *Tt* H-NOX provides a highly stable framework for coordinating metals under biological conditions.

Enhancing protein properties for MRI. Numerous strategies are available to rationally tune the properties of the protein-based agents for improved imaging and biological delivery.[5-7] The relaxivities of the proteins could be enhanced through the encapsulation of other metalloporphyrins or complexes in the heme pocket. Additionally, structure-guided mutagenesis could be used to modify the metal coordination environment to tune relaxivity and/or further enhance metal binding affinity. These changes could include the incorporation of amino acids providing oxygen ligands (since lanthanides in particular are oxophilic) or opening the heme pocket for improved water exchange with bulk solvent. Targeting groups could be appended to the protein scaffold through genetic or chemical means to enhance biological retention. Additionally, the biocompatibility of the agents could be improved and the size modulated through modification of the protein surface (e.g., through PEGylation). These strategies will allow the protein-based agents to be uniquely tailored for desired imaging applications.

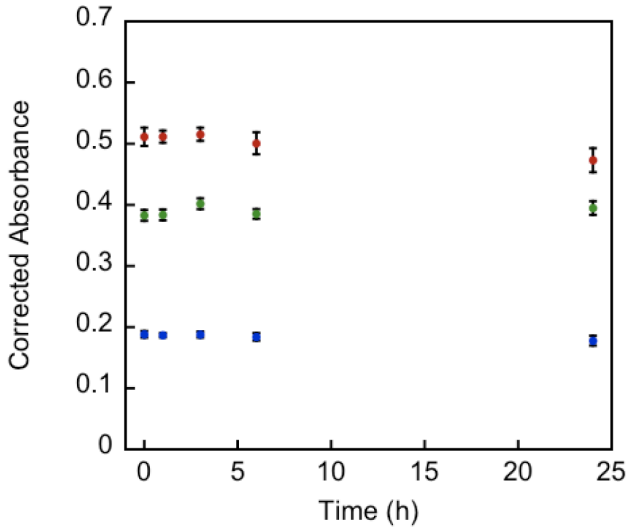

Figure 5. Plasma stability of Fe^{III} (—), Gd^{III} (—), and Mn^{III} (—) *Tt* H-NOX complexes (~2.5 mg/mL by A280) in DPBS at 37 °C over 24 h. Absorbance is plotted at 414 nm, 420 nm, and 474 nm, respectively, and corrected for the plasma background. N = 3.

Conclusion

Porphyrin-substituted H-NOX proteins are a promising prototype of contrast agents for MRI technology. H-NOX proteins stabilize metal binding under aqueous conditions and provide unique porphyrin coordination environments. We anticipate that H-NOX scaffolds can be modulated through genetic or chemical means to enhance MRI signal and/or facilitate biological targeting. In addition, alternate metalloporphyrins may be incorporated at the heme site to further improve MRI signal. Together, these strategies present opportunities to rationally design heme protein-based scaffolds with unique,

tailored properties for future biological imaging.

References

1) Moonen, C. T.; van Zijl, P. C.; Frank, J. A.; Le Bihan, D.; Becker, E. D. Functional magnetic resonance imaging in medicine and physiology. *Science.* **1990**, *250*, 53-61.
2) Datta, A.; Raymond, K. N. Gd-Hydroxypyridinone (HOPO)-based high-relaxivity magnetic resonance imaging (MRI) contrast agents. *Acc. Chem. Res.* **2009**, *42,* 948-957.
3) Caravan, P.; Ellison, J. J.; McMurry, T. J.; Lauffer, R. B. Gadolinium(III) chelates as MRI contrast agents: structure, dynamics, and applications. *Chem. Rev.* **1999**, *99*, 2293-2352.
4) Hasebroock, K. M.; Serkova, N. J. Toxicity of MRI and CT contrast agents. *Expert. Opin. Drug Metab. Toxicol.* **2009**, *5*, 403-416.
5) Winter, M. B.; McLaurin, E. J.; Reece, S. Y.; Olea, C, Jr.; Nocera, D. G.; Marletta, M. A. Ru-porphyrin protein scaffolds for sensing O2. *J. Am. Chem. Soc.* **2010***, 132,* 5582-5583.
6) Boon, E. M.; Marletta, M. A. Sensitive and selective detection of nitric oxide using an H-NOX domain. *J. Am. Chem. Soc.* **2006**, *128*, 10022-10023.
7) Weinert, E. E.; Plate, L.; Whited, C. A.; Olea, C. Jr.; Marletta, M. A. Determinants of ligand affinity and heme reactivity in H-NOX domains. *Angew. Chem. Int. Ed.* **2010**, *49*, 720-723.
8) Srivastava, T. Gadolinium(III) myoglobin: interaction of Gd(III) mesoporphyrin IX with apomyoglobin. *Current Science.* **1980**, *49*, 429-430.
9) Karow, D. S.; Pan, D.; Davis, J. H.; Behrends, S.; Mathies, R. A.; Marletta, M. A. Characterization of functional heme domains from soluble guanylate cyclase. *Biochemistry.* **2005**, *44*, 16266-16274.
10) Otwinowski, Z.; Minor, W. Processing of X-ray diffraction data collected in oscillation mode. *Method Enzymol.* **1997**, *276*, 307-326.
11) McCoy, A. J.; Grosse-Kunstleve, R. W.; Storoni, L. C.; Read, R. J. Likelihood-enhanced fast translation functions. *Acta Crystallogr. D Biol. Crystallogr.* **2005**, *61*, 458-464.
12) Humphries, M. Rare earth elements: The global supply chain (Congressional Research Service). **2010**.
13) Kummerer, K.; Helmers, E. Hospital effluents as a source of gadolinium in the aquatic environment. *Environ Sci Technol* **2000**, *34*, 573-577.
14) Strauch, R. C.; Mastarone, D. J.; Sukerkar, P. A.; Song, Y.; Ipsaro, J. J.; Meade, T. J. Reporter protein-targeted probes for magnetic resonance imaging. *J. Am. Chem. Soc.* **2011***, 133,* 16346-16349.
15) Olea, C, Jr.; Kuriyan, J.; Marletta, M. A. Modulating heme redox potential through protein-induced porphyrin distortion. *J. Am. Chem. Soc.* **2010**, *132*, 12794-12795.
16) Brunori, M.; Amiconi, G.; Antonin, E.; Wyman, J.; Zito, R.; Fanelli, A. R. The transition between 'acid' and 'alkaline' ferric heme proteins. *Biochim. Biophys. Acta.* **1968**,*154*, 315-322.
17) Tan M, Ye Z, Jeong EK, Wu X, Parker DL, & Lu ZR (2011) Synthesis and

evaluation of nanoglobular macrocyclic Mn(II) chelate conjugates as non-gadolinium(III) MRI contrast agents. *Bioconjug Chem* 22: 931-937.
18) Drahos, B.; Kubicek, V.; Bonnet, C. S.; Hermann, P.; Lukes, I.; Toth, E. Dissociation kinetics of Mn2+ complexes of NOTA and DOTA. *Dalton Trans.* **2011**, *40*, 1945-1951.
19) Woodward, J. J.; Martin, N. I.; Marletta, M. A. An *Escherichia coli* expression-based method for heme substitution. *Nat. Methods.* **2007**, *4*, 43-45.
20) Elizondo, G.; Fretz, C. J.; Stark, D. D.; Rocklage, S. M.; Quay, S. C.; Worah, D.; Tsang, Y. M.; Chen, M. C.; Ferrucci, J. T. Preclinical evaluation of MnDPDP: new paramagnetic hepatobiliary contrast agent for MR imaging. *Radiology.* **1991**, *178*, 73-78.
21) Port, M.; Idee, J. M.; Medina, C.; Robic, C.; Sabatou, M.; Corot, C. Efficiency, thermodynamic and kinetic stability of marketed gadolinium chelates and their possible consequences: a critical review. *Biometals*. **2008**, *21*, 469-490.

Chapter 7 – Improved Relaxivity and Function through Nanoparticle Synthesis

Abstract

Configuring Ln_2O_3 nanocrystals with pseudo-2D morphologies confers substantive gains in relaxivities over equivalent spherical counterparts. The most promising arises from Gd_2O_3 whose ionic transverse and longitudinal relaxivities were as high as r_1 = 12.7 mM^{-1} s^{-1} and r_2 = 17.2 mM^{-1} s^{-1} (dispersed in H_2O, T = 37 °C & B_0 = 1.41 T), pointing to new opportunities to achieve high contrast MRI while concomitantly affording longer half-life potential *in vivo*.

Introduction

While the structure of organic chelates can tune the relaxivity of the paramagnetic ion over a broad range, their small size leads to a short half-life *in vivo*.[1, 2] Macromolecular contrast agents–including micelles,[3–5] liposomes,[6–8] and other supramolecular assemblies,[9–12] (bio)polymer[13–16] or nanoparticle conjugates[17–20] and (super)paramagnetic nanocrystals[21] – on the other hand, serve to both prolong serum presence and increase relaxivities through a slowing down of the molecular tumbling rate of the contrast agent. In this manner, it is possible to substantially lower the dose for patients undergoing MRI. Furthermore, for patients with kidney ailments, a macromolecular approach where ions are chemically fixed in an inorganic lattice may also mitigate the potential for bioaccumulated contrast agent to leach into tissues and incur nephrogenic systemic fibrosis, although this is still a murky area that requires further investigation.[22]

Several inorganic lattices show promise for high-contrast MRI, including iron oxides,[23] manganese oxide,[24] manganese ferrite,[25] graphene-CoFe intermetallic composites,[26] and oxides of the rare earths.[27–29] Size dependent contrast ability for spherical nanocrystals has been determined for several of these compositions; however, much less is understood regarding the role of particle morphology in modulating the observed relaxivities and how these might offer alternatives to the widely-used molecular chelates with more tailored properties in vivo. There is a unique opportunity to do so with rare earth–based materials since both chelates and spherical nanocrystals have been widely reported. Ln_2O_3-based nanodiscs offer exciting new opportunities for high contrast MRI. We highlight the synergistic role of high-temperature, inorganic colloidal synthesis techniques to afford particles with controlled size, composition and unique morphologies alongside new polymer compositions and passivation strategies that confer efficient aqueous transfer ability and biocompatibility as required for MRI (Figure 1).

Ionic transverse and longitudinal relaxivities as high as r_1 = 9.9 mM^{-1} s^{-1} and r_2 = 10.5 mM^{-1} s^{-1} (respectively) have been reported for spherical Gd_2O_3 nanocrystals up to 2.5 nm in diameter (in pure water at T = 20 °C and a field

strength of B_0 = 1.41 T), with rapid decline thereafter since relaxivity gains with larger sizes are offset by having fewer Gd(III) at the surface.[27]

Experimental Procedures

General Synthesis of PAA_{28-x}-$mPEO_x$ Graft Copolymers (syntheses by Rob van der Weegen and Mark Bailey): PAA (28 eq–CO_2H per polymer) was dissolved in anhydrous DMF along with mPEG-NH_2 (*x* equivalents with respect to–CO_2H) before the addition of DCC (1.3 equivalents with respect to *x*). The reaction mixture was allowed to stir at RT overnight, after which a ninhydrin test indicated the reaction had gone to completion. The dicyclohexyl urea byproduct was filtered through glass wool and a short cotton plug. The graft copolymer was then precipitated with cold ether (45 mL) and centrifuged to pellet the product. The ethereal layer was decanted and the pellet dissolved in chloroform (5 mL). The process was repeated 3x. The final pellet was air-dried and then dissolved in MilliQ water prior to filtration through a PTFE syringe filter (PALL Life Sciences, 0.2 μm). Aqueous solutions of PAA_{28-x}-$mPEO_x$ graft copolymer were lyophilized to a fluffy colorless solid.

PAA_{26}-$mPEO_2$ (syntheses by Rob van der Weegen and Mark Bailey): Overall yield of 95% from PAA (270mg, 125 μmol), mPEG-NH_2 (500 mg, 250 μmol) and DCC (77 mg, 375 μmol). ^{1}H NMR (500 MHz, $CDCl_3$, δ): δ 4.0-3.1 (m, 358H), 3.2-0.7 (m, 74H) ppm; FT-IR ($CHCl_3$, **ν**): 3473(m), 2873(s), 1728(s), 1454(m), 1098(s), 949(m), 845(m) cm^{-1}.

PAA_{24}-$mPEO_4$ (syntheses by Rob van der Weegen and Mark Bailey): Overall yield of 93% from PAA (135 mg, 62.5 μmol), mPEG-NH_2 (500 mg, 250 μmol) and DCC (77 mg, 375 μmol). ^{1}H NMR NMR (500 MHz, $CDCl_3$, δ): 4.0-3.1 (m, 710H) 3.1-0.8 (m, 89H) ppm; FT-IR ($CHCl_3$, **ν**): 3500(m), 2941(s), 2870(s), 1729(s), 1651(m), 1540(w), 1453(m), 1349(m), 1292(m), 1249(m), 1109(s), 949(m), 847(m) cm^{-1}.

PAA_{22}-$mPEO_6$(syntheses by Rob van der Weegen and Mark Bailey): Overall yield of 92% from PAA (90 mg, 41.7 μmol), mPEG-NH_2 (500 mg, 250 μmol) and DCC (77 mg, 375 μmol). ^{1}H NMR (500 MHz, $CDCl_3$, δ): 4.0-3.1 (m, 999H), 3.1-0.8 (m, 83H) ppm; FT-IR ($CHCl_3$, **ν**): 3250(w), 2872(s), 1731(m), 1672(m), 1540(w), 1466(m), 1343(m), 1280(m), 1242(m), 1105(s), 949(m), 842(m) cm^{-1}.

PAA_{16}-$mPEO_{12}$: Overall yield of 89% from PAA (45 mg, 20.9 μmol), mPEG-NH_2 (500 mg, 250 μmol) and DCC (77 mg, 375 μmol). ^{1}H NMR (500 MHz, $CDCl_3$, δ): 4.0-3.1 (m, 2148H), 3.1-0.8 (m, 92H) ppm. FT-IR ($CHCl_3$, **ν**): 3477(m), 2868(s), 1724(s), 1672(m), 1544(w), 1454(m), 1348(m), 1283(m), 1248(m), 1108(s), 948(m), 844(m) cm^{-1}.

Relaxometry: T_1 and T_2 measurements were performed on a Bruker mq60 minispec relaxometer and analyzed using Bruker minispec software. T_1 and T_2 were determined at 60 MHz (1.41 T) using an inversion recovery pulse sequence. Temperature was controlled at 37.0 °C using a Julabo F25 circulating water bath. Each sample was analyzed by ICP-AES for exact Gd and Dy concentration. Relaxivity analyses were performed in triplicate at three concentrations and plotted. Samples were vortexed/sonicated prior to analysis to break up potential aggregation of nanocrystals. For T_1 measurements, the inverse of the longitudinal relaxation time of each sample ($1/T_1$,

s^{-1}) was plotted against Gd or Dy concentration (mM) and fit by linear regression ($R^2 >$ 0.99). Instrument Parameters were as follows: Scans: 4; Recycle Delay: 18.5 s; Gain: 53; Dummy Shots: 0; Detection mode: real; Bandwidth: Broad, 20,000 kHz; Monoexponential Curve Fitting, Phase Cycling. First Pulse Separation: 5 ms; Final Pulse separation: 18,500 ms, Number of data points for fitting: 20; Delay sample window: 0.05 ms; Sampling Window: 0.02 ms; Time for Saturation Curve Display: 6 s. For T_2 measurements, the inverse of the longitudinal relaxation time of each sample ($1/T_2$, s^{-1}) was plotted against Gd and Dy concentration (mM) and fit by linear regression ($R^2 >$ 0.99). Instrument Parameters were as follows: Pulse Separation: 1.000 ms; Data Points: 200; Monoexponential Curve Fitting; Phase Cycling. Data are summarized in Figures S4 & S5.

Phantom Magnetic Resonance Imaging (Dr. Suzanne L. Baker): MR Imaging was performed with a 1.5 T Siemens Avanto MRI using a small flex surface coil. The following parameters were adopted. For both the T_1- and T_2-weighted images the slice thickness was 1.0 mm with a 0.1 mm gap, in plane voxel size was 0.4 mm^2 with 16 slices, 32 images were collected and averaged to create the final image. The T_1-weighted image was collected with a spin echo pulse sequence with a TR = 180 ms and a TE = 19 ms, flip angle = 90 degrees. The T_2-weighted image was collected using a turbo spin echo pulse sequence with a TR = 4380 ms and a TE = 148 ms, flip angle = 150 degrees.

Results and Discussion

While higher values have been reported for larger Gd_2O_3 nanoparticles (d = 5-10 nm, passivated by diols),[27-29] the experimental conditions used to obtain these data make it difficult for further comparison since they were taken at a lower temperature or in thick cell culture media; both parameters are known, expected, and observed to increase r_1 and r_2 by affecting the molecular tumbling rate of the nanoscopic contrast agent.[28] Changing the morphology of RE_2O_3 nanocrystals to pseudo-2D shapes, i.e. discs or plates, should more deliberately make use of their surface area, which scales more favorably with increasing size for discs. Specifically, for an equivalent volume of RE_2O_3, $r_{sphere} = (¾\, r_{disc}^2\, t)^{1/3}$ and $SA_{disc}/SA_{sphere} = [2\pi r_{disc}^2 + 2\pi r_{disc} t]/[4\pi r_{sphere}^2] = [r_{disc}^2 + r_{disc} t]/[2(¾ r_{disc}^2\, t)^{2/3}]$. Thus, a nanodisc of r_{disc} = 5 nm and a thickness of a single unit cell (t = 1.08 nm) would have over twice the surface area of a spherical nanocrystal with r_{sphere} = 2.7 nm, i.e., the commonly reported size for spherical particles.[27, 29] We also recognize that chemical passivation of their surface sites may impinge somewhat on the overall contrast ability; however, for similar chemisorptive coatings on nanocrystals with dissimilar morphologies, trends should nevertheless manifest in a meaningful way. To test this hypothesis, reliable syntheses for producing aqueous dispersible ultrathin RE_2O_3 nanocrystals with diameters ~10 nm is critical.

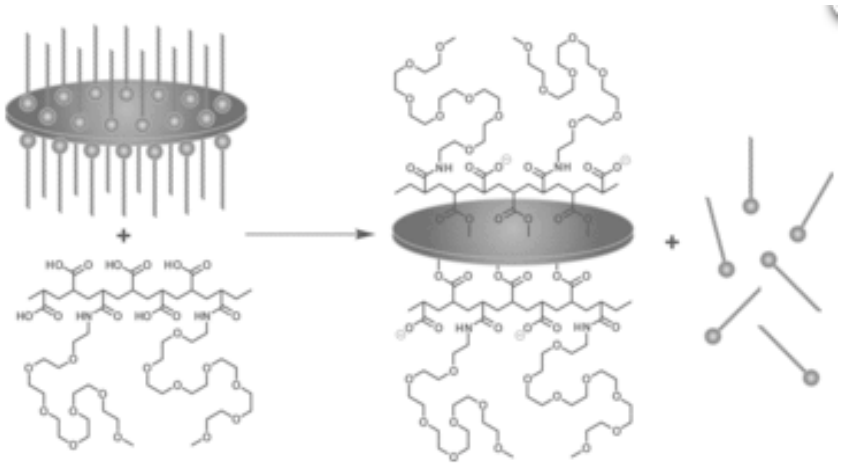

Figure 1. Direct transfer of hydrophobic oleate-passivated rare earth oxide nanodiscs into aqueous media using polyacrylic acids grafted with short, mPEO chains. The resulting nanocrystals show high contrast ability for magnetic resonance imaging (MRI).

Hydrothermal and sol-gel syntheses for preparing RE_2O_3 nanocrystals for use in MRI are ubiquitous.[27–29] These techniques generally yield small spherical nanocrystals and are thus unsuitable for producing pseudo-2D shapes. On the other hand, pyrolysis, sintering, or autoclaving–while capable of conferring a more diverse array of morphologies–produce RE_2O_3 nanocrystals with little to no control over size. Several high-temperature colloidal syntheses of RE_2O_3 in organic media have been described recently, yielding high-quality pseudo-2D RE_2O_3 nanocrystals with a thickness of only one unit-cell edge length (e.g., for Gd_2O_3, the unit cell thickness is 1.08 nm).[30–33] Here, these procedures were adapted to produce nanodiscs of RE_2O_3, where RE = Gd, Dy or Yb, by employing a higher-grade oleic acid in the synthesis. Nanodiscs of ~10-14 nm in diameter with a thickness of a single unit cell were observed by S/TEM (Figure 2), with EDS in support of the composition. The distribution in nanocrystal sizes by DLS was fairly narrow for all three samples, with slightly larger diameters than observed in the TEM reflecting contributions of the oleate surface chemical passivation. Estimated for a RE2O3 nanodisc with a 10 nm diameter and an edge thickness of 1.08 nm, as supported by S/TEM data in Figure 2 as well as by DLS. The total number of Gd(III) ions per nanodisc would be ~20,883. This number was used to determine the per nanodisc relaxivity.

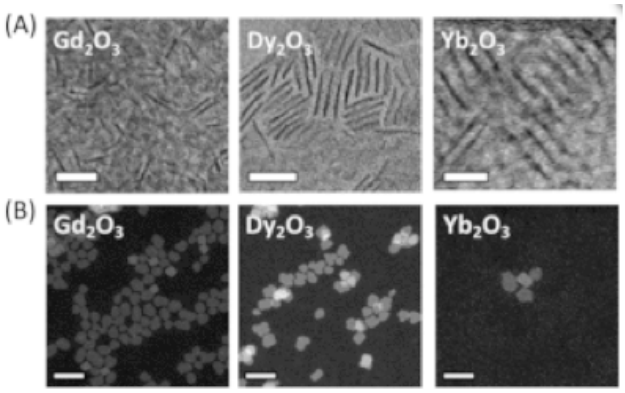

Figure 2. A) TEM of oleate-passivated rare earth oxide nanodiscs viewed edge-on. Scale bars are 10 nm; B) HAADF-STEM of oleate-passivated rare earth oxide nanodiscs viewed face-on. Scale bars are 20 nm.

Unlike spherical RE_2O_3 prepared via hydrothermal or sol-gel routes, RE_2O_3 nanodiscs passivated with hydrophobic ligands are not readily dispersible in water; thus, it was also imperative to define an efficient path to transfer these nanocrystals into aqueous media, which was not known prior to this work, for subsequent relaxometric characterization and MRI. We also sought to do so in a manner that would confer the nanocrystals with a biocompatible, stealth surface passivation. Poly(acrylic acid) (PAA) grafted with short methoxy-terminated polyethylene oxides (mPEO, M_n = 2 kg mol^{-1}) were synthesized as a robust, immunopassive yet stable chemisorptive coating for RE_2O_3nanodiscs: PAA-mPEO$_x$ where x = 2, 4, 6 or 12. The chemical synthesis of PAA-mPEO$_x$ was carried out via DCC-mediated coupling of mPEO-NH_2 to the PAA backbone. The chemisorption of the polymer onto the surface of RE_2O_3 nanodiscs was achieved under equilibrium-controlled reaction conditions. Here, the weakly acidic character of PAA-mPEO$_x$ polymers serves to establish equilibrium, allowing for the reversible association/dissociation of oleates from the surface and, eventually, the entropy-driven multivalent attachment of the polymer to the surface of the nanodiscs. Due to the number of PEO grafts, more conventional appraoches for displacing oleates from the nanocrystal surface were not immediately successful.[34–36] Instead, we found that microwave irradiation in THF at 140 °C for 12 h followed by direct transfer into borate buffer (50 mM, pH 9.0) provided the best results. Reaction conditions were optimized for a 1:5 weight ratio of RE_2O_3 nanodiscs to PAA-mPEO$_x$. While generally effective for PAA-mPEO$_x$ where x = 2, 4 or 6, RE_2O_3 nanodiscs undergoing reaction with PAA-mPEO$_{12}$ using this sequence were not dispersible in buffer, nor were they filterable. The persistence of complex aggregates of polymer and nanodiscs suggested that the mPEO grafting density might be too high for the pendant acids on the polymer backbone to access the nanocrystal surface for attachment.

The propensity for Ln(III) ions to negatively impact cell health is well known,[1, 22] thus it was imperative to determine the aqueous Ln(III) content (i.e. not chemically fixed in the nanodisc's lattice) in our materials using these synthetic procedures, which are somewhat different than the conventional dialysis purification

procedures more commonly encountered. Xylenol orange colorimetric assays were carried out using a standard curve spanning 100 μM to 200 nM. The limit of detection using this assay was determined to be ~800 nM. Samples of nanodiscs were introduced to the xylenol orange reagent (50 μM in 50 mM acetate buffer at pH 5.8), and the absorption spectrum acquired and compared to the standard curve to establish the aqueous RE(III) content in the SEC-purified stock solutions. For all samples, including aged nanocrystals, the aqueous RE(III) content was below the limit of detection (i.e. less than 0.05% of the total ion content of the samples). Direct measures of the cytotoxicity of polymer-passivated RE_2O_3 nanodiscs were also carried out. For Gd_2O_3 and Dy_2O_3 nanodiscs passivated with PAA-mPEO$_4$, MTS-based cell viability assays were carried out in HeLa cells over a concentration range of 1 mg mL^{-1} to 500 ng mL^{-1}. Cells were allowed to incubate in complete medium containing the nanodiscs for two days. No emergent cytotoxicity was observed over this concentration regime (Figure 2), consistent with the absence of significant concentrations of aqueous RE(III) ions as determined by the xylenol orange assay.

Relaxometry was performed on various compositions of RE_2O_3 nanodiscs passivated with PAA-mPEO$_x$ in order to determine whether the pseudo-2D morphology afforded enhanced contrast ability over reported values for their spherical counterparts[27] or small molecule chelates[1, 2] based on the widely-used DTPA ligand. We also sought to determine whether the specific composition of the polymer coating (i.e. the mPEO grafting density along the PAA backbone) affected these physical properties. The total RE(III) content of nanocrystal dispersions were determined by ICP-OES of samples pre-digested with HNO_3. Relaxometry was then carried out in MilliQ H_2O at 37.0 °C and a field strength of 1.41 T for meaningful comparison to data in the literature for spherical equivalents. The observed ionic longitudinal and transverse relaxivities (i.e., r_1 and r_2, respectively) are summarized in Table 1.

Table 1. Relaxometry of Gd(III)- and Dy(III)-based RE_2O_3 nanodiscs passivated with PAA-mPEO$_x$ alongside Gd-DTPA. Determinations were performed in MilliQ H_2O at T = 37 °C and B_0 = 1.41 T.

Construct	PAA-mPEO$_x$ Coating (x)	r_1 (mM^{-1} s^{-1})	r_2 (mM^{-1} s^{-1})	r_2/r_1
Gd_2O_3	2	12.7	16.5	1.30
Gd_2O_3	6	12.6	17.2	1.36
Dy_2O_3	2	3.76	6.23	1.66
Dy_2O_3	4	3.84	6.56	1.71
Gd-DTPA	NA	3.3	3.9	1.18

For both samples of Gd-based nanodiscs passivated with PAA-mPEO$_x$, their positive contrast ability exceeded by approximately 4-fold the value of observed for commercial agents based on Gd-DTPA and by 1.3-fold over previously reported Gd_2O_3 spheroidal nanocrystals measured under the same experimental conditions (i.e. in pure water, at T = 37 °C and B_0 = 1.41 T).[27, 28] Surprisingly, the chemical nature of the polymer coating did not impart significant effect on the relaxometric character. They also exhibited unusually high r_2 values (16.5-17.2 mM^{-1} s^{-1}) for Gd_2O_3-based nanomaterials, pointing to their potential to serve as negative contrast agents as well (albeit not as

effectively as some transition metal oxides, such as Fe_3O_4-based nanomaterials). For Dy-based nanodiscs, on the other hand, their positive contrast ability was not significantly improved over Gd-DTPA chelates (which is not surprising since they are generally more effective agents at higher field strengths);[37] however, their r_2 values showed a modest ~1.6-1.7-fold enhancement over Gd-DTPA and exhibited the highest r_2/r_1 values of the series tested. Again, the chemical nature of the polymer coating was not a deterministic factor in their contrast ability.

While relaxometric data presented on a per RE(III) ion basis is useful to compare molecular chelates to nanoscale constructs, it is also important to appropriately scale the per particle behavior between systems employing multiple paramagnetic species in a single construct. Macromolecular contrast agents based on dendrimers[13] have shown a per particle r_1 of up to 228 $mM^{-1}\,s^{-1}$, which is still inferior to small molecule hydroxypyridinoanates[2] whose r_1 = 304 $mM^{-1}\,s^{-1}$. On the other hand, recently reported constructs based on MS2 viral capsids[38] reached r_1 = 6,876 $mM^{-1}s^{-1}$. In the case of Gd_2O_3 nanodiscs synthesized here, the per-particle[39] relaxivity r_1 reaches ~265,215 $mM^{-1}s^{-1}$ and r_2 = 359,189 $mM^{-1}\,s^{-1}$ due to the dense packing of paramagnetic ions in the nanocrystalline lattice. Even Dy_2O_3 nanodiscs, on a per particle basis, are attractive candidates for MRI. By either measure, the data suggested that both Gd- and Dy-based contract agents would show marked improvement over DTPA analogs in MRI for both T_1 and T_2 contrast modalities.

Phantom MRI was carried out on a dilution series spanning [RE(III)] = 1.5-0.092 mM for both Gd-, Dy-, and Yb-based nanodiscs and their DTPA analogs (Figure 3). In all cases, the MRI contrast curves were consistent with the results from relaxometry. For example, nearly a four-fold increase in relaxivity when the ionic content was held constant was observed for Gd_2O_3 nanocrystals compared to Gd-DTPA. Gd_2O_3 nanocrystals were also very effective in both T_1- and T_2-weighted acquisitions; indeed, they were the only materials to produce negative contrast effectively at these concentrations. For Dy-based materials, Dy_2O_3 nanodiscs outperformed Dy-DTPA chelates by a factor of ~2 for T_1 contrast mode, and slightly less so in their performance enhancement while in the T_2 mode. Not surprisingly, Yb(III), a poor paramagnetic agent with only one unpaired electron, showed a complete lack of contrast ability as either a small molecule Yb-DTPA chelate or a polymer-wrapped nanodisc.

The stealth character of the polymer wrapped RE_2O_3 nanodiscs was also evaluated alongside the DTPA-chelate. Here ~10^7 HeLa cells were incubated with medium (as a control), medium containing Gd-DTPA (0.15 mM), or medium containing an equivalent amount of polymer wrapped Gd_2O_3 nanodiscs. Significantly, phantom MR imaging did not show any accumulation of the nanodiscs in HeLa cells above background after a 24 h incubation, whereas for Gd-DTPA higher contrast associated with accumulation was present. This suggests that the wrapped nanodiscs should be suitable for in vivo MR imaging where extravasation and eventual excretion (rather than bioaccumulation due to intracellular internalization) is the dominant mechanism for achieving contrast during the imaging period in patients.

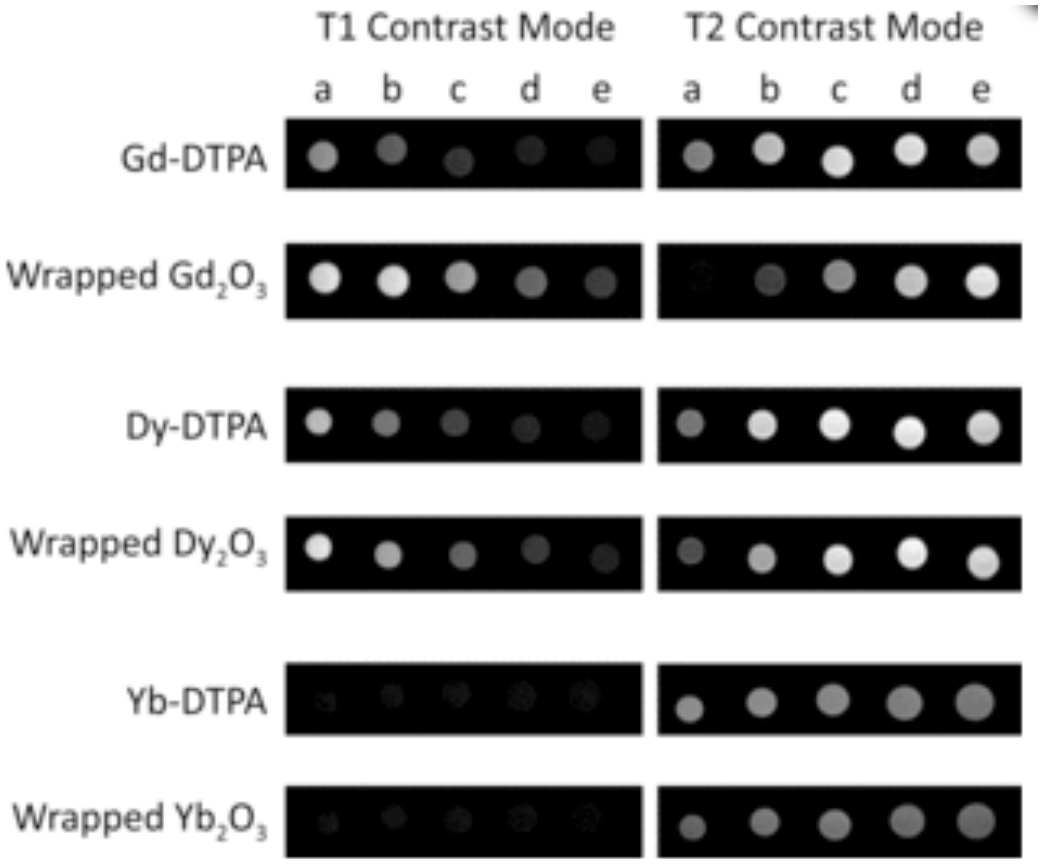

Figure 3. Phantom MRI for Gd-, Dy- and Yb-based RE_2O_3 nanodiscs and DTPA-based molecular chelates for both T_1- and T_2-weighted pulse sequences. Data were acquired for samples dispersed in MilliQ H_2O at T = 20 °C. In all cases, *a–e* spans [RE(III)] = 1.5, 0.75, 0.375, 0.183 and 0.092 mM.

Conclusion

Morphology control during RE_2O_3 colloidal nanocrystal syntheses is concommittant with excellent MRI contrast ability for pseudo-2D nanodiscs, once they are transfered into aqueous media using our PEGylated polyacrylic acid coatings. Gd_2O_3 nanodiscs in particular offer clear advantages over Gd-DTPA contrast agents now on the market and can be used for both T_1- andT_2-weighted MR imaging. Their exceptionally high per- particle relaxivity should lead to very effective targeted imaging schemes in vivo as a high amount of proton relaxation can be obtained without need for multiple small molecules to come in contact with the target. In combination with our biocompatible polymer coating, and the ability in future schemes to functionalize the outer polymer shell, this hybrid nanocrystal platform is improvement for systematic whole body imaging for medical diagnostics.[42]

References

1) Port, M.; Idee, J. M.; Medina, C.; Robic, C.; Sabatou, M.; Corot, C. Efficiency, thermodynamic and kinetic stability of marketed gadolinium chelates and their possible consequences: a critical review. *Biometals*. **2008**, *21*, 469-490.
2) Werner, E. J.; Datta, A.; Jocher, C. J.; Raymond, K. N. High-relaxivity MRI contrast agents: where coordination chemistry meets medical imaging. *Angew. Chem. Intl. Ed.* **2008**, *47*, 8568-8580.
3) Accardo, A.; Tesauro, D.; Aloj, L.; Pedone, C.; Morelli, G. Supramolecular aggregates containing lipophilic Gd(III) complexes as contrast agents in MRI. *Coor. Chem. Rev.* **2009**, *253,* 2193-2213.
4) Nicolle, G. M.; Toth, E.; Eisenwiener, K. P.; Macke, H. R.; Merbach, A. E. From monomers to micelles: investigation of the parameters influencing proton relaxivity. *J. Biol. Inorg. Chem.* **2002**, *7,* 757-769.
5) Torchilin, V. P. PEG-based micelles as carriers of contrast agents for different imaging modalities. *Adv. Drug Deliv. Rev.* **2002**, *54,* 235-252.
6) Strijkers, G. J.; Mulder, W. J. M.; van Heeswijk, R. B.; Federik, P. M.; Bomans, P.; Magusin, P. C. M. M.; Nicolay, K. Relaxivity of liposomal paramagnetic MRI contrast agents. *Magn. Res. Mater. Phys., Biol. Med.* **2005**, *18,* 186–192.
7) Mulder, W. J. M.; Strijkers, G. J.; Griffioen, A. W.; van Bloois, L.; Molema, G.; Storm, G.; Konig, G. A.; Nicolay, K. A liposomal system for contrast-enhance magnetic resonance imaging of molecular targets. *Bioconjugate Chem.* **2004**, *15*, 799-806.
8) Trubetskoy, V. S.; Cannillo, J. A.; Milshtein, A.; Wolf, G. L.; Torchilin, V. P. *Mag. Reson. Imag.* **1995,** *13,* 31–37.
9) Bruns, O. T.; Ittrich, H.; Peldschus, K.; Kaul, M. G.; Tromsdorf, U. I.; Lauterwasser, J.; Nikolic, M. S.; Mollwitz, B.; Merkell, M.; Bigall, N. C.; Sapra, S.; Reimer, R.; Hohenberg, H.; Weller, H.; Eychmuller, A.; Adam, G.; Beisiegel, U.; Hereen, J. *Nat. Nanotechnol.* **2009**, *4,* 193–201.
10) Pierre, V. C.; Botta, M.; Aime, S.; Raymond, K. N. Fe(III)-templated Gd(III) self-assemblies- a new route toward macromolecular MRI contrast agents. *J. Am. Chem. Soc.* **2006,** *128,* 9272–9273.
11) Dirksen, A.; Langereis, S.; de Waal, B. F. M.; van Genderen, M. H. P.; Hackeng, T. M.; Meijer, E. W. A supramolecular approach to multivalent target-specific MRI contrast agents for angiogenesis. **2005**, *22*, 2811-2813.
12) Bull, S. R.; Guler, M. O.; Bras, R. E.; Meade, T. J.; Stupp, S. I. Self-assembled peptide amphiphile nanofibers conjugated to MRI contrast agents. *Nano Lett.* **2005,** *5,* 1–4.
13) Floyd, III, W. C.; Klemm, P. J.; Smiles, D. E.; Kohngruber, A. C.; Pierre, V. C. Mynar, J. L.; Fréchet, J. M. J.; Raymond, K. N. Conjugation effects of various linkers on Gd(III) MRI contrast agents with dendrimers: optimizing the hydroxypyridinonate (HOPO) ligands with nontoxic, degradable (EA) dendrimers for high relaxivity. *J. Am. Chem. Soc.* **2011**, *133*, 2390-2393.
14) Langereis, S.; Dirksen, A.; Hackeng, T. M.; van Genderen, M. H. P.; Meijer, E. W. Dendrimers and magnetic resonance imaging. *New J. Chem.* **2007***, 31,* 1152–1160.

15) Reynolds, C. H.; Annan, N.; Beshah, K.; Huber, J. H.; Shaber, S. H.; Lenkinski, R. E.; Wortman, J. A. Gadolinium-loaded nanoparticles: new contrast agents for magnetic resonance imaging. *J. Am. Chem. Soc.* **2000**, *122,* 8940-8945.
16) Torchilin, V. P. Polymeric contrast agents for medical imaging. *Curr. Pharm. Biotech.* **2000**, *1,* 183–215.
17) Manus, L. M.; Mastarone, D. J.; Waters, E. A.; Zhang, X. Q.; Schultz-Sikma, E. A.; MacRenaris, K. W.; Parigi, G.; Luchinat, C.; Ho, D.; Meade, T. J. Gd(III)-Nanodiamond conjugates for MRI contrast enhancement. *Nano. Lett.* **2010**, *10*, 484-489.
18) Rowe, M. D.; Chang, C.-C.; Thamm, D. H.; Kraft, S. L.; Harmon, Jr., J. F.; Vogt, A. P.; Sumerlin, B. S.; Boyes, S. G. Tuning the magnetic resonance imaging properties of positive contrast agent nanoparticles by surface modification with RAFT polymers. *Langmuir.* **2009**, *25,* 9487–9499.
19) Song, Y.; Xu, X.; MacRenaris, K. W.; Zhang, X-Q.; Mirkin, C. A.; Meade, T. J. Multimodal gadolinium-enriched DNA-gold nanoparticle conjugates for cellular imaging. *Angew. Chem. Intl. Ed.* **2009**, *48,* 9143-9147.
20) Turner, J. L.; Pan, D.; Plummer, R.; Chen, Z.; Whittaker, A. K.; Wooley, K. L. Synthesis of Gadolinium-labeled shell-crosslinked nanoparticles for magnetic resonance imaging application. *Adv. Funct. Mater.* **2005**, *15,* 1248–1254.
21) Na, H. B.; Song, I. C.; Hyeon, T. Inorganic nanoparticles for MRI contrast agents. *Adv. Mater.* **2009**, *21,* 2133–2148.
22) Zou, Z.; Lin, M. Nephrogenic Systemic Fibrosis/ Nephrogenic Fibrosing Dermopathy: A Decade-old Disease. *Indian J. Dermatol.* **2007,** *52*, 125-130.
23) Laurent, S.; Forge, D.; Port, M.; Roch, A.; Robic, C.; Elst, L. V.; Muller, R. N. Magnetic iron oxide nanoparticles: synthesis, stabilization, vectorization, physicochemical characterizations, and biological applications. *Chem Rev.* **2008**, *108*, 2064–2110.
24) Na, H. B.; Lee, H. H.; An, K.; Park, Y. I.; Park, M.; Lee, I. S.; Nam, D.-H.; Kim, S. T.; Kim, S.-H.; Kim, S.-w.; Lim, K.-H.; Kim, K.-S.; Kim, S.-O.; Hyeon, T. Development of a T1 contrast agent for magnetic resonance imaging using MnO nanoparticles. *Angew. Chem. Int. Ed.* **2007**, *46*, 5397–5401.
25) Tromsdorf, U. I.; Bigall, N. C.; Kaul, M. G.; Bruns, O. T.; Nikolic, M. S.; Mollwitz, B.; Sperling, R. A.; Reimer, R.; Hohenberg, H.; Parak, W. J.; Forster, S.; Beisiegel, U.; Adam, G.; Weller, H. Size and surface effects on the MRI relaxivity of manganese ferrite nanoparticle contrast agents.
26) Seo, W. S.; Lee, J. H.; Sun, X.; Suzuki, Y.; Mann, D.; Liu, Z.; Terashima, M.; Yang, P. C.; McConnell, M. V.; Nishimura, D. G.; Hongjie, D. FeCo/graphite-shell nanocrystals as an advanced magnetic-resonance-imaging and near-infrared agents. *Nat. Mater.* **2006***, 5*, 971–976.
27) Park, J. Y.; Baek, M. J.; Choi, E. S.; Woo, S.; Kim, J. H.; Kim, T. J.; Jung, J. C.; Chae, K. S.; Chang, Y.; Lee, G. H. Paramagnetic ultrasmall gadolinium oxide nanoparticles as advanced T-1 MR1 contrast agent: account for large longitudinal relaxivity, optical particle diameter, and in vivo T-1 MR images. *ACS Nano.* **2009**, *3*, 3663–3669.

28) Engstrom, M.; Klasson, A.; Pedersen, H.; Vahlberg, C.; Kall, P.-O.; Uvdal, K. High proton relaxivity for gadolinium oxide nanoparticles. *Magn. Reson. Mater. Phys., Biol. Med.* **2006**, *19*,180–186.
29) Bridot, J. L.; Laurent, S.; Riviere, C.; Billotey, C.; Hiba, B.; Janier, M.; Josserand, V.; Coll, J. L.; Elst, L. V.; Muller, R.; Roux, S.; Perriat, P.; Tillement, O. Hybrid gadolinium oxide nanoparticles: multimodal contrast agents for in vivo imaging. *J. Am. Chem. Soc.* **2007**, *129*, 5076–5084.
30) Huo, Z.; Tsung, C.-K.; Huang, W.; Fardy, M.; Yan, R.; Zhang, X.; Li, Y.; Yang, P. Self-organized ultrathin oxide nanocrystals. *Nano Lett.* **2009**, *9*, 1260–1264.
31) Si, R.; Zhang, Y.-W.; Zhou, H.-P.; Sun, L.-D.; Yan, C.-H. Controlled-synthesis, self-assembly behavior, and surface-dependent optical properties of high quality rare-earth oxide nanocrystals. *Chem. Mater.* **2007**, *19*, 18–27.
32) Si, R.; Zhang, Y.-W.; You, L.-P.; Yan, C.-H. Rare-earth oxide nanopolyhedra, nanoplates, and nanodisks. *Angew. Chem. Int. Ed.* **2005**, *44*, 3256–3260.
33) Cao, Y. C. Synthesis of square gadolinium-oxide nanoplates. *J. Am. Chem. Soc.* **2004**, *126*, 7456–7467.
34) Park, Y. I.; Piao, Y.; Lee, N.; Yoo, B.; Kim, B. H.; Choi, S. H.; Hyeon, T. Transformation of hydrophobic iron oxide nanoparticles to hydrophilic and biocompatible maghemite nanocrystals to use as a highly efficient MRI contrast agent. *J. Mater. Chem.* **2011**, *21*, 11472–11477.
35) Taboada, E.; Rodriguez, E.; Roig, A.; Oro, J.; Roch, A.; Muller, R. N. Relaxometric and magnetic characterization of ultrasmall iron oxide nanoparticles with high magnetization. Evaluation as potential T-1 magnetic resonance imaging contrast agents for molecular imaging. *Langmuir.* **2007**, *23*, 4583–4588.
36) Song, H.-T.; Choi, J.-S.; Huh, Y.-M.; Kim, S.; Jun, Y.-W.; Suh, J.-S.; Cheon, J. Surface modulation of magnetic nanocrystals in the development of highly efficient magnetic resonance probes for intracellular labeling. *J. Am. Chem. Soc.* **2005**, *127*, 9992–9993.
37) Norek, M.; Kampert, E.; Zeitler, U.; Peters, J. A. Tuning the size of Dy2O3 nanoparticles for optimal performance as an MRI contrast agent. *J. Am. Chem. Soc.* **2008**, *130*, 5335–5340.
38) Garimella, P. D.; Datta, A.; Romanini, D. W.; Raymond, K. N.; Francis, M. B. Multivalent, high-relaxivity MRI contrast agents using rigid cysteine-reactive gadolinium complexes. *J. Am. Chem. Soc.* **2011**, *133*, 14704–14709.
39) Harris, J. M. Laboratory synthesis of polyethylene glycol derivatives. *Macromol. Sci. C: Polym. Rev.* **1985**, *25*, 325–373.
40) Brunisholz, G.; Randin, M. *Helv. Chim. Acta* **1959**, *42*, 1927–1938.
41) Barge, A.; Cravotto, G.; Gianolio, E.; Fedeli, F.*Contrast Med. Mol. Imaging* **2006**, *1*, 184–188.
42) Bailey, M. J.; van der Weegen, R.; Klemm, P. J.; Baker, S. L.; Helms, B. Direct transfer of hydrophobic rare earth oxide nanodiscs into aqueous media using PEGylated polyacrylic acids for magnetic resonance imaging. *Adv. Healthcare Mat.* **2012**, *1*, 437-442.

Chapter 8 – Improved Attachment Strategies and Per-Gadolinium Relaxivity Through Gold Nanoparticle Conjugation

Abstract

Magnetic resonance imaging (MRI) contrast agents (CA) are limited in their function and modalities by low relaxivity (r_1). Gd(III)-based CA complexes have the potential for increased relaxivity and lower dosage when they are immobilized on a macromolecular solid support. Gold nanoparticles are an excellent choice due to their facile synthesis, low toxicity, and tailorable surface chemistry. Here, hexadentate Gd-HOPO (6-methyl-3-hydroxy-pyridin-2-one) complexes have been conjugated using short, rigid linkers to limit local motion of Gd(III) on gold nanoparticles and increase relaxivity. These complexes have *q* values of 2-3 water molecules coordinated to the inner sphere of Gd(III) for increased water exchange rates. We find that single-tether attachment to a scaffold produces similar relaxivity gains, regardless type of macromolecular scaffold. These results indicate a limit to relaxivity improvements achievable via single attachment. To overcome this limitation, we introduce a system that uses multiple scaffold links per CA complex. These materials exhibit *per Gd* relaxivities up to 79 $mM^{-1}s^{-1}$ at 60 MHz and 37 °C; the highest per Gd relaxivities reported to date, under physiological conditions.

Introduction

Inorganic nanoparticles, when chelated to a paramagnetic conjugate, have been shown to have large per particle relaxivities[1-3] and may be easily functionalized by a myriad of chemical groups.[3-4] These particles have potential for generating CAs with improved relaxivity, low toxicity, and high multivalency. To illustrate this potential we have designed a system to leverage each aspect of both the nanoparticle and CA architecture. First, we introduce a new macrocycle building block, which contains an uncharged functional group that can be used for both additional chemical modification (such as with cell-targeting groups) as well as scaffold conjugation. CAs based on these ligands are then appended to gold nanoparticle (AuNPs) scaffolds which are attractive supports due to their facile synthesis,[5] unique optical features,[6-7] low toxicity,[8] and tailorable surface chemistry.[35] For example, AuNPs can be used as light-triggered therapeutics due to their surface plasmon resonances,[8] making these particles a multifunctional platform (or "theranostic"). Importantly, we hypothesized that a single-tether between scaffold (of any type) and CA, would reach a plateau for r_1 improvement at fixed tether length. Here, we synthesize and test three hexadentate Gd-HOPO complexes coordinated to the nanoparticle surface with 1, 2, or 3 surface-binding moieties (Gd-1, Gd-2, and Gd-tripod; respectively; Figure 1).

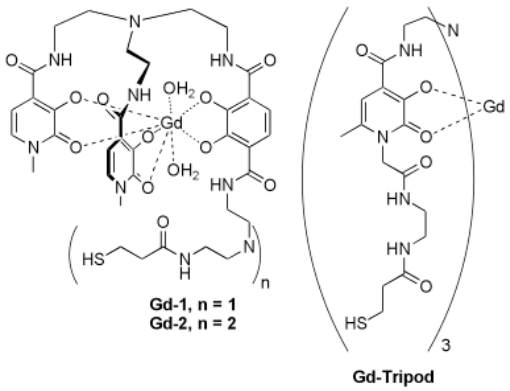

Figure 1. Gd-N1, Gd-N2 possess one and two thiol moieties, respectively for nanoparticle conjugation The Gd-Tripod is a novel ligand with three binding moieties which should dramatically slow the local motion of the Gd(III) center.

Experimental Procedure

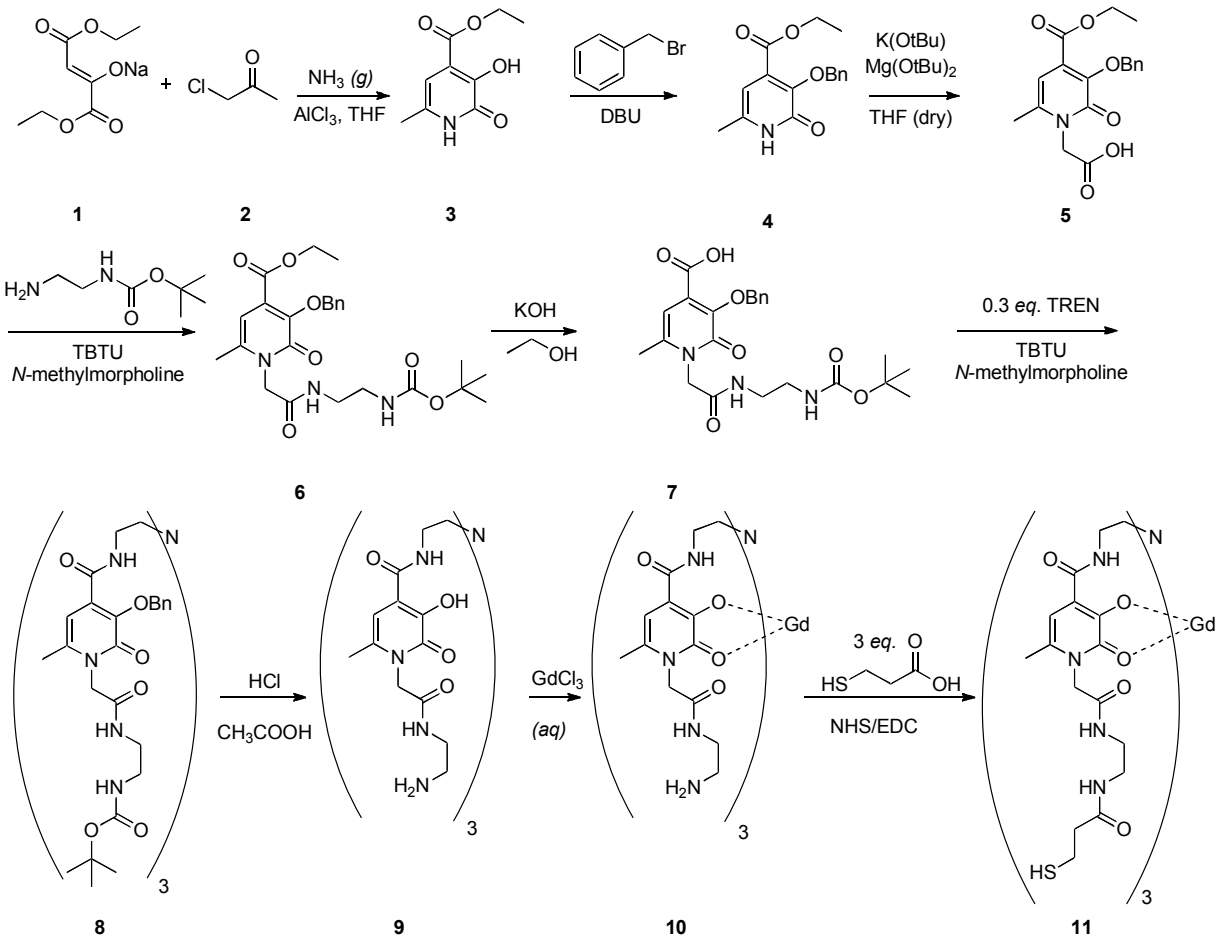

Figure 2. Synthesis of Gd-Tripod, by Michelle N. Keyser.

1. Purchased commercially from Aldrich Chemistry.
2. Purchased commercially from Aldrich Chemistry.
3. Previously reported in Doble, D. M. J.; Melchior, M.; O'Sullivan, B.; Siering, C.; Xu, J.; Pierre, V. C.; Raymond, K. N. *Inorg. Chem.* 2003, *42*, 4930-4937.
4. Previously reported in Doble, D. M. J.; Melchior, M.; O'Sullivan, B.; Siering, C.; Xu, J.; Pierre, V. C.; Raymond, K. N. *Inorg. Chem.* 2003, *42*, 4930-4937.
5. Potassium tert-butoxide (K(OtBu), 0.065 g, 0.59 mmol, 1 *eq*.) and magnesium di-tert-butoxide ($Mg(OtBu)_2$, 0.20 g, 0.59 mmol, 1 *eq.*) were added to 4 (0.168 g, 0.586 mmol, 1 *eq.*) in a round bottom flask in a nitrogen atmosphere. Tetrahydrofuran (THF, 10 mL) was added to the mixture. Bromoacetic acid (0.200 g, 1.46 mmol, 2.5 *eq*.) was dissolved in a separate solution of THF (10 mL). The bromoacetic acid solution was added to the mixture containing 4 and stirred overnight at room temperature under N_2 (g), until producing a yellowish brown liquid (TLC conditions: 2:98 MeOH:DCM. The product was quenched using 3.0 M HCl (10 mL), then extracted using dichloromethane (DCM, 3 x 20 mL). The organic layer was washed with Millipore water (2 x 15 mL). The organic layers were dried over anhydrous $MgSO_4$. The solution was filtered dried *in vacuo*, producing a brown oil. Diisopropyl ether was added to the oil and stirred overnight. The product was filtered and dried producing 5 (0.149 g), a cream colored solid (74%). ^{1}H NMR ($CDCl_3$ + TMS, 400 MHz), δ (ppm): 1.29 (t, 3H, CH_3, J = 7.1 Hz), 2.28 (s, 3H, CH_3), 4.30 (q, 2H, CH_2, J = 7.1 Hz), 4.78 (s, 2H, CH_2), 5.21 (s, 2H, CH_2), 6.28 (s, 1H, CH), 7.27-7.35 (m, 3H, Ph), 7.45-7.53 (m, 2H, Ph). ^{13}C NMR ($CDCl_3$ + TMS, 400 MHz), δ (ppm): 14.09, 20.16, 46.49, 61.83, 74.27, 105.47, 128.30 (t), 131.42, 136.95, 140.08, 144.97, 160.98, 164.88, 170.15. ESI-MS (-): *m/z* 344.1149 $[M-H]^-$ ($C_{18}H_{18}NO_6$, expected 344.1134). Anal. Calculated (found) for $C_{18}H_{19}NO_6$: C, 62.60 (62.39); H, 5.55 (5.42); N, 4.06 (3.99). MP: 242.9-245.7 ºC.
6. Compound 5 (0.994 g, 2.88 mmol, 1 *eq.*) and O-(Benzotriazol-1-yl)-*N,N,N′,N′*-tetramethyluronium tetrafluoroborate (TBTU, 0.924 g, 2.88 mmol, 1 *eq.*) were dissolved in *N*,*N*-dimethylformamide (DMF, 25 mL) under N_2 (g). *N*-methylmorpholine (0.582 g, 5.76 mmol, 2 *eq*.) was added and the mixture was stirred for 20 min at room temperature. *N*-*tert*-butyl-carbonyl-amide (*N*-Boc, 0.461 g, 2.88 mmol, 1 *eq.*) was prepared by dissolving ethylene diamine (26.4 g, 0.439 mol, 6 *eq*.) in dichloromethane (100 mL). This solution. Boc was added to 1,000 mL of DCM in a 1 L addition funnel. Boc was added dropwise very slowly to the ethylenediamine solution at ~0º C in a saturated salt bath with vigorous stirring overnight. Excess solvent was removed *en vacuo* and Millipore water added to produce a yellow solution. This was filtered on a glass frit, extracted twice with 250 mL DCM, and dried with $MgSO_4$. After the solid was filtered off, the *N*-Boc was dried *en vacuo* to a pale yellow solution at a 76% yield (11.7 g).
   N-Boc was dissolved in DMF to reduce the viscosity of the compound and added to Compound 5. The mixture was stirred at room temperature for 18 h, producing a brown viscous oil from which the solvent was removed *in vacuo*. The product was taken into DCM (25 mL) and washed with 1.0 M HCl (2 x 12 mL), resulting in a dark brown organic layer. The solution was washed with 1.0 M NaOH (3 x 12 mL), leading to an opaque brown organic layer. The mixture was washed with Millipore water (2 x 12 mL).

The product was dried over Na_2SO_4 and filtered. The filtrate was dried *in vacuo*, resulting in viscous brown oil. Compound 6 (1.22 g) was washed with diisopropyl ether and filtered, turning the solution an opaque white solid (86%). ^{1}H NMR ($CDCl_3$ + TMS, 400 MHz), δ (ppm): 1.28 (t, 3H, CH_3, J = 7.0 Hz), 1.56 (s, 9H, CH_3), 2.39 (s, 3H, CH_3), 4.29 (q, 2H, CH_2, J = 7.0 Hz), 4.68 (s, 2H, CH_2), 5.22 (s, 2H, CH_2), 6.25 (s, 1H, CH), 7.30-7.35 (m, 3H, Ph), 7.47-7.49 (m, 2H, Ph). ^{13}C NMR ($CDCl_3$ + TMS, 400 MHz), δ (ppm): 14.11, 20.40, 28.37, 40.59, 48.96, 61.75, 74.12, 79.66, 105.05, 128.32 (t), 137.04, 160.91, 164.94, 167.43. ESI-MS (+): *m/z* 488.2400 $[M+H]^+$ ($C_{25}H_{34}N_3O_7$, expected 488.2397), 510.2219 $[M + Na]^+$ ($C_{25}H_{33}N_3O_7Na$ expected 510.2216). Anal. Calculated (found) for $C_{25}H_{33}N_3O_7$: C, 61.59 (61.79); H, 6.82 (6.77); N, 8.62 (8.56). MP: 275.2-277.3 ºC.

7. Compound 6 (1.01 g, 2.07 mmol, 1 *eq*.) was stirred in KOH (0.116 g, 2.07 mmol, 1 *eq*.) in MeOH (30 mL). The mixture was stirred at 60 ºC for four days and the solution turned to a brownish orange color with pH = 8. The mixture was dried *in vacuo* and full conversion was confirmed by ^{1}H NMR. Distilled water (40 mL) was added to the product forming an orange tinted brown liquid. The mixture was placed in an ice bath and hydrochloric acid (20 mL) was subsequently added to acidify the solution (pH = 1), turning the solution an opaque orange liquid containing the aqueous precipitate. The mixture was filtered, producing a light orange solid. Diethyl ether (50 mL) was stirred overnight with the solid, forming 7 (0.202 g), a whitish powder (21%). ^{1}H NMR ($CDCl_3$ + TMS, 400 MHz), δ (ppm): 1.45 (s, 9H, CH_3), 2.44 (s, 3H, CH_3), 4.73 (s, 2H, CH_2), 5.26 (s, 2H, CH_2), 6.29 (s, 1H, CH), 7.32-7.41 (m, 3H, Ph), 7.53-7.54 (m, 2H, Ph). ^{13}C NMR ($CDCl_3$ + TMS, 400 MHz), δ (ppm): 14.11, 20.40, 28.37, 40.37, 40.62, 48.97, 61.75, 74.11, 105.05, 128.09, 128.33, 128.51, 130.89, 137.04, 140.52, 145.04, 160.91, 164.94, 167.43. ESI-MS (-): *m/z* 458.1938 $[M-H]^-$ ($C_{23}H_{28}N_3O_7$, expected 458.1927). Anal. Calcd (found) for $C_{23}H_{29}N_3O_7$: C, 60.12 (59.80); H, 6.36 (6.50); N, 9.14 (8.92). MP: 202.3-204.6 °C.
8. Compound 7 (0.536 g, 1.17 mmol, 1 *eq*.) and TBTU (0.370 g, 1.17 mmol, 1 *eq*.) were combined in DMF (10 mL) under nitrogen gas in EDTA-washed glassware, producing a yellow solution. *N*-methylmorpholine (0.241 g, 2.34 mmol, 2 *eq*.) was added. The reaction was stirred for 20 min at room temperature (25 ºC). Tris(2-aminoethyl)amine (TREN, 0.057 g, 0.389 mmol, 0.33 *eq*.) was then added to the mixture and the reaction was stirred at room temperature for 72 h. DMF was removed *in vacuo*, producing a yellowish brown oil. The product was taken into DCM (10 mL) and an extraction was performed using water. The product was washed and stirred with diisopropyl ether twice and filtered, producing 8, (0.533 g) a rose colored solid (31%). ^{1}H NMR ($CDCl_3$ + TMS, 400 MHz), δ (ppm): 1.38 (9H, CH_3), 2.26 (3H, CH_3), 2.53 (3H, CH_2), 3.26 (3H, CH_2), 3.42 (3H, CH_2), 3.66 (3H, CH_2), 4.20 (3H, CH_2), 4.97 (3H, CH_2), 6.60 (3H), 7.38 (9H, CH), 7.47 (6H, CH). ^{13}C NMR ($CDCl_3$ + TMS, 400 MHz), δ (ppm): 18.9, 28.4, 37.6, 37.8, 40.6, 51.8, 53.7, 70.9, 79.5, 107.7, 111.3, 127.1, 127.6, 128.9, 136.1, 150.1, 155.9, 159.0, 159.4, 170.7. ESI-MS (+): *m/z* 1470.7312 $[M + H]^+$ ($C_{75}H_{100}N_{13}O_{18}$, expected 1470.7311). Anal. Calcd (found) for $C_{75}H_{100}N_{13}O_{18}$ + $3H_2O$: 59.08 (58.92); H, 6.94 (6.72); N, 11.94 (11.98). MP: 168.6-171.4 °C.
9. A. A one-to-one mixture of hydrochloric acid and acetic acid (12.0 M, 50 mL:50 mL) were added to an EDTA-washed round bottom flask containing 8 (0.150 g, 0.1665 mmol,

1 *eq*.). The solution was stirred at room temperature for 3 h and then solvent was removed *in vacuo*. The solid was resuspended in methanol and centrifuged (Sorvall RC-5B Refrigerated Superspeed Centrifuge, 6,000 rpm, 30 min) three times with the supernatant decanted. The solid was dried and stirred in diisopropyl ether (anhydrous) and filtered. The resulting product 9 (0.0091 g) was a white powder (60%).

B. In 5 mL glacial acetic acid 8 (0.150 g, 0.1665 mmol, 1 *eq*.) was dissolved. To this solution 0.5 mL H_2O was added with 10 mg Pd/C (10% weight, wet, 25% by weight of 8). This solution was placed in a Parr bomb. The Parr bomb was flushed with H_2 two times and filled with H_2 to a pressure of 1,100 psi, which was maintained for 40 h. After 40 h, the bomb was vented and the Pd/C filtered off with a fine frit. The solution was washed with acetic acid, after which the acid was removed *in vacuo*. The product 9 (0.101 g) was obtained as a white powder (67%). ^{1}H NMR ($CDCl_3$ + TMS, 400 MHz), δ (ppm): 2.26 (3H, CH_3), 2.53 (3H, CH_2), 2.76 (3H, CH_2), 3.26 (3H, CH_2), 3.66 (3H, CH_2), 4.20 (3H, CH_2), 6.60 (3H, H), 8.03 (6H, NH). ^{13}C NMR ($CDCl_3$ + TMS, 400 MHz), δ (ppm): 18.9, 37.8, 39.8, 40.3, 51.8, 53.7, 107.7, 114.9, 150.1, 155.9, 159.4, 170.7, 182.3. ESI-MS (+): *m/z* 900.43 $[M + H]^+$ ($C_{39}H_{58}N_{13}O_{12}$, expected 900.43).

10. Compound 9 (75 mg, 85 mmol, 1 *eq*.) was dissolved in minimal methanol in an EDTA washed scintillation vial. Pyridine was added (three drops) and $GdCl_3$ *(aq)* (3.0 mL, 85 mmol, 1 *eq*.) was added to the reaction (via EDTA washed pipet) and stirred overnight. Diethyl ether was added to precipitate the product. The ether mixture was centrifuged, the supernatant decanted and the residue dried *in vacuo*. The product 10 was a yellow crystalline solid (52 mg, 58%). ESI-MS (+): *m/z* 1058.35 $[M + H]^+$ ($C_{39}H_{58}N_{13}O_{12}Gd$, expected 1058.35).

    To a 25 mL EDTA washed scintillation vial containing 25 mg (0.024 mmol, 1 *eq*.) of gadolinium complex 10 was added 9.0 mg (0.075 mmol, 3.1 *eq*.) of 3-mercaptopropionic acid. To this was added 20. mg (0.17 mmol, 7 *eq*.) of *N*-hydroxysuccinimide (NHS). The solids were dissolved in 1 mL DMSO and 4.7 mg (0.024 mmol, 1 *eq*.) of EDC (EDAC or EDCI, 1-ethyl-3-(3-dimethylaminopropyl) carbodiimide) was added and the reaction was allowed to stir overnight at room temperature under nitrogen atmosphere. After overnight stirring, the solvent was removed *in vacuo* and solids were taken into 5 mL DCM. After filtering solids the solution was precipitated by addition to 20 mL diethyl ether (anhydrous) to give a light yellow solid. The solids were isolated by centrifugation give 19 mg (59%) of conjugate 13 as a pale yellow solid. ESI-MS (+): *m/z* 1319.64 $[M + H]^+$ ($C_{28}H_{67}N_{13}O_{15}GdS_3$, expected 1319.66).

<u>*Relaxivity:*</u> ICP-OES Analysis and Ligand Loading Determination: ICP-OES (Optical Emission Spectroscopy) analysis was performed using a Perkin-Elmer Optima 7000 DV with Argon flow. Samples were prepared by first dissolving the nanoparticle conjugates in a solution 0.1 M aqua regia in water for 3 h. These samples were than diluted in a 2 % HNO_3 matrix for analysis. The concentration of Au found in the samples was compared to a standard curve with a range of 1-100 ppb, and made from a standard gold solution (Sigma Aldrich, 10,000 ppm in 2% HNO_3). Samples were diluted to concentrations within the range of the standard curve. The concentration of Au was then converted into number of nanoparticles by dividing the number of gold atoms in the sample by the

number of gold atoms per nanoparticle (For a nanoparticle of d = 15 nm, the number of gold atoms is estimated by the unit cell of gold and the volume of the gold particle: ~1.04 x 10^5 atoms/particle). The concentration of Gd was determined from the same samples. For Gd, samples were compared to a standard curve with a range of 0.1 – 10 ppm, and made from a standard Gd solution (Sigma Aldrich, 1,000 ppm in 2% HNO_3). The ratio of Gd atoms to nanoparticles was used to estimate the average Gd-complex loading on the nanoparticle surface.

Relaxivity Studies: T_1 and T_2 measurements were performed on a Bruker mq60 minispec relaxometer. T_1 and T_2 were determined at 60 MHz (1.41 T) using an inversion recovery pulse sequence. Temperature of the samples, in Millipore water (pH 6) or 0.1 M HEPES buffer (pH 7.4), was controlled at 37.0 °C using a Julabo F25 circulating water bath. Each sample was analyzed by ICP-OES for exact Gd, concentration. The inverse of the longitudinal relaxation time of each sample ($1/T_1$, s^{-1}) was plotted against Gd concentration (μM) and fit by linear regression ($R^2 > 0.99$). Relaxivity analyses were performed in triplicate (three samples, three times to report experimental and instrument error) and averages reported. Samples were vortexed and shaken prior to each measurement to discourage aggregation.

Relaxivity Instrument Parameters: Scans: 4; Recycle Delay: 18.5 s; Gain: 53; Dummy Shots: 0; Detection mode: real; Bandwidth: Broad, 20,000 kHz; Monoexponential Curve Fitting, Phase Cycling. First Pulse Separation: 5 ms; Final Pulse separation: 18,500 ms, Number of data points for fitting: 20; Delay sample window: 0.05 ms; Sampling Window: 0.02 ms; Time for Saturation Curve Display: 6 s.

<u>*Nanoparticle Synthesis:*</u>

Preparation of Nanoparticle Conjugates (by Patrick J. Straney): Aliquots of the nanoparticle solution were washed with Nanopure™ water three times by centrifugation (14, 000 rpm for 15 minutes; Eppendorf 5804R, Eppendorf, Inc.). After the third removal of supernatant, the particle pellet was resuspended in 1 mL of a 10 μM aqueous solution of thiolated polyethylene glycol (PEG-SH), where displacement of the citrate was carried out by standard mass-action transfer over 12 hours at 22°C under constant agitation (1000 rpm, Eppendorf Thermomixer R, Eppendorf, Inc.) as 3. PEG-SH functionalized particles were purified again by centrifugation (14,000 rpm for 15 minutes; Eppendorf 5804R, Eppendorf, Inc.) and diluted with 0.01% w/v SDS (*aq*) to 1 mL. To these solutions was added 2 μL of Gd-1, Gd-2, or Gd-Tripod at concentrations of 1 mM in DMSO. Conjugation of the contrast agents was carried out by standard mass-action transfer over 12 h at 22°C under constant agitation (1000 rpm, Eppendorf Thermomixer R, Eppendorf, Inc.).

UV-Vis-NIR Spectrophotometry and TEM Analysis (by Patrick J. Straney and Dr. Christopher M. Andolina): Nanoparticles and nanoparticle conjugates were characterized by ultraviolet-visible-near infrared spectroscopy (UV-Vis-NIR) using a Cary 5000 spectrophotometer (Agilent Technologies, Inc.) baselined to the spectrum of NANOpure™ water. All measurements were made using 1 cm pathlength quartz

cuvettes. All nanostructures were imaged using an FEI Morgagni 268 transmission electron microscope (TEM) at 80 kV. Samples were prepared by dropcasting 10 μL of purified, concentrated nanoparticle solution onto Formvar coated, Cu TEM grids (Ted Pella, Inc.). TEM images were analyzed by the computer program ImageJ (http://rsbweb.nih.gov/ij/), using the PSA-r12 Particle Sizing Analyer macro. Over 1250 particles were analyzed to determine the average size particle diameter of 19 ± 3 nm.

Dynamic Light Scattering Analysis (by Patrick J. Straney): Dynamic Light Scattering measurements (DLS, photon correlation spectroscopy) were performed using a Malvern Zetasizer (Nano Series ZS90, Malvern Instruments, Inc.). Nanoparticle samples were purified by centrifugation (three cycles of 15 minutes at 14,000 RPM) and resuspended in 0.01% w/v SDS (*aq*) and diluted to approximately one-tenth the original concentration. Measurements were obtained using 1 cm pathlength quartz cuvette (Hellma, Inc.) using the refractive index of gold (n = 0.999, k = 2.39x 10^{-6}) at 25.0 °C. Zeta potential was measured with a Pd-electrode dip cell (Malvern Universal Dip Cell kit ZEN1002).

Table 1. Summary of size and surface charge as measured by DLS. (Standard deviations are based on variation in three measurements of 11 scans each measurement.)

	Average Hydrodynamic Diameter (nm)	Polydispersity Index	Zeta Potential (mV)
PEG-SH AuNPs	28.2 ± 1.77	0.278 ± 0.03	-26.1 ± 0.70
Gd-1	32.7 ± 0.24	0.275 ± 0.00	-17.1 ± 1.27
Gd-2	27.8 ± 0.31	0.322 ± 0.08	-10.9 ± 4.09
Gd-Tripod	26.4 ± 0.15	0.252 ± 0.02	0.02 ± 0.03

Results and Discussion

Each Gd-HOPO complex is conjugated to the nanoparticle surface using 7 or less non-planar atom linkers to limit local motion of Gd(III) on gold nanoparticles and increase relaxivity. A unique feature of the Gd-Tripod CA, is that it is designed to form a macro-tricycle on the surface of the AuNP. In order to understand the impact of this binding motif, we compare the relaxivity of Gd-Tripod to two previously investigated ligand architectures, Gd-1 and Gd-2. Analogues to Gd-1 and Gd-2 have previously exhibited relaxivities up to 38 $mM^{-1}s^{-1}$ when conjugated to an esteramide dendrimer (40 kDa) or the MS2 viral capsid. Here, these compounds are appended with terminal thiol moieties which serve as linkers to bind directly to the AuNP surface. Like Gd-1 and Gd-2, Gd-Tripod is also hexadentate binding chelator, allowing space for q = 2-3 water sites for coordination. However, Gd-Tripod uses three HOPO moieties, which leaves the overall complex with a neutral charge.

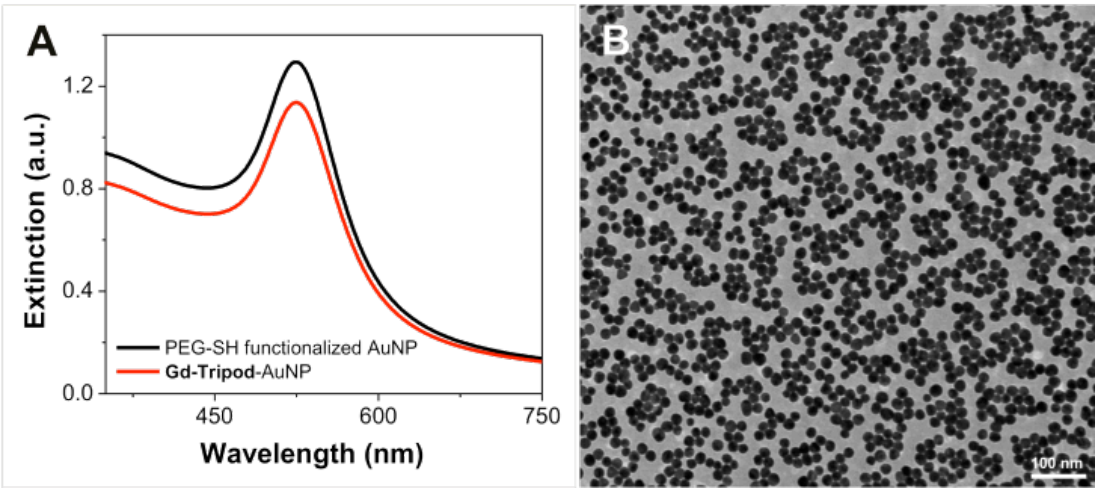

Figure 3. (A) Extinction spectra and (B) TEM image of gold nanoparticles after functionalization with Gd-Tripod.

Gd-Tripod synthesis begins with the previously described (6-Me)-3,2-HOPO chelator 3, which has been successfully imaged in mice with Gd(III).[9] The HOPO ring is formed with an ethyl ester at the four-position. Following this, an ethylene diamine *N*-boc protected bottom linker was added to the compound. The ethyl ester 6 was saponified and three of these moieties were bridged using a tris-(2-aminoethyl)-amine (TREN) cap to form a hexadentate species. After a global deprotection of benzyl and *N*-boc groups under acidic conditions, the Gd(III) was complexed to the TREN-*tris*-(6-Me)-3,2-HOPO-amine 9. In order to provide a SH group to the ligand, 3-mercaptopropionic acid was reacted with compound 10. (Scheme 1).

With these three Gd-HOPO complexes in hand (Gd-1, 13, Gd-2, 14, Gd-Tripod, 11; Figure 1), I evaluated their relaxivity properties when appended to an AuNP scaffold. We examined the efficiency of particle functionalization using these compounds, as well as the stability of the AuNP architecture and optical features upon functionalization.

It is important that these conjugates maintain key features of the AuNP scaffold including optical properties and particle dispersity, as these are often key features of both diagnostic and therapeutic applications of gold nanoparticles.[6-7] Figure 2 shows transmission electron microscopy (TEM) images and extinction spectra of the particles before and after conjugation. It is well known that gold nanoparticle aggregation causes a red-shift and broadening of the nanoparticle spectral features.[10-11] However, extinction spectra taken of the particle colloid before and after conjugation indicate similar optical properties (Figure 2A). Next, the colloid was examined by TEM. Although TEM is not a definitive characterization technique for the presence of aggregates, it can indicate coalescence or degradation of particles that may have occurred as a result of the functionalization or testing procedures. TEMs taken after CA conjugation indicate robust AuNPs (Figure 2B).

Last, dynamic light scattering (DLS) was used to evaluate the average size of the particles in solution. One particular challenge when using ligands with multiple binding

sites is the formation of nanoparticle dimers (and higher order aggregates). As is well-known, the intensity of light scattering is skewed toward larger particles and therefore DLS serves a sensitive technique for identifying aggregates in solution.[12] Before conjugation, DLS measurements indicate that the average hydrodynamic diameter of particles is approximately 28 ± 2 nm, and after conjugation their size was measured as 33, 28, and 27 nm for Gd-1, Gd-2, and Gd-Tripod, respectively. The slightly smaller radii observed after conjugation are due to loss of particles during successive centrifugation and purification steps, and are consistent with the observed absorption spectra, which do not red-shift after conjugation (as would be expected due to a change in surface dielectric environment).

For relaxivity analysis of these materials, I first analyze the degree of particle functionalization with each ligand. Gd-1-AuNP conjugates exhibit a complex loading density of 2,350 molecules per particle as characterized by inductively coupled plasma optical emission spectroscopy (ICP-OES). The relaxivity value of Gd-1-AuNP is 40 ± 2 $mM^{-1}s^{-1}$, similar to previously reported relaxivity values for scaffold immobilized CAs (37 ^{o}C and 60 MHz). This similarity may be related to a plateau in the attenuation of local complex motion that is afforded by a single scaffold attachment strategy. Indeed, the same per-Gd(III) relaxivity of 38 $mM^{-1}s^{-1}$ is also observed for both the esteramide dendrimer (~40 kDa) and MS2 viral capsid(~2 MDa) systems at the same conditions.

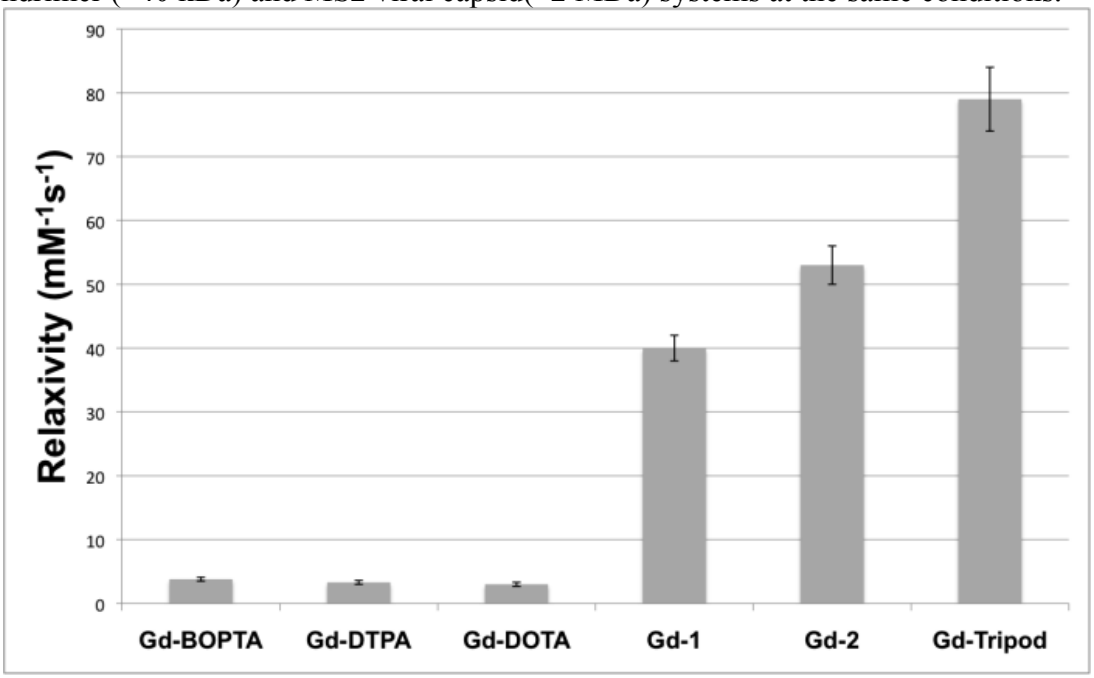

Figure 4. A comparison of the per gadolinium relaxivities of several clinical Gd(III) CAs,[2] macromolecular Gd-HOPO CAs, and gold nanoparticle contrast agents investigated in this study.

However, by using a "multi-linked" approach, the local motion of the Gd(III) center may be slowed further as compared to the molecular tumbling time of the

macromolecule. A second CA, Gd-2, was prepared and contained two thiol gold surface binding moieties. Relaxivity of AuNP conjugates functionalized with Gd-2 exhibit values of 53 ± 3 $mM^{-1}s^{-1}$ (Gd-2-AuNP) and complex loadings of 1,150 Gd-2 complexes per particle by ICP-OES. This rise in r_1 is notable: with only one portion of the molecule (the TAM chelator) bound in two locations, the relaxivity increases to the largest relaxivity value reported for Gd-HOPO-based complexes to date.

The full Gd-Tripod complex increased relaxivity to a maximum of 79 ± 5 $mM^{-1}s^{-1}$ (Figure 3). The structure of the Gd-Tripod monolayer was evaluated in a similar manner to the Gd-1-AuNP and Gd-2-AuNP conjugates (*vide supra*), and showed the lowest loading values of all the conjugates, as expected with its larger surface area footprint (720 complexes per particle by ICP). Indeed, Gd-1 showed approximately twice the complex loading of Gd-2, and three times the loading of Gd-Tripod throughout condition optimization.

AuNPs are an ideal platform for the multilinked approach. Binding sites on dendrimers and proteins are often dispersed throughout the molecule, whereas the number of adjacent binding sites on a gold nanoparticle allows for the *on-particle* formation of supramolecular architectures which maximize the rigidity of the CA both in terms of global (through the chelator) and local (through multiple particle tethers) motion. Because the number of Gd complexes per particle increases with the particle diameter as a function of increasing surface area, by definition larger particles tend to exhibit larger per particle relaxivities. However, several scaffolded CA systems are evaluated in this manner, and we report a Gd-Tripod-AuNP per particle relaxivity of approximately 25,000 $mM^{-1}s^{-1}$, which compares favorably with other reported values.[1] Yet, this metric is to be taken with caution: smaller particles are preferred for renal clearance,[13] and the total amount of Gd needed to obtain clear images with minimal toxicity is the figure of merit in these investigations.

Conclusion

In summary, it has been demonstrated that using conjugation to highly biocompatible and readily synthesized gold nanoparticles improves the relaxivity of HOPO-based TREN capped Gd(III) complexes over commercial agents without compromising clinical relevance and safety. Importantly, further improvements in Gd-based CA performance may be accessed through scaffold-conjugation strategies aimed at decreasing local CA tumbling rates in addition to attenuation of CA global motion. Conjugates presented here contain novel tripod conjugated gadolinium(III) complexes that exhibit relaxivities of up to 79 $mM^{-1}s^{-1}$ under the clinically relevant conditions of 60 MHz and 37 ^{o}C.

Literature

1) Song, Y.; Xu, X.; MacRenaris, K. W.; Zhang, X.-Q.; Mirkin, C. A.; Meade, T. J. Multimodal gadolinium-enriched DNA-gold nanoparticle conjugates for cellular imaging. *Angew. Chem. Intl. Ed.* **2009,** *48,* 9143-9147.

2) Lee, S.-M.; Song, Y.; Hong, B. J.; MacRenaris, K. W.; Mastarone, D. J.; O'Halloran, T. V.; Meade, T. J.; Nguyen, S. T. Modular polymer-caged nanobins as a theranostic

platform with enhanced magnetic resonance relaxivity and pH-responsive drug release. *Angew. Chem. Intl. Ed.* **2010,** *49,* 9960-9964.
3) Steinbacher, J. L.; Lathrop, S. A.; Cheng, K.; Hillegass, J. M.; Butnor, K. J.; Kauppinen, R. A.; Mossman, B. T.; Landry, C. C. Gd-labeled microparticles in MRI: in vivo imaging of microparticles after intraperitoneal injection. *Small.* **2010**, *6,* 2678-2682.
4) Bohren, C. F.; Huffman, D. R. Absorption and Scattering of Light by Small Particles. **1983**, John Wiley & Sons.
5) Daniel, M.-C.; Astruc, D. Gold nanoparticles: assembly, supramolecular chemistry, quantum-size-related properties, and applications toward biology, catalysis, and nanotechnology. *Chem. Rev.* **2004,** *104,* 293-346.
6) Chi, X.; Huang, D.; Zhao, Z.; Zhou, Z.; Yin, Z.; Gao, J. Nanoprobes for in vitro diagnostics of cancer and infectious diseases. *Biomaterials.* **2011,** *33,* 189-206.
7) Huang, Z.; Neretina, S.; El-Sayed, M. A. Gold nanorods: from synthesis and properties to biological and biomedical applications. *Adv. Mater.* **2009,** *21*, 4880-4910.
8) Giljohann, D. A.; Seferos, D. A.; Daniel, W. L.; Massich, M. D.; Patel, P. C.; Mirkin, C. A. Gold nanoparticles for biology and medicine. *Angew. Chem. Intl. Ed.* **2010**, *49*, 3280-3294.
9) 40) Choi, H. S.; Liu, W.; Misra, P.; Tanaka, E.; Zimmer, J. P.; Ipe, B. I.; Bawendi, M. G.; Frangioni, J. V. Renal clearance of quantum dots. *Nat. Biotechnol.* **2007,** *25,* 1165-1170.
10) Mout, R.; Moyano, D. F.; Rana, S.; Rotello, V. M. Surface functionalization of nanoparticles for nanomedicine. *Chem. Soc. Rev.* **2012,** *41,* 2539-2544.
11) Frens, G. Controlled nucleation for the regulation of the particle size in monodisperse gold suspensions. *Nature Phys. Sci.* **1973,** *241*, 20-22.
12) Hill, H. D.; Mirkin, C. A. The bio-barcode assay for the detection of protein and nucleic acid targets using DTT-induced ligand exchange. *Nat. Protoc.* **2006**, *1*, 324-336.
13) Mirkin, C. A.; Letsinger, R. L.; Mucic, R. C.; Storhoff, J. J. A DNA-based method for rationally assembling nanoparticles into macroscopic materials. *Nature*, **1996,** *382*, 607-609.

Chapter 9- Conclusions and Future Directions

Many different macromolecular platforms and scaffolds to improve MRI –CA have been developed. Using unique chemistry and materials science developed in the laboratories of various collaborators, the forefront of macromolecular conjugation has been combined with high-efficiency small molecule MRI-CA, including Gd-HOPO and other oxygen donor chelators, to vastly improve per-Gd relaxivity, per-particle relaxivity, and kinetic stability of the metal center in the compound. These experiments offer new insight into how to best harness the potential of macromolecules to make a superior contrast agent. The design of contrast agents involves the simultaneous optimization of safety, signal, and rapid excretion; , these examples each highlight superior features and the prospects that different macromolecules have to offer.

All particle options (gold, silica, $NaYF_4$) are of great interest due to their abundance of loading sites. Many loading sites allow for a larger molar concentration of gadolinium, as well as huge per-particle relxivities, and sites available for further modification and improvement. With these loading sites, future work will include adding imaging modalities (e.g. optical imaging, PET), therapeutics (e.g. irradiation of gold nanoparticles), solubilizing groups (e.g. PEG chains), and targeting moieties (e.g. antibodies, folate, etc.). The protein structure, while a loading of only one metal per macromolecule, offers a new type of structure- that in which a kinetically stable wrapping is used around the metal. This wrapping is unique in that it not wrapped so tight so as to still allow for solvent exchange and therefore high relaxivity, but cannot allow the metal out of its shell. From an inorganic and metal binding perspective, this general type of system has not been explored in the literature and should make for a very interesting direction to further research and clinical exploration when higher molar relaxivity can be obtained. Dendrimers with degradable cores offer an option to allow larger molecules to function without the worry of renal clearance of high-molecule weights. These have been shown to increase relaxivity, function, and have the most precise, controlled, and high-yield of the macromolecules explored. These attributes will be essential in further exploration toward *in vivo* models.

Future exploration into these topics will work on uniting the superior qualities defined individually into one contrast agent, and eventually, one multimodal contrast agent and treatment therapy.